Influence of 3D tumor cell/fibroblast co-culture on monocyte differentiation and tumor progression in pancreatic cancer

DOCTORAL DISSERTATION

submitted to the

Faculty of Biology,

Julius-Maximilians University Würzburg,

for fulfillment of the requirements for the degree of

DOCTOR OF NATURAL SCIENCES

(DR. RER. NAT.)

presented by

Janina Kuen

born in

Fulda, Germany

Würzburg, Year 2017

The work presented in this doctoral thesis was started in October 2013 and completed in July 2017 at Roche Diagnostics GmbH, Pharma Research and Early Development (pRED), Department Discovery Oncology, Cancer Immunotherapy I (CIT1), in Penzberg under supervision of Dr. Meher Majety and Prof. Dr. Manfred Lutz and PD Dr. Alois Palmetshofer from the Julius-Maximilians University of Würzburg.

Doctoral thesis submitted: ……………………………………………………………………

Members of the Thesis Committee:

Chairman: ………………………………………………………………………….
Official Reviewer: ………………………………………………………………………….
Official Reviewer: ………………………………………………………………………….

Dissertation will be defended on: …………………………………………………………..
Graduation certificate received on: …………………………………………………………..

Name: Kuen, Janina
Address: Johann-Dreher-Straße 6, 82377 Penzberg
Mobile: +49 178 722 61 11
E-Mail: janina.kuen@outlook.com

Erklärungen nach §4 Abs. 3 Satz 3, 5, 8 der Promotionsordnung der Fakultät für Biologie

Affidavit

I hereby declare that my thesis entitled: „Influence of 3D tumor cell/fibroblast co-culture on monocyte differentiation and tumor progression in pancreatic cancer" is the result of my own work.

I did not receive any help or support from commercial consultants. All sources and / or materials applied are listed and specified in the thesis.

Furthermore I verify that the thesis has not been submitted as part of another examination process neither in identical nor in similar form.

Eidesstattliche Erklärung

Hiermit erkläre ich an Eides statt, die Dissertation: „Influence of 3D tumor cell/fibroblast co-culture on monocyte differentiation and tumor progression in pancreatic cancer", eigenständig, d. h. insbesondere selbständig und ohne Hilfe eines kommerziellen Promotionsberaters, angefertigt und keine anderen, als die von mir angegebenen Quellen und Hilfsmittel verwendet zu haben.

Ich erkläre außerdem, dass die Dissertation weder in gleicher noch in ähnlicher Form bereits in einem anderen Prüfungsverfahren vorgelegen hat.

Penzberg, den 18.07.2017

_____

Unterschrift, Janina Kuen

Acknowledgements

So eine Arbeit wird eigentlich nie fertig,
man muss sie für fertig erklären,
wenn man nach Zeit und Umständen
das Möglichste getan hat.

(Johann Wolfgang von Goethe)

Table of content

Parts of this thesis have already been published:

Publication

Janina Kuen, Diana Darowski, Tobias Kluge, Meher Majety

Pancreatic cancer cell/fibroblast co-culture induces M2 like macrophages that influence therapeutic response in a 3D model.

Published in PLoS ONE 12(7): e0182039 (27th of July 2017)

Poster

Janina Findeis and Meher Majety

Influence of 3D tumor cell/fibroblast co-culture on monocyte differentiation and tumor growth in pancreatic cancer.

Immunotherapy of Cancer Conference 2 (ITOC2), March 2015, Munich, Germany

Abstract published in European Journal of Cancer Vol 51 (1) Page S1 (March 2015)

Abstract

Pancreatic cancer (PC) remains one of the most challenging solid tumors to treat with a high unmet medical need as patients poorly respond to standard-of-care-therapies. Prominent desmoplastic reaction involving cancer-associated fibroblasts (CAFs) and the immune cells in the tumor microenvironment (TME) and their cross-talk play a significant role in tumor immune escape and progression. To identify the key cellular mechanisms induce an immunosuppressive tumor microenvironment, we established 3D co-culture model with pancreatic cancer cells, CAFs, monocyte as well as T cells.

Using this model, we analysed the influence of tumor cells and fibroblasts on monocytes and their immune suppressive phenotype. Phenotypic characterization of the monocytes after 3D co-culture with tumor/fibroblast spheroids was performed by analysing the expression of defined cell surface markers and soluble factors. Functionality of these monocytes and their ability to influence T cell phenotype and proliferation was investigated.

3D co-culture of monocytes with pancreatic cancer cells and fibroblasts induced the production of immunosuppressive cytokines which are known to promote polarization of M2 like macrophages and myeloid derived suppressive cells (MDSCs). These co-culture spheroid polarized monocyte derived macrophages (MDMs) were poorly differentiated and had an M2 phenotype. The immunosuppressive function of these co-culture spheroids polarized MDMs was demonstrated by their ability to inhibit autologous CD4$^+$ and CD8$^+$ T cell activation and proliferation *in vitro*, which we could partially reverse by 3D co-culture spheroid treatment with therapeutic molecules that are able to re-activate spheroid polarized MDMs or block immune suppressive factors such as Arginase-I.

In conclusion, we generated a physiologically relevant 3D co-culture model, which can be used as a promising tool to study complex cell-cell interactions between different cell types within the tumor microenvironment and to support drug screening and development. In future, research focused on better understanding of resistance mechanisms to existing cancer immunotherapies will help to develop new therapeutic strategies in order to combat cancer.

Zusammenfassung

Bei Bauchspeicheldrüsenkrebs handelt es sich um eine maligne Tumorerkrankung, deren Behandlung Ärzte noch immer vor große Herausforderungen stellen und die zur dritthäufigsten krebsbedingten Todesursache der westlichen Welt zählt. Desmoplastische Reaktionen im Tumorgewebe sind hierbei ein besonderes Merkmal dieser Erkrankung. Dabei spielen tumor-assoziierte Fibroblasten sowie unterschiedliche Zellen des Immunsystems und deren Interaktionen eine essentielle Rolle hinsichtlich Tumorwachstum und der Herunterregulation des Immunsystems. Um zelluläre Mechanismen, die ein immunsuppressives Tumormilieu induzieren, zu identifizieren, entwickelten wir ein 3D Ko-Kultur Modell mit Bauchspeicheldrüsenkrebszellen, tumor-assoziierten Fibroblasten sowie Monozyten und T-Zellen.

Mit Hilfe dieses Modells konnten wir den Einfluss von Tumorzellen und Fibroblasten auf den Phänotyp und das Verhalten von Monozyten untersuchen. Dazu wurden Monozyten in einer 3D Tumorzell/Fibroblasten Ko-Kultur kultiviert und differenziert, um anschließend die Expression definierter Zelloberflächenmarker und löslicher Faktoren zu analysieren. Des Weiteren wurde das Verhalten dieser 3D Ko-Kultur differenzierten myeloiden Zellpopulation sowie ihre Fähigkeit den Phänotyp von T Zellen und deren Proliferation zu beeinflussen untersucht.

Die 3D Ko-Kultur der Monozyten zusammen mit den Tumorzellen und den Fibroblasten führten zur Produktion immunsuppressiver Zytokine und Chemokine, wodurch die Differenzierung der Monozyten in M2-ähnliche Makrophagen induziert wurde. Diese durch die 3D Tumorzell/Fibroblasten Sphäroide polarisierten aus Monozyten herangereiften M2-ähnlichen Makrophagen besaßen außerdem immunsuppressive funktionelle Eigenschaften, indem sie in der Lage waren, die Aktivierung und Proliferation von autologen CD4$^+$ und CD8$^+$ T Zellen *in vitro* zu inhibieren. Die Suppression sowohl der CD4$^+$ als auch der CD8$^+$ T Zellen konnte durch die Behandlung therapeutischer Moleküle, die die Re-Aktivierung der immunsuppressiven 3D Sphäroid polarisierten Makrophagen stimulierten oder suppressive Faktoren wie Arginase-I blockierten, wieder aufgehoben und die T Zell Proliferation teilweise wiederhergestellt werden.

Unser etabliertes 3D Ko-Kultur System repräsentiert ein vielversprechendes physiologisch relevantes Modell, welches genutzt werden kann, um Zell-Zell Interaktion und Kommunikation im Tumormilieu zu untersuchen und dadurch die Wirkung von Medikamenten zu verbessern. Ein gezieltes besseres Verständnis von Tumorresistenz Mechanismen gegen bereits bestehende Immun Therapien fördert die Entwicklung neuer therapeutischer Ansätze zur Bekämpfung von Krebs.

1. Introduction

1.1 Pancreatic ductal adenocarcinoma

Pancreatic ductal adenocarcinoma (PDAC) is one of the most lethal solid malignancies worldwide. The American Cancer Society estimates that there will be 53 670 people diagnosed in 2017 in the United States with an estimated 43 090 patients dying from it, which makes pancreatic cancer the third leading cause of cancer deaths (Fig. 1) [1]. Early detection methods and improved treatment therapies have led to an overall decrease of cancer-related deaths in the past 20 years, but nevertheless pancreatic cancer patients still only have a 5-year survival rate of 8%, if diagnosed with localized and potentially curable tumors in early stages and once the tumor has spread to nearby lymph nodes or distant sites, such as liver or lung, the 5-year survival rate decreases to 3% [1].

Estimated new cases, 2017 By cancer type, both sexes combined		Estimated deaths, 2017 By cancer type, both sexes combined	
Breast	255,180	Lung and bronchus	155,870
Lung and bronchus	222,500	Colorectum	50,260
Prostate	161,360	Pancreas	43,090
Colorectum	135,430	Breast	41,070
Melanoma of the skin	87,110	Liver and intrahepatic bile duct	28,920
Urinary bladder	79,030	Prostate	26,730
Non-Hodgkin lymphoma	72,240	Leukemia	24,500
Kidney and renal pelvis	63,990	Non-Hodgkin lymphoma	20,140
Leukemia	62,130	Urinary bladder	16,870
Uterine corpus	61,380	Brain and other nervous system	16,700
Thyroid	56,870	Esophagus	15,690
Pancreas	53,670	Kidney and renal pelvis	14,400
Oral cavity and pharynx	49,670	Ovary	14,080
Liver and intrahepatic bile duct	40,710	Myeloma	12,590

Figure 1: Cancer statistics.
Obtained from the American Cancer Society showing estimated new cancer cases (left) and estimated cancer deaths (right) in 2017 in the United States for both males and females [1].

Pancreatic cancer is commonly found in elderly people and occurs more often in males than in females [2]. Only 10% of patients develop this tumor below the age of 50 [2]. Numbers of risk factors have been linked to the incidence of pancreatic cancer, but environmental risk factors seem to be accountable for the majority of cases. Cigarette smoking, by far the leading preventable cause of pancreatic cancer, has been shown to double the risk of developing pancreatic cancer and 25% of diagnosed pancreatic tumors is thought to be due to smoking [3, 4]. Other risk factors that have been associated with the development of pancreatic cancer include obesity, long-standing diabetes mellitus as well as high meat and fat diets [2, 5]. Several studies reported an increased risk for patients suffering from chronic pancreatitis which often results from excessive alcohol and cigarette consumptions as well as rather rare hereditary forms. Patients with chronic pancreatitis are 14-times more likely to develop PDAC [4]. Furthermore, pancreatic cancer incidence has also been associated with genetic predisposition and individuals with a family history of pancreatic cancer affecting four or more family members have a 57-times higher risk of developing PDAC [6]. Numerous inherited germ-line mutations are known to cause pancreatic cancer, including BRCA2, PALB2, KRAS2 and CDKN2A and patients with a strong family history or hereditary pancreatitis can benefit from germ-line mutation screenings in specialized centres with high expertise and suitable equipment [2, 6].

1.1.1 Pathophysiology, diagnosis and staging of PDAC

Pancreatic ductal adenocarcinoma accounts for 90% of all pancreatic cancers and is an invasive malignant exocrine epithelial neoplasm with glandular ductal differentiation. PDAC grossly forms a firm and highly sclerotic poorly defined white-yellow fibrotic mass which often occurs on the distal common bile duct or the main pancreatic duct [7]. Pancreatic cancer is accompanied by a strong desmoplastic reaction with only the minority of cells being neoplastic. Ductal adenocarcinomas tend to strongly infiltrate into lymphatic, vascular and perineural spaces. By the time of detection, PDAC has usually metastasized into distant sites such as liver, peritoneum, lungs and pleurae [8]. The non-invasive and histologically distinct precursor lesions that arise in a step-wise progression of PDAC can be categorized into intraductal papillary mucinous neoplasm (IPMN), mucinous cystic neoplasm (MCN) and pancreatic intraepithelial neoplasia (PanIN), which are sub-classified into PanIN-1, PanIN2 and PanIN-3 depending on the degree of cytological and architectural tissue degeneration (Fig. 2 A). PanINs can often be found adjacent to ductal adenocarcinoma and it is documented that PanINs may also develop into infiltrating pancreatic cancer [9].

On molecular basis it is confirmed that PanINs harbour the most frequent genomic alterations which can typically also occur in PDAC, most notably activation point mutations in codon 12 of the *K-ras* gene found early and predominantly in PanIN1 lesions, but also in tumor-suppressor genes such as *p16*, *p53* and *BRCA2* occurring later in PanIN2 and PanIN3 lesions [8, 9]. IPMNs, accounting for 5-10% of all pancreatic precursor lesions, are mucin-producing epithelial neoplasms with a mostly papillary architecture that mainly expresses the mucin MUC-2 compared to PanINs commonly expressing MUC1. The loss of the *STK11/LKB1* gene is commonly observed in this type of lesion whereas *SMAD4* inactivation can only be observed for the minority of IPMNs [8]. The third histologically relevant precursor lesion is the MCN, which are primarily found in women. MCNs have a distinct ovarian-type stroma and consist of mucin-producing epithelial cells, and in contrary to PanINs and IPMNs, MCNs do not interact with the larger pancreatic duct. So far, there is also not much known about genetic alterations in MCN [8]. Even though all precursor lesions are able to progress to invasive PDAC over time, IPMNs and MCN have higher chances of being detected at an early stage as they are significantly larger than lesions of the PanIN type (Fig. 2 B) [8].
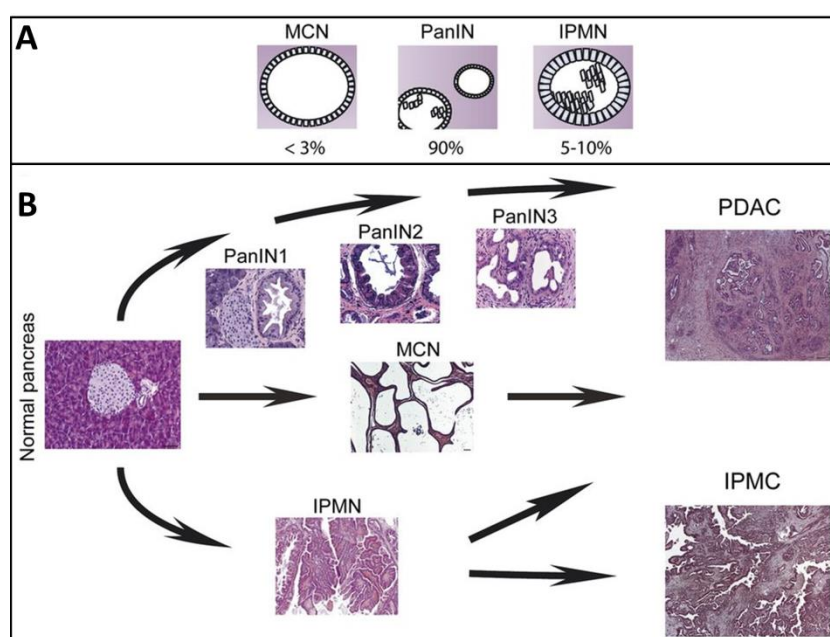
Figure 2: Progression of pancreatic ductal adenocarcinoma.
A) Non-invasive precursor lesions of PDAC can be divided into MCN, PanIN and IPMN, whereas 90% of identified lesions can be attributed to PanIN lesions. B) Development of PDAC from normal pancreas via the different precursor lesions MCN, PanIN and IPMN with PanIN lesions graded from 1 to 3 based on morphological changes (modified from Mazur et al. [10]).

Early detection of the tumor is critical to the patient´s survival. The majority of tumors have already disseminated to surrounding tissue and distant organs once it is diagnosed, so that only 20% of patients can receive a potentially curative tumor resection. Tumor staging is based on the resectability by means of imaging using contrast-enhanced spiral CT and performed by the American Joint Committee on Cancer (AJCC) classification. T1, T2 and T3 tumors are considered to be potentially resectable, whereas T4 tumors already involving the superior mesenteric artery and celiac axis, are unresectable [6]. The most common serum biomarkers to identify advanced PDAC are the sialyated Lewis blood group antigen CA19-9 and the carcinoembryonic antigen (CEA), which show low sensitivity in patients with localized or small tumors but up to 80% sensitivity in patients with advanced disease [11]. If clinical examination suggests the need of further diagnostic tests, a tri-phasic (i.e. arterial, late and venous phases) pancreatic protocol computed tomography (CT) with a sensitivity of 89%-97% serves as the standard for tumor diagnosis and staging [12].

1.1.2 Inflammatory tumor microenvironment

In recent years, pancreatic cancer research has focused on the role of the tumor microenvironment in tumor growth, progression and metastasis. One of the hallmarks of pancreatic adenocarcinoma is a dense heterogeneous desmoplastic reaction (DR) that is largely composed out of pancreatic stellate cells (PSCs), extracellular matrix (ECM) proteins including collagen I/III and fibronectin, but also contains endothelial cells, pericytes and immune cells (Fig. 3) [13]. Dense DR in primary tumors has been associated with worse clinical outcomes. In pancreatic cancer it can form up to 80% of the tumor mass and has been shown to contribute to the aggressive character of the tumor by promoting metastasis and tumor growth as well as mediating therapy resistance [14]. Along the development from pre-neoplastic precursor lesions to invasive PDAC, the tumor microenvironment is not static, but constantly changing in composition.
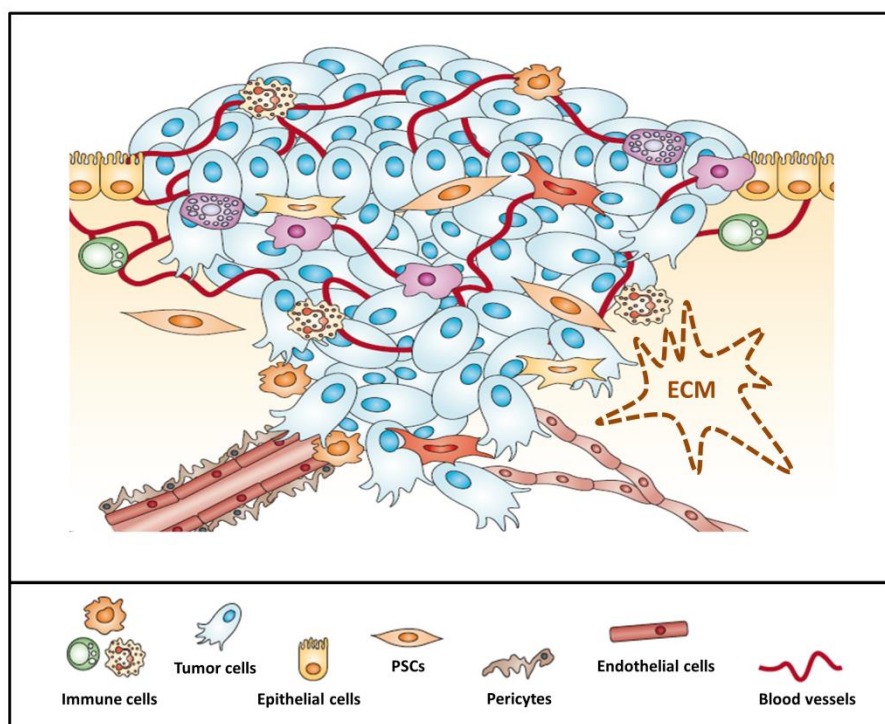
Figure 3: The primary tumor microenvironment.
Cancer cells in primary tumors are surrounded by an abundant desmoplastic stroma that accumulates as tumorigenesis progresses and that consists of numerous cells such as pancreatic stellate cells, pericytes, endothelial cells of blood vessels and different types of immune cells such as macrophages, neutrophils and lymphocytes (modified from Joyce and Pollard [15]).

Targeting tumor stroma is hence being discussed controversially and contradictory findings have raised concerns about efficacy of stroma depletion as treatment [16]. Better understanding of cellular constituents of the DR in pancreatic cancer and how different cell types interact with each other and influence tumor growth and drug resistance can improve treatment therapies, leading to an increased overall survival rate.

Stromal fibroblasts – the pancreatic stellate cells (PSCs)

The major cellular components of the tumor stroma in PDAC are PSCs and fibroblasts. PSCs have first been identified, isolated and cultured by Bachem and Apte in 1998. The origin of PSCs is unclear, but it is assumed that they arise from mesenchymal and endodermal precursor cells. Under normal conditions, PSCs are quiescent and found in periacinar spaces in the normal pancreas where they comprise only 4% of the pancreatic cell population and are responsible for regulating ECM turnover and homeostasis of matrix degrading enzymes and tissue inhibitors of metalloproteinases (TIMPs)

[17]. PSCs and fibroblasts play an important role in persistent pancreatitis and the development of PDAC. Once PSCs are activated or recruited from local fibroblasts, they lose the ability to store cytoplasmic vitamin A lipid droplets, acquire myofibroblastic characteristics and start expressing α-smooth muscle actin (α-SMA). Activated PSCs can also impair organ function due to the abundant production and deposition of ECM proteins, increased cell proliferation and secretion of growth factors and cytokines [17, 18]. It has been reported that PSCs respond to a number of cytokines such as the transforming growth factor (TGF-β), epidermal growth factor (EGF) or fibroblast growth factor (FGF), thus transforming into an active state with increased cell proliferation. Fibroblasts co-cultured with TGF-β expressing Panc-1 tumor cells strongly increased proliferation as well as expression of fibronectin and type I collagen. Orthotopic injection of these TGF-β secreting Panc-1 cells into nude mice led to enhanced tumor growth and desmoplastic reactions as shown by Lohr and colleagues [19]. Just as tumor-derived soluble factors influence the activation of tumor stroma, growth factors, cytokines and proteins secreted by PSCs regulate the composition of the ECM and also contribute to enhanced pancreatic cancer cell invasion. Gene expression profiles of PSCs co-cultured with pancreatic cancer cells revealed up-regulation of angiogenic molecules like interleukin-8 (IL-8), CCL-2 and GRO-1/2 as well as proteolytic enzymes including matrix metalloproteinases (MMPs) such as MMP-9, MMP-2 and MMP-1 [13, 18]. It is reported that PSCs significantly contribute to the resistance against chemo and irradiation therapy by the excessive production of ECM proteins. These inturn alter vascularization of the tumor which negatively affects drug delivery and promotes the epithelial-mesenchymal transition (EMT) in cancer cells thus facilitating metastatic spread and resistance to apoptosis of the tumor cells [13]. Identification of major signalling pathways of activated PSCs in contact with pancreatic cancer cells and targeting molecules specifically influencing PSCs may have a positive impact on tumor behaviour.

Extracellular matrix (ECM)

The ECM describes the non-cellular constituents present within all tissues and provides a structural scaffold for cellular components. It mainly consists of water, polysaccharides and proteins and mediates homeostasis and the retention of water as well as morphological changes, hence maintaining the physiological function by binding of growth factors and interaction with cell-surface receptors to support signal transduction and gene transcription [20]. The ECM forms the mechanical and biochemical characteristics of each organ and tissue; however it undergoes constant dynamic change and is being continuously remodelled. Changes of ECM properties are typically related to

pathology and can be induced in response to acute injuries. The ECM is composed of two main macromolecules – fibrous proteins and proteoglycans [20]. Fibrous proteins comprise collagen, elastin, laminins and fibronectin with collagen being the most abundant protein with a total mass of 30%. These scaffolding proteins regulate cell adhesion, tissue strength, chemotaxis and cell migration and are produced by stromal fibroblasts or surrounding tissues [21]. The second major component of the ECM – proteoglycans – consist of glycosaminoglycan chains covalently linked to a protein core and is classified into three main families comprising small leucine-rich proteoglycans (SLRPs), modular proteoglycans and cell surface proteoglycans. Proteoglycans are highly hydrophilic und form a hydrogel filling the extracellular interstitial space within tissues that are arranged in matrices solid enough to withstand high compressive forces [22]. While SLRPs are involved in signalling pathways such as EGF receptor activation and cell surface proteoglycans function as co-receptors for signal transduction, modular proteoglycans regulate cell adhesion, migration and proliferation and can act as pro- and antiangiogenic factors [20, 22]. In tumors, loss of tissue organization and deviant behaviour of cellular components is characteristic and often induced by genetic mutations and epigenetic alterations. Tumors are comparable to wounds failing to heal and activated PSCs and fibroblasts promote tissue desmoplasia as well as the production and deposition of ECM proteins which in turn potentiates tumor growth and survival [20, 21].

Immune cells in PDAC

The tumor microenvironment of solid tumors reveals numerous types of immune cells which, depending on tumor type, tumor stage and differentiation status, play an important regulatory role in tumor development and have the ability to either promote or inhibit tumor growth. Studies revealed that chronic inflammation, as seen in chronic pancreatitis, increases the risk and influences every step of carcinogenesis through the presence of cytokines, chemokines, growth factors, reactive oxygen species (ROS) and nitrogen oxide synthases (NOS) produced by immune cells [23]. Evaluation of leukocyte complexity, which differs in their immunosuppressive activity, has been done by flow cytometry of human and murine tumors. The tumor microenvironment was found to contain multiple types of innate immune cells such as macrophages, which are termed tumor-associated macrophages (TAMs), neutrophils, myeloid-derived suppressor cells (MDSCs) and natural killer (NK) cells and adaptive immune cells namely T and B lymphocytes [24, 25].

The most predominant cell populations within the tumor microenvironment are T cells and TAMs. T cells are classified into CD8$^+$ T cells, also termed cytotoxic T lymphocytes (CTL), and CD4$^+$ T

helper (Th) cells including T regulatory (Treg), Th1, Th2 and Th17 cells, according to their effector functions. Increased numbers of CTLs and Th1 cells correlate with better patient survival in some cancers such as pancreatic cancer [23]. As CD8^{+} T cells appear to play a distinct role in anti-tumor immunity by the direct lysis of malignant cells and the production of cytotoxic cytokines, CD4^{+} T cells seem to exert both tumor-promoting and suppressing effects due to the broad CD4^{+} T lymphocyte heterogeneity [24]. In pancreatic cancer, tumor cells and surrounding tumor stroma induce an immunosuppressive milieu by the production of cytokines such as interleukin-10 (IL-10), transforming growth factor-β (TGF-β) and the enzyme indoleamine-2,3-dioxygenase (IDO), which suppresses T cell proliferation by metabolizing tryptophan to kynurenine, leading to T cell starvation [26]. PDAC also expresses immune checkpoint ligands such programmed cell death ligand 1 (PDL1) and down-regulates the expression of the major histocompatibility complex (MHC) class I molecules, which reduces T cell activation and interferes with T cell antigen presentation [26].

The presence and distribution of TAMs in pancreatic cancer, which typically resemble M2 macrophages, closely correlates with worse clinical prognosis. They are the most abundant cell population within PDAC microenvironment and can promote tumor cell proliferation, stimulate angiogenesis and stroma remodelling and suppress other immune cells such as NK and T cells (Fig. 4) [27]. Along some other factors, the chemotactic molecules CCL2 or colony-stimulating factor-1 (CSF-1), which derive from tumor cells and stroma, directly mediate the recruitment of monocytes to the primary tumor site, where monocytes differentiate into macrophages according to environmental stimuli. Based on their function, macrophages can be classified into classically activated, pro-inflammatory M1 or alternatively activated anti-inflammatory M2 macrophages. M1 macrophages, activated by interferon-γ (IFN-γ) and lipopolysaccharide (LPS), typically secrete inflammatory cytokines such as IL-1, IL-6 or tumor necrosis factor-α (TNF-α) while M2 macrophages, induced by IL-4, IL10 and IL-13, produce immunosuppressive molecules such as TGF-β, IL-10 and Arginase-I [23, 27].
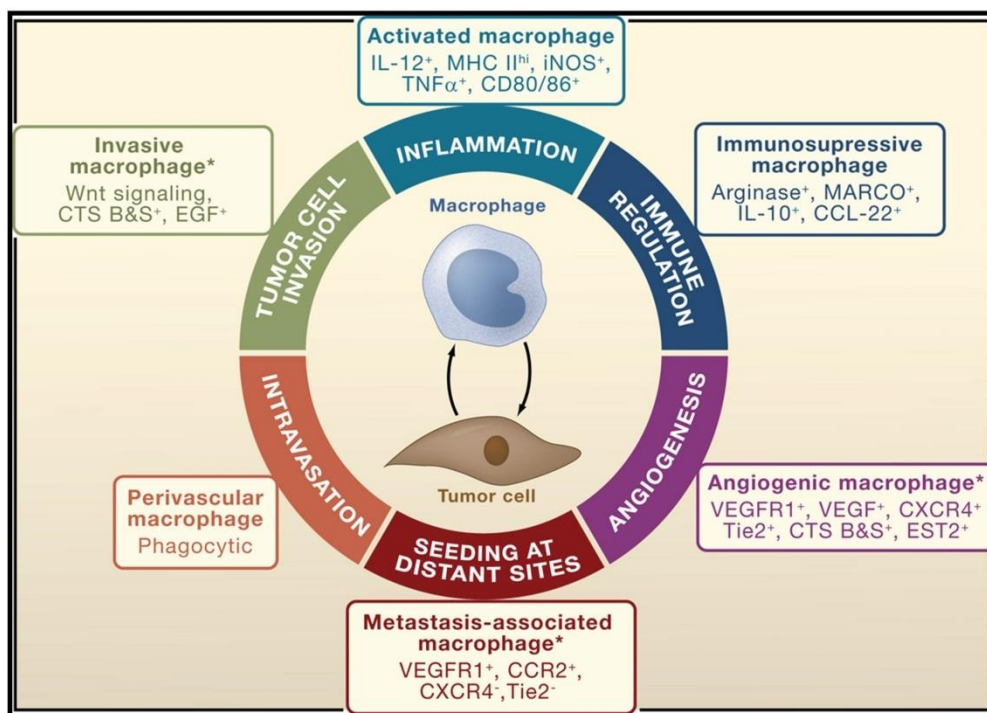
Figure 4: The role of pro-tumoral functions of TAMs in the cancer.
Macrophages develop into subtypes due to environmental stimuli, thus acquiring a unique phenotype and performing specific activities to support tumor growth and progression (adapted from Quatromoni and Eruslanov [28]).

However, most confirmed tumor promoting factors are commonly termed ´M1 cytokines` while it has been shown that IL-10 may also behave tumor suppressive for colorectal cancer, indicating the plasticity of macrophage polarization in response to surrounding stimuli [29, 30]. To discriminate macrophage populations within the tumor microenvironment, cell surface marker such as HLA-DR, CD86 and CD11c are used to identify M1 macrophages while the expression of CD163, CD204 and Arginase-I define M2 macrophages [26]. Nevertheless, flow cytometry and gene expression profiling have shown that human TAMs skew towards M2-like phenotype with a high variability and coexist in tumors depending on the location they reside within the tumor microenvironment [31]. TAM derived cytokines and proteases such as IL-10, IL-8, CCL22, Arginase-I and cathepsins strongly contribute to TAM mediated immunosuppression. The production of IL-10 leads to suppression of M1 cytokines like IL-12 and IFN-γ, thus inhibiting T cell differentiation and promoting immune cell evasion, while CCL22 or CCL17 promote Treg and Th2 cell infiltration into the tumor. The enzyme Arginase-I metabolizes L-arginine into polyamine and proline, consequently causing a dysregulation of T cell receptor (TCR) signalling that impairs T cell activation [32]. Studies revealed that TAMs also limit the efficacy of chemotherapy (e.g. paclitaxel, cyclophosphamide) by releasing chemo-protective factors, such as the lysosomal enzymes cathepsins B and S, therefore protecting cancer cells from paclitaxel-

induced cell death. Depletion of TAMs by anti-CSF1 antibodies has shown enhanced efficacy of treatment with combinational chemotherapy (5-fluorouracil, methotrexate or gemcitabine) [31]. Targeting immune cells in pancreatic cancer is considered one of the most promising therapeutic treatment options in future and strongly relies on elucidating the important and often paradoxical roles of immune cell types and their ability to function or dysfunction in the pancreatic cancer microenvironment.

1.1.3 Treatment of PDAC

Patients receive treatment against the tumor depending on the stage of the disease. Patients with a resectable tumor are able to undergo potentially curative surgery, which aims at complete tumor resection with clear resection margins (R0 resection). However, this only accounts for 10 to 20% of all patients. A multidisciplinary team of oncology experts and surgeons performs operative procedures, which, depending on the location of the tumor, include cephalic pancreatoduodenectomy (also called Whipple procedure), distal or total pancreatectomy [6]. The majority of patients are histologically staged as R1, which describes the complete resection of macroscopic tumor with positive resections margins, whereas patients staged as R2, resulting in incomplete tumor clearance, are treated like patients with locally advanced pancreatic cancer and may have to undergo further chemo- and irradiation therapy [6, 33]. Despite complete pancreatic resection, the overall 5-year survival of patients remains at around 15% due to recurrence of the tumor after surgery, emphasizing the need of additional adjuvant therapies [34]. Adjuvant therapy is usually given after recovery from surgery and significantly improves the patient´s length of survival. Numerous studies have investigated positive effects of systemic chemotherapy, irradiation therapy or the combination of both. In the 1970s, the first randomized clinical trials testing 5-fluorouracil (5-FU)-based therapies showed a superior overall median survival compared to patients that only received surgery (19.7 versus 14 months) [35]. For a long time, 5-FU was considered the standard-of-care therapy for pancreatic cancer patients until 20 years later a pivotal phase III study proved gemcitabine to be a more effective treatment of PDAC with lower toxicity compared to 5-FU alone (5.7 versus 4.4 months of prolonged overall median survival) with a significantly higher 5-year survival rate of 18% compared to 2% for those treated with 5-FU [34, 35]. So far, the benefit of a combination of chemotherapy and irradiation therapy remains controversial, as randomized controlled studies failed to show increased survival of patients [36]. Neoadjuvant therapy aims at the elimination of metastatic cancer cells and the reduction of the tumor mass prior surgery and is

usually given to patients with borderline resectable tumors where tumors have already spread to surrounding tissue in order to improve primary treatments. Nevertheless, the benefit of neoadjuvant treatment remains elusive, since it comes at the cost of delaying surgery and clinical studies showed limited response rates. To date, no clinical phase III trials exist to directly compare outcomes of adjuvant and neoadjuvant therapy [34, 36].

The need to identify and develop more efficient treatment options has led researchers to focus on cancer immunotherapy, aiming at targeting the immune network within PDAC microenvironment and stimulating the host immune cells to recognize and eliminate tumor cells. During tumorigenesis, tumor cells start expressing specific tumor-associated antigens (TAA) also known as neoantigens that fundamentally differ from normal cellular antigens and can be recognized by the immune system [37]. In a process called immunoediting, tumor cells are usually eliminated by immune cells, however tumors develop escape and tolerance mechanisms by up-regulation of inhibitory molecules such as PDL1, IDO, IL-10 and TGF-β, therefore creating an immunosuppressive tumor microenvironment [37]. Our understanding of these immune-inhibitory pathways has led to the development of immune-based strategies that target and block immune checkpoint markers such as PD1, PDL1 or CTLA-4 to promote anti-tumor T cell responses or activating molecules such as CD40 to activate T cells and revert pro-tumoral TAMs into anti-tumor M1 macrophages [38]. Unfortunately, outcomes of clinical trials testing PDL1 or CTLA-4 inhibitors in patients with locally advanced or metastatic pancreatic cancer were disappointing, despite showing promising clinical activities in melanoma and other malignancies [38]. Poor clinical outcomes of studies with single agent therapies emphasize the need for combination therapies that focus on multiple immune cells and checkpoint markers to treat tumors of patients who do not respond to single agent therapies.

1.1.4 Therapy resistance of PDAC

One of the biggest challenges and a major reason for limited therapeutic efficacy in PDAC is its resistance to treatment (Fig. 5). Over the past decades, several molecular resistance mechanisms have been unravelled, but are still not well understood. Pancreatic cancer is intrinsically highly chemoresistant due to dense desmoplastic stroma, a unique feature of PDAC. Excessive desmoplastic reactions as well as the hypoxic tumor microenvironment negatively affect drug penetration and pancreatic stroma cells act as physical barrier to delivery of chemotherapeutic agents [39]. In contrast to intrinsic resistance mechanisms, acquired resistance mechanisms may take months to develop and include genetic and epigenetic alterations such as mutations in the proto-oncogene *kras*

or *brca2* and aberrant expression of genes associated with cellular survival and apoptosis like *survivin*, *plk1* and *snail* have been implicated in resistance to gemcitabine treatment [39, 40].
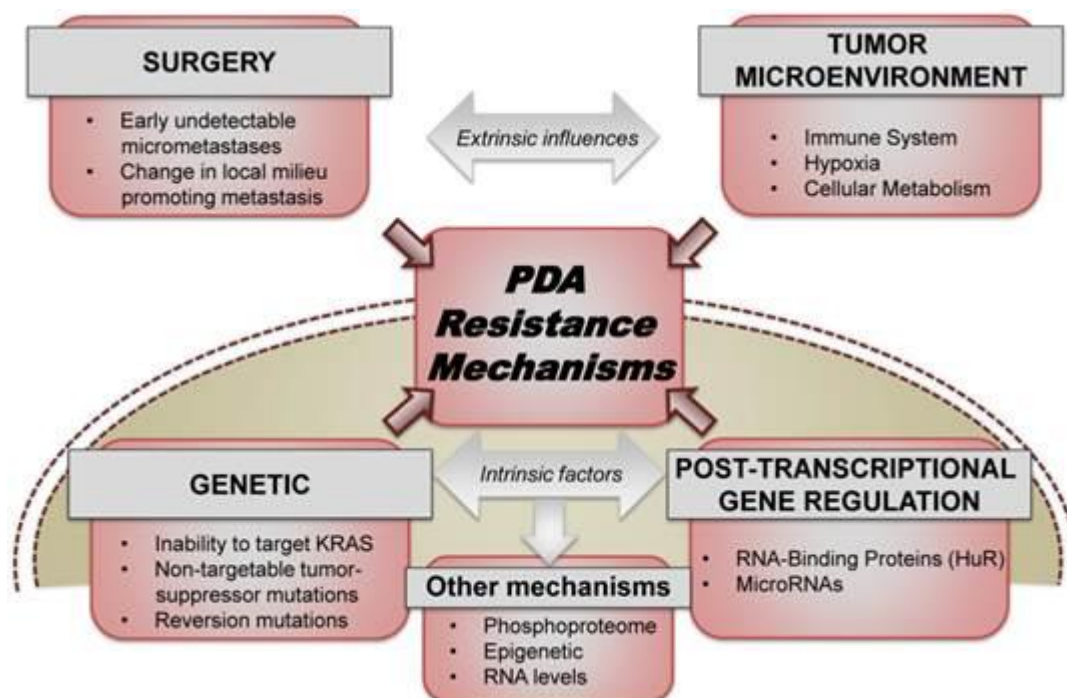
Figure 5: Resistance mechanisms in PDAC.
Extrinsic factors such as the tumor microenvironment or the role of surgery as well as intrinsic factors, including genetic mutations or dysregulation of signalling pathways, significantly contribute to acute or acquired resistance to chemotherapeutical agents or immune-modulatory molecules in treatment of PDAC (from Chand and al. [40]).

Additionally, dysregulation of key signalling pathways including nuclear factor κB (NF-κB), Akt and Notch pathways as well as downstream transcription factors like survivin, B cell lymphoma-extra large (Bcl-xL) and c-inhibitor of apoptosis protein (c-IAP) have been associated with reduced efficacy of gemcitabine and studies showed that down-regulation of these signalling pathways lead to chemo sensitization of PDAC to conventional drug therapies [39]. Immune cells have also been shown to contribute to chemoresistance in PDAC, however molecular mechanisms remain elusive and still need to be explored in more detail. Ireland and colleagues observed that TAMs and myofibroblasts can directly be associated with gemcitabine resistance by production and secretion of insulin-like growth factors (IGF) 1 and 2 [41]. IGF 1 and 2 activate insulin/IGF receptors, which were expressed on 72% of tumor samples tested from pancreatic cancer patients. Activated insulin/IGF receptors correlated with increased TAM infiltration in tumors and reduced efficacy of gemcitabine treatment [41]. Understanding the complex interactions between intrinsic and acquired molecular and cellular

resistance mechanisms, and investigating potential targets to overcome drug resistance will hopefully lead to increased treatment efficacy by sensitizing PDAC to chemotherapy in future.

1.1.5 Preclinical pancreatic cancer models – Established human cell lines

Precise, standardized and reliable preclinical models are needed as a tool to understand the biology of pancreatic cancer and to design biology-based therapeutic approaches that are more effective than standard-of-care therapies such as gemcitabine. To date, more than 20 human pancreatic cancer cells have been characterized und are commonly used as a starting point to investigate specific cellular and molecular mechanisms of PDAC development and to design proof-of-concept studies. Cell lines are homogenous and can simply be maintained in culture using fetal calf serum (FCS) and a defined medium condition, which facilitates the performance of functional assays as well as high-throughput screening with chemical compounds. Using transient or stable RNA interference (RNAi), cells can easily be genetically manipulated *ex vivo* to identify new potential therapeutic targets [42, 43]. PDAC cell lines also harbour several distinct mutations with corresponding transcription profiles and therefore can be used to develop prognostic biomarkers for patient groups based on gene expression profiling. Despite the advantages of using established human cell lines, they clearly do not represent the complex *in vivo* situation of the human disease [43]. In conventional 2 dimensional (2D) monolayer cultures, cells lack the structural organization and multifaceted tumor microenvironment, which is a hallmark of pancreatic cancer. During long-term culturing, phenotypic and genotypic changes may also occur in morphology and development, leading to genetic drift and a loss of tumor heterogeneity [42]. Numerous discoveries have been made using pancreatic cancer cell lines in 2D *in vitro* cell culture such as EMT signalling and chromatin remodelling, nevertheless, additional approaches are needed to potentially reflect and investigate pancreatic cancer biology and therapy [43]. Among *in vitro* cell culture models, various animal models have been used to mimic human disease, hereby establishing tumors in rodent models by implanting tumor cells or generating genetically engineered animals that spontaneously develop human-like tumors [43]. Nevertheless, these models often fail to translate into therapeutic options. To better exploit the chance of successful discovery and development of therapeutic agents, cell-based systems that close the gap between 2D *in vitro* experiments and *in vivo* animal models are needed [44]. Thus, researchers strongly focus on the establishment of 3D *in vitro* systems by customizing tumor microenvironments using primary cells or cell lines which mimic *in vivo* cell behaviour more realistically and are able to provide more predictable results.

1.2 The 3D cell culture model

In the preclinical phase, fast and cost-effective *in vitro* cell culture systems typically precede large scale cost-intensive animal testing and for years, research routinely relied on 2D cell culture monolayers as initial model system to evaluate proof-of-concept studies, drug efficacy and safety of potential therapeutic molecules. However, 2D cell culture models poorly represent the 3D architecture of tissues and tumors and lack physiologically relevant information such as cell-cell interaction and communication [45]. As a consequence, 3D cell culture systems have gained importance in drug discovery and screening due to the reflection of a more realistic *in vivo* situation. They represent a simplified model of *in vivo* organisms and are able to mirror the heterogeneity of cells and their behaviour in a more physiological environment, hereby overcoming spatial limitations set by 2D cell culture systems (Fig. 6) [45].
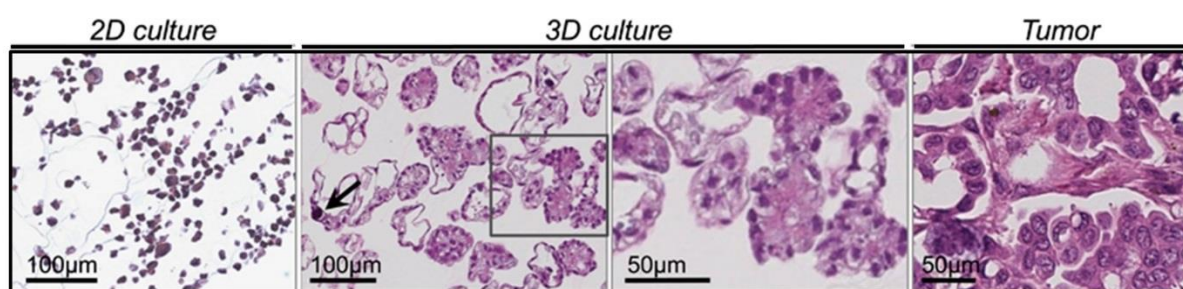
Figure 6: OAW42 epithelia ovarian cancer cells grown in 2D and 3D culture.
OAW42 cultured in 3D represent architectural and histological features that closely resemble a well-differentiated serous ovarian tumor shown on the far right (from Lee et al. [46]).

1.2.1 Characteristics of 3D cell culture compared to 2D cell culture models

As 2D cell culture systems do not consider surrounding tissues and ECM, they often provide misleading data for *in vivo* responses which can lead to failure due to lack of efficacy or unacceptable toxicity. Cells cultured in 2D strongly differ from 3D with regard to morphology, differentiation and gene expression. While 2D monolayers are typically cultured on tissue culture polystyrene flasks, there are several ways to generate 3D cell aggregates or spheroids, using a variety of scaffold systems, synthetic-based materials or even scaffold-free in suspension medium [47]. Regardless of the method, 3D cell culturing provides a more natural environment, allowing cells to interact and communicate with each other and influencing cellular functions such as proliferation, differentiation and responses to external stimuli. In 2D models, cells seeded as monolayer can be equally supplied by homogeneous amounts of nutrients and growth factors from the medium. Viable cells proliferate

and remain attached to the flask bottom, stretching out more flatly than they would in their physiological environment, whereas necrotic cells usually detach and are removed with medium change [44]. In contrast to 2D monolayer culture, 3D cells form aggregates and spheroids within a matrix or in suspension. Close cell-cell contact leads to bi-directional cell communication and interaction, so that 3D cells strongly resemble their *in vivo* counterparts in shape and morphology.
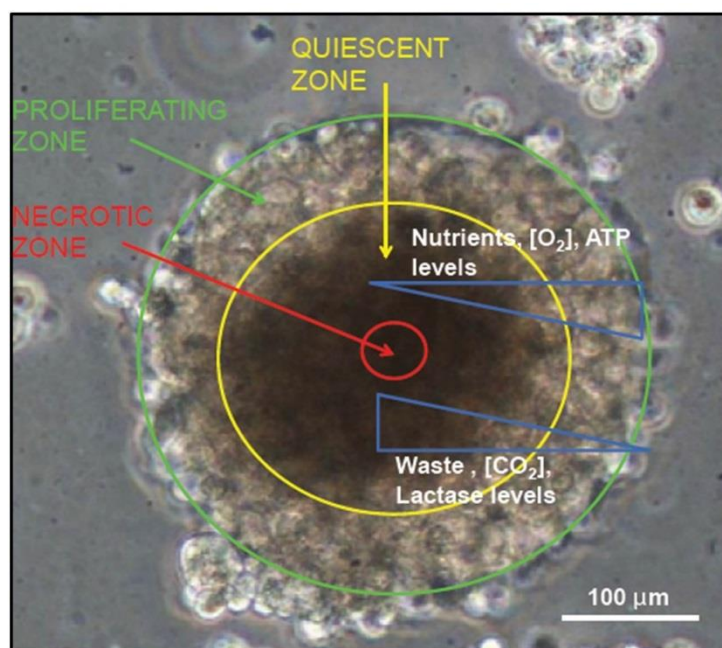
Figure 7: Schematic diagram of a tumor spheroid.
Different zones and the pathophysiologic gradient within a 3D spheroid (from Chandrasekaran and King [48]).

Cells in different stages including proliferating, quiescent, apoptotic, hypoxic or necrotic cells can be found within 3D cell aggregates and spheroids [49]. This heterogeneity of cells closely reflects *in vivo* tissues and cellular processes, particularly in tumors. The outer rim of a spheroid typically consists of proliferating cells, since the medium can provide an optimal supply of nutrients and growth factors, while the inner core receives less oxygen and nutrients, forcing cells into a quiescent or hypoxic state and often leading to necrotic cores (Fig. 7) [44]. The structure and morphological appearance of 3D spheroids are cell line dependent and vary from tight round shapes to grape-like loose cell aggregations with poor cell adhesion. Studies found that cellular morphology does not correlate with migratory or proliferative capacity of cell lines, but rather depends on the 3D culture method that is being used [50]. Although, 3D culture models more closely resemble the *in vivo* situation than 2D monolayers, they still lack the complex extracellular matrix structure as well as a vascular system that supports tissues *in vivo* with oxygen, nutrients and enables waste removal, which presents a

challenge particularly for large 3D spheroids, since nutrients and oxygen can only be exchanged by a diffusion gradient (Fig. 7) [48].

Different cellular behaviour of cells in 2D and 3D culture can be attributed to differential gene expression patterns that influence proliferation, migration, morphology and drug sensitivity. Tumor cells that are removed from their original tissue and cultured *in vitro* quickly lose their native characteristics and adapt to 2D culturing conditions, commonly up-regulating genes that induce morphological changes and promote rapid growth and proliferation [51]. However, original characteristics can be restored to a certain extent when placing cells back into an *in vivo* environment such as an animal model, emphasizing the importance of mimicking the *in vivo* situation *in vitro* by using 3D cell culture systems to maintain transcriptional and translational functions [51]. A number of studies also found that 2D monolayers are considerably more sensitive to chemotherapeutic compounds than 3D spheroids. Loessner and colleagues showed that the viability of ovarian cancer cells was reduced by 80% when cultured in 2D and treated with paclitaxel compared to 40% - 60% in 3D culture models [52]. Differences in the response to chemotherapeutic drugs are most likely due to several combined factors. As cells in 2D systems grow as monolayers, drugs in the growth medium can be effectively distributed to all cells, whereas it is hard to penetrate large compact 3D spheroids. Furthermore, drugs show different effects on each cell within 3D spheroids due to the diverse differentiation stages of cells, which eventually reduces overall drug efficacy compared to 2D monolayers [44]. These studies highlight the significant role of *in vitro* 3D culture as an essential tool in drug discovery and development.

1.2.2 Methods to generate multicellular spheroids

In order to implement spheroid models for improved drug development and predictability of cell-based drug screening systems, it is essential to choose the appropriate 3D method depending on the utilized cell types and scaffold materials. Currently, a wide variety of techniques exist to generate 3D multicellular spheroids either as mono- or as co-cultures (Fig. 8). These techniques can be grouped into scaffold-free and scaffold-based methods.
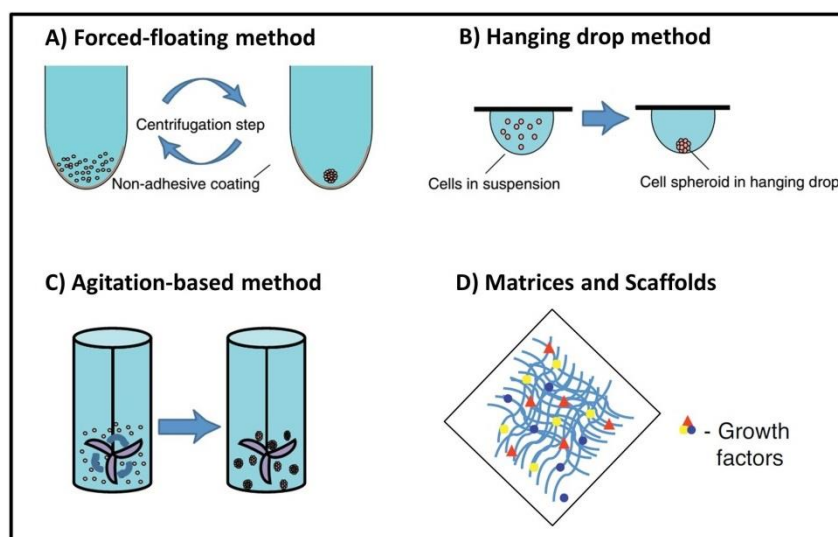
Figure 8: Most commonly used methods to generate multicellular 3D spheroids.
A) forced-floating of cells, B) hanging drop method, C) agitation-based approaches and D) the use of scaffold-based models (adapted from Breslin and O´Driscoll [53]).

A relatively simple method to create 3D spheroids is the scaffold-free liquid overlay, also known as forced-floating method (Fig. 8 A). Cells are seeded onto non-adhesive surfaces such as positively charged surfaces or surfaces coated with thin Agarose films or albumin, which prevent cell attachment and leading to cell-cell aggregation and spheroid formation [53]. This method is suitable for high-throughput testing as it is inexpensive and spheroids are easily accessible for further analyses. Using the forced-floating technique, Ivascu and Kubbies have developed a high-throughput method using poly-2-hydroxyethylmethacrylate (poly-Hema), which is coated on 96 well u-bottom plates for three days before addition of cells. To obtain spheroids similar in size and morphology, fixed cell numbers are seeded per well into poly-Hema coated 96 well plates and then centrifuged to facilitate spheroid formation [54]. The drawback of this method is the labour-intensive plate-coating that comes along particularly with high-throughput approaches. Another option to generate spheroids in a scaffold-free manner is the hanging drop method (Fig. 8 B). Here, only small amounts of cell suspension up to 50 µl are used and pipetted into wells of a 60 or 96 micro well tray. Similar to the forced-floating method, spheroid size can be altered depending on the number of cells seeded. Once cells are seeded, the tray is subsequently inverted, turning aliquots of cell suspension into hanging drops that are kept in place due to surface tension [55]. Cells accumulate at the tip of the drop and form tight spheroids that are being kept in bioassay dishes to maintain moisture levels. Since specialized plates are needed, this method is more expensive and difficult in handling than the forced-floating method and the small culture volume complicates medium exchange without disturbing the cells [53]. Agitation-based approaches such as the spinner flasks and gyrators also prevent cell adhesion by keeping cells in motion using rotator systems (Fig. 8 C) [49]. It can be used

for large-scale spheroid production, however spheroid size cannot be controlled and cells may be damaged due to shear forces in the spinner [53]. Advantages of scaffold-free models are the complete native cellular organization through migration and cell-cell interactions. The absence of scaffolds also facilitates experiment analysis and read-outs such as imaging, since there is less interference with optical assessments or absorption by scaffold materials. Nevertheless, scaffold-based methods are necessary to support certain survival of cell lines and to provide the possibility of adding a natural source of growth factors, hormones and other molecules depending on the scaffold material that is being used (Fig. 8 D). A variety of scaffolds and matrices are currently available and choosing the appropriate one depends on the cell type used and the aim of the study. The most commonly used scaffolds are natural and bio-degradable substances such as collagen, laminin or fibronectin which are processed to form hydrogels that mimic the native extracellular matrix and provide physical and structural support [47]. As these hydrogels are derived from natural sources, they promote numerous cellular functions such as cell viability, proliferation and differentiation. Scaffold hydrogels can be manipulated to suit experimental requirements, including changes of pore size and stiffness, thus allowing nutrients, oxygen and drugs to reach cells within the scaffold [53]. Even though scaffold-based models provide an optimal physiological environment, potential drawbacks of using natural scaffold materials are the varying composition between batches, a cost-intensive large-scale production as well as difficulties retrieving cells from matrices for further analyses [53].

1.2.3 Applications of 3D culture models

While traditional 2D cell culture has helped unravel complex cellular physiology, 3D culture models are able to go one step closer to the *in vivo* situation, slowly decreasing the gap between *in vitro* cell culture and *in vivo* animal models. So far, 3D culture models have been applied in a wide variety of studies, including applications in cancer research, differentiation studies, cell cytoskeleton and motility studies, gene and protein expression as well as in drug discovery. 3D models have become prominent especially in cancer research, where they are used to mimic the complex *in vivo* tumor microenvironment [47]. 3D spheroids typically consist of three different layers, which comprise the outer proliferating rim, the inner quiescent circle and the necrotic centre similar to *in vivo* tumors (Fig. 7) [44]. These features enable researchers to better understand cancer biology, particularly signalling pathways, expression and interaction with the ECM and studies on biomarkers that can be used for diagnostic purposes or as potential drug targets [47]. Further insights into the complex

physiology of tumors and behaviour of cells can be gained by using 3D models to establish heterogeneous co-cultures. This is essential especially for tumors which strongly rely on stromal cells with regard to tumor growth and progression such as pancreatic cancer. Studies have already shown that tumor cells co-cultured with fibroblasts in a 3D model show increased proliferation rates as well as increased resistance to therapeutic agents [56, 57]. Research on drug resistance strongly advanced with the help of 3D culture systems as they effectively present an authentic *in vitro* model to mirror tumor tissues, thus improving drug screening and identification of toxic chemotherapeutic substances. Moreover, 3D models reduce the ethically controversial usage of animal testing for drug screening and lower the cost of drug discovery by providing more predictive data before molecules reach clinical phases [47].

1.2.4 Limitations of 3D culture models

Despite offering an easy and improved possibility to reflect *in vivo* situations better than 2D monolayers, 3D culture models have several disadvantages and limitations that still remain unresolved. Depending on the aim of the study, it is essential to choose and establish the appropriate 3D culture model. Optimization of a 3D culture model can be a lengthy and complex process, since spheroid size, cell number, cell culture duration or drug concentrations need to be determined [58]. Some models such as the agitation-based approaches may also produce spheroids in different sizes and shapes, making it difficult to compare experimental outcomes. When using biologically derived scaffolds or matrices, the variability between batches may also lead to limited reproducibility of experimental results [44]. Even though, 3D models represent an improved *in vitro* model to mimic *in vivo* tumors, they are still simplified and lack a vascular system, which plays a pivotal role in drug delivery and tumor growth [59]. Spheroids grown in scaffolds are difficult to extract for analysis and the quality of images strongly depend on the scaffold size, material and on the microscope [58]. Once spheroids have been extracted from scaffolds or collected from scaffold-free systems, the production of a single cell suspension still remains a rough procedure, easily damaging cells and thus decreasing cell viability. Properties such as reproducibility, experimental consistency and lack of appropriate analytical tools need to be addressed and improved in long-term experiments to enable usage as a routine tool for *in vitro* studies [58].

1.3 Scientific objective

Pancreatic cancer has a high unmet medical need and patients still poorly respond to standard-of-care therapy. Hallmarks of this disease include a strong desmoplastic stromal reaction as well as a diverse inflammatory tumor microenvironment. Increased infiltrations of immune cells, particularly TAMs, have been shown to play an important role in tumor growth and resistance to therapy. However, novel *in vitro* models to investigate the interaction between different cell types within the tumor microenvironment need to be developed and optimized in order to gain more physiologically relevant information.

This thesis aims to establish a 3D co-culture model with pancreatic cancer cell lines, fibroblasts and monocytes to study the influence of direct cell-cell contact on monocyte differentiation and functionality.

In this study, the following aspects have been addressed:

    I.   Establishment of a viable 3D pancreatic cancer cell, fibroblast and monocyte co-culture model

    II.   Phenotypic characterization of the monocytes that survive and differentiate in the 3D tumor cell/fibroblast co-culture in terms of cell surface marker and cytokine expression

    III.   Functional characterization of the spheroid differentiated monocytes with regards on tumor cell survival, T cell activation and proliferation

    IV.   Investigating the influence of the immune cells on the development of resistance to therapeutic agents

This study provides critical insight into the role of the inflammatory tumor microenvironment of pancreatic cancer and its interaction with desmoplastic fibroblasts in cancer progression and therapy. The established 3D model contributes to better understand cell-cell communication between tumor cells, fibroblasts and monocytes, which may lead to the identification of potential targets and key mechanisms operating in this lethal malignancy.

2. Material

2.1 Equipment

Equipment	Trade name	Supplier
Autotechnikon	ASP6025	Leica Microsystems, GER, Wetzlar
Cell counter	Cellometer Auto T4	Nexcelom Bioscience, USA, Lawrence
Centrifuge	Heraeus Megafuge 3.0R	Heraeus, GER, Hanau
Centrifuge	Heraeus Megafuge 40R	Thermo Fisher Scientific, USA, Waltham
Centrifuge, small	Mini Star	VWR, GER, Ismaning
Confocal microscope	Nikon Eclipse Ti	Nikon Instruments Inc., USA, New York
Cooling plate	TES 99	Medite, GER, Burgdorf
Flow cytometer	FACS Canto II	BD Diagnostics, USA, Franklin Lakes
Flow cytometer	FACS LSR II	BD Diagnostics, USA, Franklin Lakes
Flow Hood Class 2	HeraSafe KS	Thermo Fisher Scientific, USA, Waltham
fridge and freezer	-	Liebherr, CHE, Bulle
Immunohistochemistry staining system	Benchmark XT	Ventana Medical Systems Inc., USA, Tucson
Incubator	Heraeus	Thermo Fisher Scientific, USA, Waltham
Inverted light microscope	DMIL LED	Leica Microsystems, GER, Wetzlar
Light sheet microscope	UltraMicroscope II	LaVision BioTec, GER, Bielefeld
Light microscope	Axiovert 25	Zeiss, GER, Oberkochen
Magnetic stirrer	RH basic	IKA, GER, Staufen
Magnetic system for cell isolation	EasySepTM "The Big Easy"	STEMCELL^{TM} Technologies, CAN, Vancouver

Magnetic system for cell isolation	EasySepTM Magnet	STEMCELL^{TM} Technologies, CAN, Vancouver
Magnet system for cell isolation, Starter Kit	130 091 051	Miltenyi Biotec, GER, Bergisch Gladbach
Microcentrifuge	5415 R	Eppendorf, GER, Hamburg
Microplate reader	BioTek Synergy 2	WESSAMAT, GER, Kaiserslautern
Microtome	Microm HM 3555	Thermo Fisher Scientific, USA, Waltham
Multiplex array reader	Bio-Plex 200 System	BioRad Laboratories, USA, Hercules
Multiwell pipet (8-well/12-well)	Multipipette Plus	Eppendorf, GER, Hamburg
Paraffin Embedding station	Tissue-Tek	Sakura, GER, Staufen
Pipetboy	-	Integra Biosciences, GER, Biebertal
Plate shaker	Titramax 101	Heidolph, GER, Schwabach
Plate washer	Bio-Plex Pro2	BioRad Laboratories, USA, Hercules
Pump	Vacusafe	Integra Biosciences, GER, Biebertal
Rotator	Hula Mixer	Thermo Fisher Scientific, USA, Waltham
Scale	-	Sartorius AG, GER, Göttingen
Tissue homogenizer	Medimachine	BD Biosciences, GER, Heidelberg
Vortexer	Vortex Genie	VWR, GER, Ismaning
Water bath	Julabo	Julabo, GER, Seelbach

2.2 Consumable supplies

Name	Reference number	Supplier
μ-tissue slides angiogenesis	81501	ibidi GmbH, GER, Martinsried
BD Vacutainer	367525	BD Diagnostics, GER, Heidelberg

Cell counting chambers	CHT4-PD100-002	Nexcelom Bioscience, USA, Lawrence
Cell culture flask, T300	90301	TPP, CHE, Trasadingen
Cell culture flask, T175	353112	Corning, GER, Kaiserlautern
Cell culture flask, T75	353136	Corning, GER, Kaiserlautern
Cell culture plates, 6 well flat bottom, clear	3516	Corning, GER, Kaiserlautern
Cell culture plates, 96 well flat bottom microplates, black	655209	greiner bio one
Cell culture plates, 96 well u bottom, clear	3799	Corning, GER, Kaiserlautern
Cell strainer, 70µm	352350	Corning, GER, Kaiserlautern
Disposable bags	759705	Brand, GER, Wertheim
FACS tubes, 5ml round bottom	352054	Corning, GER, Kaiserlautern
Falcon tubes, 15ml	188261	greiner bio one, AUT, Kremsmünster
Falcon tubes, 50ml	227261	greiner bio one, AUT, Kremsmünster
Histology cassettes	1000957	Thermo Fisher Scientific, USA, Waltham
Lymphocyte separating columns	P04-60125	Pan^{TM}Biotech, GER, Aidenbach
Microscope SuperFrost tissue slides	1014356190	Thermo Fisher Scientific, USA, Waltham
Nitrile gloves	97612	Kimberly-Clark, USA, Roswell
Pipette tips, 10 µl	0030073 401	Eppendorf, GER, Hamburg
Pipette tips, 1000 µl	0030073 460	Eppendorf, GER, Hamburg
Pipette tips, 200 µl	0030073 428	Eppendorf, GER, Hamburg
Reagent reservoir, 100ml	95128085	Thermo Fisher Scientific, USA, Waltham
Reagent reservoir, 25ml	95128095	Thermo Fisher Scientific, USA, Waltham
Safe-lock tubes, 1.5ml	30120086	Eppendorf, GER, Hamburg
Safe-lock tubes, 2ml	30120094	Eppendorf, GER, Hamburg

Serological pipettes, 10ml	607180	greiner bio one, AUT, Kremsmünster
Serological pipettes, 25ml	760180	greiner bio one, AUT, Kremsmünster
Serological pipettes, 50ml	768180	greiner bio one, AUT, Kremsmünster
Serological pipettes, 5ml	606180	greiner bio one, AUT, Kremsmünster
Stericup filtration system, 500ml	SCGPU05RE	Merck, GER, Darmstadt
Storage bottle, 500ml	8393	Corning, GER, Kaiserlautern
Tubes, 14ml round bottom	352057	Corning, GER, Kaiserlautern

2.3 Chemicals and reagents

Name	Reference number	Supplier
1400W dihydrochloride	1415	Tocris Bioscience, GB, Bristol
5-Flurouracil	F6627	Sigma-Aldrich, USA, St. Louis
Agarose	11388991001	Roche Diagnostics GmbH, GER, Mannheim
Benzyl alcohol	1 09626 1000	Sigma-Aldrich, USA, St. Louis
Benzyl benzoate	B6630-250ML	Sigma-Aldrich, USA, St. Louis
CD3/CD28 Dynabeads	11131D	Thermo Fisher Scientific, USA, Waltham
Cell Titer Glo Luminescence assay	G7571	Promega, GER, Mannheim
CFSE	C34554	Thermo Fisher Scientific, USA, Waltham
DAPI	10236276001	Roche Diagnostics GmbH, GER, Mannheim
DMSO	P60-36720100	Pan™Biotech, GER, Aidenbach
Doxorubicin hydrochloride	D1515-10MG	Sigma-Aldrich, USA, St. Louis
EDTA	15575-038	Thermo Fisher Scientific, USA, Waltham
Ethanol	MC1009836010	Merck, GER, Darmstadt
Formaldehyde 37%	1040031000	Merck, GER, Darmstadt

Human CD40 ligand	130-096-714	Miltenyi Biotec, GER, Bergisch Gladbach
LPS	2204	Novus Biologicals, USA, Littleton
N-hydroxy-nor-L-arginine	399275-5MG	Merck, GER, Darmstadt
Poly-Hema	18894	PolySciences, GER, Hirschberg an der Bergstraße
Qtracker 525	Q25041MP	Thermo Fisher Scientific, USA, Waltham
Qtracker 585	Q25011MP	Thermo Fisher Scientific, USA, Waltham
RNAase ZAP	R2020	Sigma-Aldrich, USA, St. Louis
TL8-506	tlrl-tl8506	Invivogen, USA, San Diego
Triton X100	10789704001	Roche Diagnostics GmbH, GER, Mannheim
TrypanBlue	93595	Sigma-Aldrich, USA, St. Louis
Tween 20	655205	Merck, GER, Darmstadt
Water, sterile, pyrogenfree, hypotonic	32551	ROTH, GER, Karlsruhe

2.4 Ready-for-use Kits

Name	Reference number	Supplier
Human cytokine/chemokine multiplex kit	HCYTOMAG-60K	Merck, GER, Darmstadt
CD11b Microbeads, human	130 049 601	Miltenyi Biotec, GER, Bergisch Gladbach
ChromoMAP DAB kit	766 159	Ventana Medical Systems Inc., USA, Tucson
Human GM-CSF Quantikine ELISA kit	SGM00	R&D Systems, USA, Minneapolis
Human M-CSF Quantikine ELISA kit	SMC00B	R&D Systems, USA, Minneapolis
Human monocyte isolation kit	19359	STEMCELL^{TM} Technologies, CAN, Vancouver
Human T cell isolation kit	17951	STEMCELL^{TM} Technologies, CAN, Vancouver
PicoPure RNA Isolation Kit	12204-01	Thermo Fisher Scientific, USA, Waltham

2.5 Enzymes and Cytokines

Enzymes	Reference number	Supplier
Collagenase D	11088882001	Roche Diagnostics GmbH, GER, Mannheim
Dispase II	4942078001	Roche Diagnostics GmbH, GER, Mannheim
Dnase I	11284932001	Roche Diagnostics GmbH, GER, Mannheim
Hyaluronidase	H-4272	Sigma-Aldrich, USA, St. Louis

Cytokines	Reference number	Supplier
GM-CSF, human recombinant	572905	Biolegend, USA, San Diego
IFN-γ, human recombinant	570206	Biolegend, USA, San Diego
IL-10, human recombinant	571008	Biolegend, USA, San Diego
IL-6, human recombinant	570806	Biolegend, USA, San Diego
M-CSF, human recombinant	716602	Biolegend, USA, San Diego

2.6 Antibodies

Myeloid cell panel, human	Label	Clone	Isotype	Reference number	Supplier
CD163	PE	MAC-2-48	mouse IgG1	CD163-48P	Trillium Diagnostics LLC, USA, Bangor
CD14	APC Cy7	M5E2	mouse IgG2a	301820	Biolegend, USA, San Diego
CD33	PerCP Cy5.5	WM53	mouse IgG1	303414	Biolegend, USA, San Diego
CD206	APC	19.2	mouse IgG1	550889	BD Pharmingen, GER, Heidelberg
HLA-DR	APC	L243	mouse IgG2	347403	BD Pharmingen, GER, Heidelberg
CD80	FITC	L304.4	mouse IgG1	557226	BD Pharmingen, GER, Heidelberg
CD86	PE	2331	mouse IgG1	555658	BD Pharmingen, GER, Heidelberg
CD16	PE	3G8	mouse IgG1	555407	BD Pharmingen, GER, Heidelberg
CD40	FITC	5C3	mouse IgG1	334306	Biolegend, USA, San Diego
CD11b	PE Cy7	ICRF44	mouse IgG1	301322	Biolegend, USA, San Diego

PD-L1	APC	29E.2A3	mouse IgG2b	329708	Biolegend, USA, San Diego
ARG-1 , intracellular	APC	-	sheep IgG	IC5868A	R&D Systems, USA, Minneapolis

T cell panel, human	Label	Clone	Isotype	Reference number	Supplier
CD122	PE	Mik-β2	mouse IgG2a	554522	BD Pharmingen, GER, Heidelberg
CTLA-4 (CD152)	BV421	BNI3	mouse IgG2a	562743	BD Horizon, GER, Heidelberg
4-1BB (CD137)	APC	4B4-1	mouse IgG1	561702	BD Pharmingen, GER, Heidelberg
CD25	APC	M-A251	mouse IgG1	555434	Biolegend, USA, San Diego
CD25	PE Cy7	M-A251	mouse IG1	557741	BD Pharmingen, GER, Heidelberg
PD1 (CD279)	BV510	EH12.1	mouse IgG1	563076	BD Horizon, GER, Heidelberg
CD8	PerCP Cy5.5	SK1	mouse IgG1	565310	BD Pharmingen, GER, Heidelberg
CD8	PE	HIT8a	mouse IgG1	555635	BD Biosciences, GER, Heidelberg
CD4	APC	SK3	mouse IgG1	345771	BD Biosciences, GER, Heidelberg
CD4	FITC	SK3	mouse IgG1	345768	BD Biosciences, GER, Heidelberg
CD69	BV510	FN50	mouse IgG1	310936	Biolegend, USA, San Diego
Ox40 (CD134)	PE	L106	mouse IgG1	340420	BD Biosciences, GER, Heidelberg
CD45RO	BV421	UCHL1	mouse IgG2a	562641	Biolegend, USA, San Diego
Fixable Viability Stain 780	-	-	-	565388	BD Horizon, GER, Heidelberg

Isotype control	Clone	Isotype	Reference number	Supplier
APC Cy7	MOPC-173	mouse IgG2a	400230	Biolegend, USA, San Diego
APC	MOPC-21	mouse IgG1	555751	BD Biosciences, GER, Heidelberg
APC	G155-178	mouse IgG2a	555576	BD Biosciences, GER, Heidelberg
APC	11711	mouse IgG1	IC002A	R&D Systems, USA,

				Minneapolis
APC	polyclonal	sheep IgG	IC016A	R&D Systems, USA, Minneapolis
BV421	G155-178	mouse IgG2a	562439	BD Biosciences, GER, Heidelberg
BV510	MOPC-21	mouse IgG1	400172	Biolegend, USA, San Diego
BV510	X40	mouse IgG1	562946	BD Biosciences, GER, Heidelberg
FITC	MOPC-21	mouse IgG1	555748	BD Biosciences, GER, Heidelberg
FITC	MOPC-21	mouse IgG1	400108	Biolegend, USA, San Diego
PE	G155-178	mouse IgG2a	555574	BD Biosciences, GER, Heidelberg
PE	MOPC-21	mouse IgG1	554680	BD Biosciences, GER, Heidelberg
PE Cy7	MOPC-21	mouse IgG1	400126	Biolegend, USA, San Diego
PerCP Cy5.5	MOPC-21	mouse IgG1	400150	Biolegend, USA, San Diego

2.7 Media and supplements

Name	Reference number	Supplier
DMEM	P04-03500	Pan^{TM}Biotech, GER, Aidenbach
Accutase	P10-21100	Pan^{TM}Biotech, GER, Aidenbach
Cell culture freezing medium	C6295	Sigma-Aldrich, USA, St. Louis
EGF, human recombinant	E3374-04H.100	biomol GmbH, GER, Hamburg
Fetal Calf Serum	P30-3702	Pan^{TM}Biotech, GER, Aidenbach
HAMS F12 with L-glutamine	P04-15500	Pan^{TM}Biotech, GER, Aidenbach
Horse Serum	26050-088	Thermo Fisher Scientific, USA, Waltham
Hydrocortisone	Cay18226-1	biomol GmbH, GER, Hamburg
Insulin, human recombinant	87402.1	biomol GmbH, GER, Hamburg
L-Glutamine	P04-80100	Pan^{TM}Biotech, GER, Aidenbach
MEM Eagle EBSS (EMEM)	P04-08050	Pan^{TM}Biotech, GER, Aidenbach
MEM NEAA	P08-32100	Pan^{TM}Biotech, GER, Aidenbach
Panexin (w/o hormones, insulin)	P04-957001	Pan^{TM}Biotech, GER, Aidenbach
PBS	P04-36500	Pan^{TM}Biotech, GER, Aidenbach
Penicillin/Streptomycin	P06-07100	Pan^{TM}Biotech, GER, Aidenbach
RPMI 1640	P04-17500	Pan^{TM}Biotech, GER, Aidenbach

Sodium pyruvate	11360-039	Thermo Fisher Scientific, USA, Waltham
Transferrin	10652202001	Roche Diagnostics GmbH, GER, Mannheim
β-Mercaptoethanol	31350010	Thermo Fisher Scientific, USA, Waltham

2.8 Eukaroytic cell lines

All tumor cell lines used in this work were derived from the in-house CELLO cell bank, which was established and characterized by Chugai Pharmaceutical Co., a member of the Roche Group.

<u>Pa-Tu 8902</u>

pancreas adenocarcinoma; established from primary ductal pancreatic adenocarcinoma (grade II) from a 44-year old woman

<u>BxPC3</u>

pancreas adenocarcinoma; established from the body of the pancreas of a 61-year old woman without metastasis

<u>HPAC</u>

pancreas adenocarcinoma; established from the head of the pancreas of a 64-year old woman with moderate to well differentiated pancreatic adenocarcinoma of ductal origin

<u>MiaPaCa-2</u>

Pancreas adenocarcinoma; established from the body and tails of the pancreas of a 65-year old man with periaortic metastasis

<u>MRC5</u>

fibroblasts; derived from normal lung tissue of a 14-week old male fetus

Pa-Tu 8902 was obtained from the Leibniz Institute DSMZ-German Collection of Microorganisms and Cell Cultures, Braunschweig, Germany. The other cell lines were obtained from the American Type Culture Collection (ATCC), Manassas, VA, USA.

2.9 Applied computer software

For the generation, analysis and visualization of data, the following computer software were used:

Software	Intended use
BD FACS Diva V8.01	BD flow cytometer Canto II and LSR II
Bio-Plex Manager V6.1	Multiplex Array reader
FlowJo V10.1	Flow cytometer analysis
Graphpad Prism V6.07	Evaluation and visualization of data
Imspector V4.0	Light sheet microscope
Leica Application Software V4.4	Inverted light microscope
Microplate Gen5 V2	Microplate reader
Microsoft Excel 2010	Data analysis
Microsoft Powerpoint 2010	Generation of graphics
NiS Elements V4.5	Confocal microscope

3. Methods

3.1 Cell culture

3.1.1 Culturing of cell lines

Pancreatic cancer cell lines and MRC5 fibroblasts were cultured in 35 ml of the appropriate medium at 37° C and 5 % CO_2 in the incubator. For splitting of cell cultures, medium was removed from the culturing flask, cells were washed once with 10ml PBS and 5ml Accutase per T175 flask was added to remove cells from the substrate. After 10 to 15 min, cells detached from the flask bottom, 30 ml medium was added und single cell suspension was transferred into new flasks with splitting ratios depending on the cell line or application. For all experiments, cells between passage 4 and 15 were used and medium was changed to serum free macrophage medium.

Pa-Tu 8902 and BxPC3 medium:

500 ml RPMI 1640

10 % FCS

2 mM L-glutamine

0.1 mM NEAA

1 mM Sodium pyruvate

5 ml Penicillin/Streptomycin

HPAC medium:

250 ml DMEM

250 ml HAMS F12

5 % FCS

0.002 mg/ml Insulin

0.005 mg/ml Transferrin

40 ng/ml Hydrocortisone

10 ng/ml EGF

5 ml Penicillin/Streptomycin

MiaPaCa-2 medium:

500 ml DMEM

10 % FCS

2.5 % Horse serum

2 mM L-glutamine

5 ml Penicillin/Streptomycin

MRC5 medium:

500 ml EMEM

10 % FCS

2 mM L-glutamine

0.1 mM NEAA

1 mM Sodium pyruvate

5 ml Penicillin/Streptomycin

3.1.2 Freezing, thawing and counting of cells

For cryopreservation of cells, single cell suspensions were pelleted by centrifugation (1000 rpm, 5 min, 4° C), re-suspended in cell freezing medium containing DMSO (Sigma-Aldrich) and up to 1×10^7 cells per ml were aliquoted into pre-cooled cryovials. The vials were then transferred into a pre-cooled Mr. Frosty and placed in a -80° C freezer. One day later, vials were transferred into a liquid nitrogen tank for long-term storage. To thaw cells, cryovials were retrieved from the liquid nitrogen tank and carefully placed into 37°C water bath. When half of the cell suspension has thawed, cells were transferred into pre-warmed medium and washed once with 10ml warm medium by centrifugation to remove DMSO. After washing, the pellet was resuspended in warm medium and the cell number was determined. An aliquot of the cell suspension was diluted 1:2 with 0.04 % trypan blue solution (Sigma-Aldrich) to quantify the viable number of cells. Cells were counted in Nexcelom cell counting chambers and the viable number of cells was determined using the following calculation:

Average cell number/chamber squares x dilution factor x 10^4

3.1.3 Monocyte isolation from whole blood

For this study, obtaining cells from whole blood of healthy donors was approved by the local ethics committee (Bayerische Landesärztekammer, Munich) and subjects gave written informed consent. Monocytes were isolated from whole blood by negative selection using the EasySep® Human Monocyte Isolation Kit (Stemcell™ Technologies) according to manufacturer´s instructions. Blood from healthy donors was collected and gently mixed 1:1 with isolation buffer (PBS + 2 % FCS + 1 mM EDTA). The mixed solution was transferred into Pancoll separation columns (Pan™ Biotech GmbH) and PBMCs were obtained by a density gradient and centrifugation (300xg, 20 min, RT without brakes). The plasma interface containing PBMCs was collected and washed 3 times with isolation buffer (300xg, 10 min, RT). PBMCs were counted and cell number was adjusted to 5×10^7/ml. The cell suspension was incubated with antibody isolation cocktail (50 µl/ml) and platelet removal cocktail (50 µl/ml) for 5 min followed by addition of magnetic beads (50 µl/ml). Negative selection of monocytes was then performed by removal of unwanted cells through magnetic separation of beads using EasySep magnets (Stemcell™ Technologies).

3.1.4 Macrophage and MDSC *in vitro* differentiation

For monocyte differentiation into activated M1 and M2c macrophages, 1.2×10^6 freshly isolated monocytes were seeded in 2 ml macrophage medium in a 6 well plate for 6 days in the presence of appropriate cytokines. For M1 macrophage polarization, monocytes were incubated with 100 ng/ml recombinant human GM-CSF (Biolegend) for 3 days and then activated with 10 ng/ml LPS (Novus Biologicals) and 50 ng/ml recombinant human IFN-γ (Biolegend) for 3 additional days. For M2c macrophage polarization, monocytes were incubated with 100 ng/ml recombinant human M-CSF (Biolegend) and 10 ng/ml recombinant human IL-10 (Biolegend). Myeloid-derived suppressor cells (MDSCs) were obtained by incubation of monocytes with 100 ng/ml recombinant human GM-CSF and 50 ng/ml recombinant human IL-6 (Biolegend). Phenotypical and functional characterization was assessed after 6 days. For generation of spheroid-polarized myeloid-derived macrophages (MDMs), 1×10^4 monocytes were added to co-culture spheroids per well on day 5 of spheroid formation. The co-cultures were incubated for 6 additional days without addition of polarizing cytokines.

Macrophage medium:

500 ml DMEM

5 % Panexin NTA

2 mM L-glutamine

0.1 mM NEAA

5 ml Penicillin/Streptomycin

3.1.5 T cell isolation from whole blood

CD3$^+$ T cells were isolated from whole blood by negative selection using the EasySep® Human T cell Isolation Kit (Stemcell™ Technologies) according to manufacturer´s instructions. Blood from healthy donors was collected and gently mixed 1:1 with isolation buffer. The mixed solution was transferred into Pancoll separation columns (Pan™ Biotech GmbH) and PBMCs were obtained by a density gradient and centrifugation (300xg, 20 min, RT without brakes). The plasma interface containing PBMCs was collected and washed 3 times with isolation buffer (300xg, 10 min, RT). PBMCs were counted and cell number was adjusted to 5×10^7/ml. The cell suspension was incubated with the antibody isolation cocktail (50 µl/ml) for 5 min followed by addition of magnetic beads (40 µl/ml).

Negative selection of T cells was then performed by removal of unwanted cells through magnetic separation of beads using EasySep magnets (Stemcell™ Technologies). For cultivation, T cell numbers were adjusted to $1x10^6$/ml, seeded in T cell medium in cell culture flasks and kept in incubator at 37° C and 5 % CO_2.

T cell medium:

500 ml RPMI 1640	0.1 mM β-Mercaptoethanol	0.1 mM NEAA
10 % FCS	5 ml Penicillin/Streptomycin	
2 mM L-glutamine	1 mM Sodium pyruvate	

3.1.6 Establishment of the 3D culture model

For 3D culture, 96 well u-bottom plates were coated with 100 µl and 6 well flat-bottom plates with 3 ml poly-2-hydroxyethyl methacrylate solution (poly-Hema) (Polysciences). To produce 100 ml poly-Hema solution, 90.8 ml of absolute ethanol were mixed with 5 ml autoclaved water and 4.2 ml poly-Hema stock solution. Plates were placed into an incubator, dried at 37° C for 5 days and then kept at a dry and dark place for storage.

Tumor cells and fibroblasts were detached from cell culture flask using Accutase and cell numbers were determined as described above. For all following 3D culture experiments, the cell culture medium was switched from the original cell line specific medium to the serum free macrophage medium mentioned before. In a poly-Hema coated 96 well u-bottom plate, 5000 tumor cells were seeded per well for mono-culture and 2000 tumor cells and 3000 MRC-5 fibroblasts per well for co-cultures in a final volume of 100 µl per well (Fig. 9).
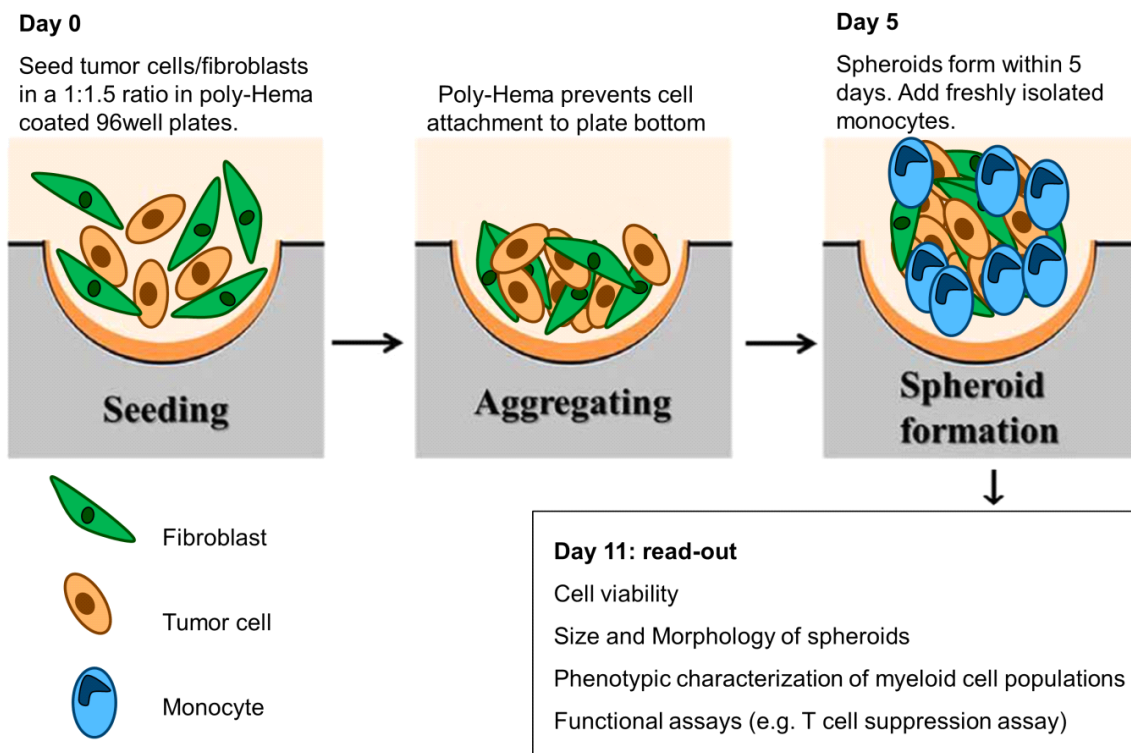
Figure 9: Experimental set-up of 3D co-cultures.
Briefly, 5000 tumor cells or 2000 tumor cells and 3000 MRC5 fibroblasts are seeded in a poly-Hema coated 96 well u-bottom plates in 100 µl medium. Plates are centrifuged to facilitate cell aggregation and within 5 days co-culture spheroids are formed. On day 5, freshly isolated monocytes are added and differentiated for 6 days until further analysis.

To facilitate cell aggregation, plates were centrifuged at 300xg for 5 min at RT. Monocultures and co-cultures were carefully placed in the incubator and cultured for 5 days at 37° C and 5 % CO_2 until spheroids were formed. In poly-Hema coated 6 well flat-bottom plates, 2.5×10^5 tumor cells were seeded per well as mono-culture and 1×10^5 tumor cells and 1.5×10^5 MRC-5 fibroblasts per well for co-cultures in a final volume of 2 ml medium per well. The 3D mono and co-culture models were extended by the inclusion of freshly isolated monocytes 5 days after spheroid formation. In poly-Hema coated 96 well u-bottom plates with spheroids, 10.000 freshly isolated monocytes in a volume of 50 µl were seeded per well, whereas 1×10^6 monocytes in a volume of 1 ml per well were added into poly-Hema coated 6 well flat-bottom plates. 3D co-cultures were then further incubated for 6 days at 37° C and 5 % CO_2. On day 11, 3D spheroids were collected for analysis.

3.1.7 T cell suppression assay

Isolated CD3^{+} T cells were washed twice with PBS to remove FCS and centrifuged at 300xg for 8 min at RT. The cell pellet was re-suspended in PBS and labelled with 5µM Carboxyfluorescein succinimidyl ester (CFSE) for 5 min in the dark. On day 11 of 3D spheroid formation, $5x10^4$ T cells were seeded in a volume of 50 µl per well in a poly-Hema coated 96 well u-bottom plate already containing 3D co-culture spheroids without or with spheroid-polarized MDMs that have been added on day 5 after spheroid formation. As proliferation controls, 50.000 T cells were also incubated either alone or with 10.000 monocytes only. To activate T cells, anti-CD3 and anti-CD28 activation beads (Invitrogen™) were washed twice with a magnet column and added to wells using a ratio of 1 bead per 16 T cells. In order to restore T cell proliferation, 3D co-cultures were treated with either 1 mM Arginase-I inhibitor (nor-NOHA, MerckMillipore), 500 µM iNOS inhibitor (1400W dihydrochloride, Tocris), 25 ng/ml TLR8 ligand (TL8-506, Invivogen), 250 ng/ml human CD40 ligand (Miltenyi Biotec) or Arginase-1/iNOS inhibitor and TLR8/CD40 ligand combinations one day prior T cell addition. Surface marker expression was analysed and suppression of T cell proliferation was determined by CFSE dilution using a BD Canto II or a BD LSR II on day 6 after addition of activation beads.
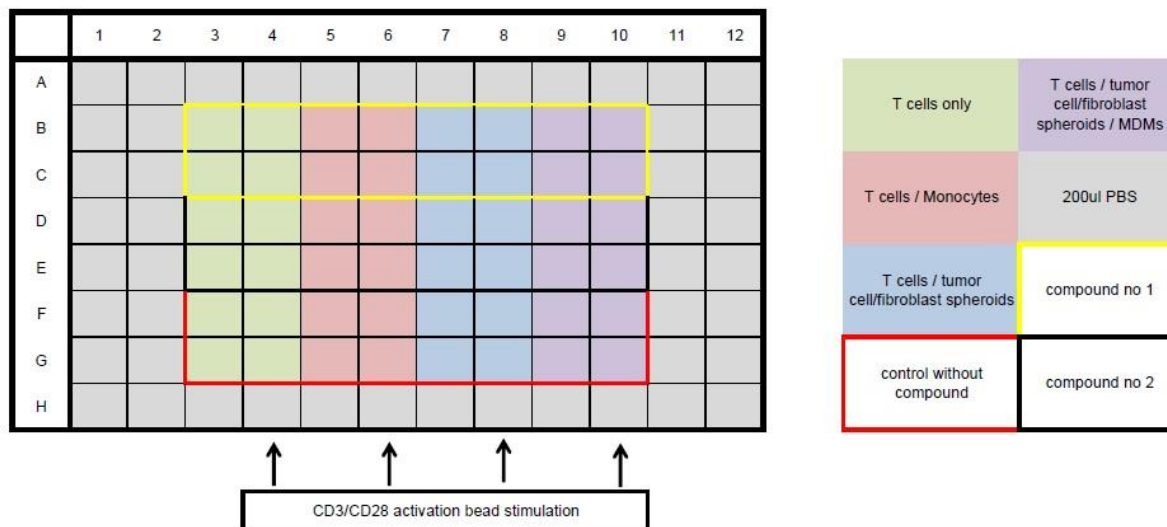

Figure 10: Seeding and treatment scheme for T cell suppression assays.
The outer wells of a poly-Hema coated 96 well u-bottom (grey) were filled with PBS to prevent medium evaporation. T cells (green), T cells with monocytes (red), T cells with tumor cell/fibroblast spheroids (blue) and T cells with tumor cell/fibroblast spheroids and MDMs (purple) were seeded and either activated with CD3/CD28 beads or not. All approaches were then left untreated or stimulated with various compounds in duplicates (red, black and yellow border) and proliferation of CFSE labelled T cells was measured using flow cytometry.

3.1.8 Cell viability assay

The cell viability of the 3D mono- and co-culture spheroids was evaluated using a CellTiterGlo luminescence assay (Promega) on day 5, 7, 9 and 11 according to the supplier's instructions. In this assay, the cell viability is determined by a method based on cell lysis and quantification of total adenosine triphosphate (ATP), a metabolic indicator of active cells, with the help of luminescence detection. For this assay, an equal volume of CellTiterGlo reagent was added to the wells containing 3D mono/co-culture spheroids with and without monocytes in medium in poly-Hema coated 96 well u-bottom plates and incubated for 45 min at RT on a shaker. 150 µl of the cell suspension was then transferred into a black 96 well clear flat-bottom plate and the relative luminescence units (RLU) were measured using a microplate reader (Synergy 2 Plate reader, Bio-Tek). For comparison between spheroids with and without monocytes, the number of monocytes added to spheroids was compensated by subtracting RLU values of a measured monocyte-only control.

3.2 Human cytokine/chemokine multiplex assay

To analyse multiple soluble cytokines and chemokines in the supernatants of 3D co-cultures, a bead-based multiplex system using the Luminex technology was used. The assay was performed in a 96 well flat-bottom plate and the supplier´s instructions were followed. Using de-ionized water, the wash buffer was diluted 1:10 and quality controls were reconstituted in 250 µl for 5 to 10 min. Standards were then prepared using de-ionized water and a 1:5 serial dilution was performed, ranging from 10.000 pg/ml to 3.2 pg/ml. Beads used in the assay were vortexed thoroughly before transferring 60 µl of each vial into the mixing bottle and using bead diluent to reach a final volume of 3 ml. After preparation of reagent, the plate was washed once with 200 µl wash buffer for 10 min at RT. Wash buffer was decanted and 25 µl of standard and quality controls were added to appropriate wells. Assay buffer was used as background reference and added to sample wells. When assaying supernatants, 25 µl control culture medium was added to background, standard and quality control wells. After addition of 25 µl undiluted supernatant to appropriate wells, mixed Luminex beads were included into each well. Samples, standards and controls were measured in duplicates. The plate was sealed with plate sealer and incubated with agitation on a plate shaker for 2 hours at RT. Well contents were then removed and the plate was washed twice using 200 µl wash buffer on a magnetic plate washer before adding 25 µl detection antibody for 1 hour at RT on a plate shaker. After 1 hour, 25 µl streptavidin-PE was added without a washing step and incubated for 30min at RT

on a plate shaker. At the end, all contents were removed by 2 washing steps and mixture was re-suspended in 150 µl sheath fluid for analysis on the multiplex array reader.
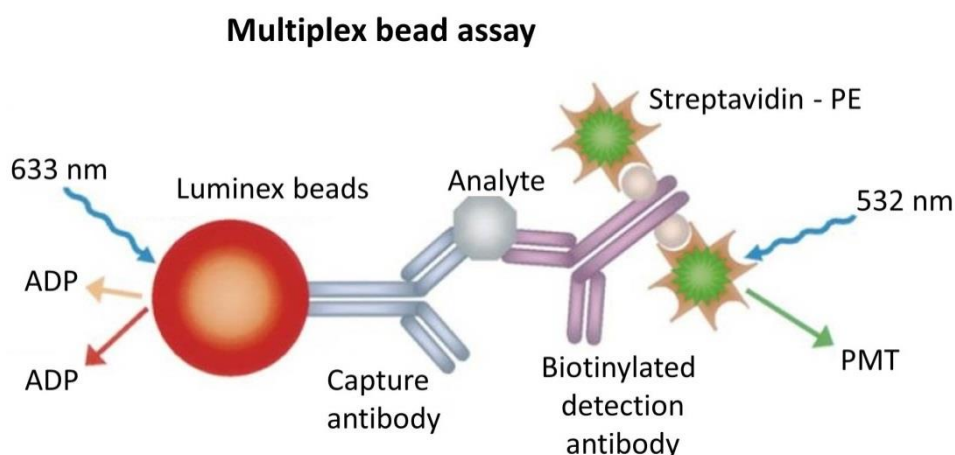
Multiplex bead assay

Figure 11: Bead-based multiplex assay using Luminex technology.
In a 96 well plate, standard or samples are mixed with Luminex beads and assay buffer and incubated for 2 hours at RT. The plate is washed twice and a biotinylated antibody cocktail is added for 1 hour at RT. For final detection, streptavidin-PE is added and further incubated for 30 min. Lastly, the plate is washed again twice, the mixture is re-suspended in sheath fluid and analysed on a Luminex plate reader (modified from B. Cunningham [60].

3.3 Human M-CSF and GM-CSF Quantikine ELISA

For detection of human M-CSF and GM-CSF in the supernatants of 3D co-cultures, a quantitative sandwich enzyme immunoassay technique was performed. Monoclonal antibodies specific for human M-CSF or GM-CSF has been pre-coated onto a 96 well flat-bottom microplate. First, 20 ml of wash buffer was filled up with 480 ml de-ionized water and colour reagent A and B was mixed in equal volumes to obtain 200 µl substrate solution, which must be kept protected from light and used within 15 min after mixing. For M-CSF, the standard was reconstituted with the appropriate Calibrator Diluent to produce a stock solution of 5000 pg/ml, whereas the standard for GM-CSF was reconstituted to obtain a stock solution of 500 pg/ml. 1:2 serial dilutions were performed, ranging from 5000 pg/ml to 78.1 pg/ml for M-CSF and from 500 pg/ml to 7.8 pg/ml for GM-CSF. For each assay, 100 µl assay diluent was added to all wells followed by 100 µl of standard, control and sample per well within 15 min of time. All samples and controls were measured in duplicates. The plate was covered with plate sealer and incubated for 2 hours at RT. After 3 washing steps using 400 µl wash buffer, the plate was further incubated with 200 µl M-CSF conjugate for 2 hours and GM-CSF conjugate for 1 hour at RT. The aspiration and washing steps were repeated again 3 times and 200 µl

substrate solution was added to each well for 30 min at RT protected from light. Addition of 50 µl stop solution changed the colour in the wells from blue to yellow and within 30 min, the optical density of each well was determined using a microplate reader at 450nm.

3.4 Flow cytometry

Flow cytometry is a laser-based technology that is used to measure multiple characteristics of single particles such as cells. It rapidly provides information regarding cell numbers, size, granularity and the expression of cell surface or intracellular biomarkers in a heterogeneous cell population using fluorescent-labelled antibody detection proteins or ligands that can bind cell-associated molecules such as CFSE binding to DNA. For the analysis of cell surface receptor expression, *in vitro* differentiated MDMs were detached from 6 well flat-bottom plates by gently scraping them off after incubation with Accutase at 37° C for 30 min. MDMs cultured in 3D tumor cell/fibroblast co-culture spheroids were dissociated from spheroids by incubation at 37°C for 45 minutes with either Accutase or digestion buffer (PBS with Calcium + 1 mg/ml Dispase II + 2.5 mg/ml Collagenase D + 30 µg/ml Hyaluronidase + 10 µg/ml DNase I) and carefully re-suspended by pipetting up and down every 10 minutes. A 70µm cell strainer (Corning) was used to remove clumps and obtain a single cell suspension. When using the Medimachine (BD Biosciences) instead of Accutase or digestion buffer, spheroids were collected and inserted into the Medicon with 1 ml PBS. The Medicon with a pore size of 50 µm was run 3 times on the Medimachine for 40 seconds to obtain the cell suspension in the bottom of the Medicon. Cells were then washed with PBS with 2% FCS at 300xg for 10 min at 4° C, blocked with human IgG (Invitrogen[TM]) for 15 min and stained for 30 min with conjugated antibodies or matching isotype controls using the concentration as indicated on the datasheet. DAPI (Roche) staining with 200ng/ml for 10 min was performed right before measurement to discriminate dead cells. For intracellular staining, single cells were fixed in 4 % Formaldehyde in PBS for 20 min on ice and washed once in PBS followed by cell membrane permeabilization using 0.5 % Triton-X100 in PBS for 5 min on ice. After another washing step, intracellular staining with conjugated antibodies and matching isotypes was performed according the manufacturer´s instructions. All steps were performed at 4°C (on ice). Sample acquisition was performed using a FACS Canto[TM] II (BD Biosciences) and a LSR[TM] II (BD Biosciences). Geometric mean fluorescence intensities (MFI) and cell proliferation were analysed by FlowJo 10.1 software (TreeStar Inc.).

3.5 Confocal microscopy

Confocal microscopy represents an optical imaging technique that is able to achieve high resolution images of complex tissues or cell structures by the use of spatial filtering through a pinhole placed at the confocal plane of the lens to eliminate out-of-focus light. A process called optical sectioning enables the reconstruction of 3D objects from multiple images at different depths based on illuminating a diffraction-limited spot of the specimen by a focused laser light beam. Within this spot, fluorescence dyes become excited and emit light. The light is refocused in the objective image plane and by passing the pinhole, out-of-focus signals can be removed to create a high resolution image. Selective excitation of fluorophores ensures detection of labelled molecules in several optical sections and at different depths of the specimen without losing signal intensity. To evaluate if spheroid polarized MDMs infiltrate the 3D tumor cell/fibroblast spheroids, freshly isolated monocytes were labelled with Qtracker 525 green-fluorescent nanocrystals (ThermoFisher Scientific). To prepare a 10 nM labelling solution, 1 μl Qtracker component A and 1 μl component B were mixed together in equal volumes, incubated for 5 min at RT followed by addition of 0.2 ml macrophage culture medium to label $1x10^6$ cells. Monocytes were pelleted, re-suspended in the labelling solution and incubated for 45 min at 37° C. To remove any residual Qtracker nanocrystals, cells were washed twice with PBS and seeded into 3D co-culture wells on day 5 of spheroid formation as described above. After 6 days, spheroids were collected, washed once in PBS and fixed with 4 % Formaldehyde in PBS for 1 hour at RT. To counterstain nuclei, cells were washed in PBS followed by cell membrane permeabilization using 0.5 % Triton-X100 in PBS for 5 min on ice and 500 ng/ml DAPI was added for 20 min at 4° C. Optical images were obtained using the Nikon Eclipse Ti confocal microscope and the NiS Elements V4.5 software.

3.6 Multispectral fluorescence light sheet ultramicroscopy

To be able to analyse whole specimens in a non-destructive way, ultramicroscopy was used to image spheroid polarized MDM infiltration into 3D tumor cell/fibroblast spheroids. Ultramicroscopes illuminate whole specimen by using 6 focused laser lights for double-sided, in-focus plane imaging and fluorescence light is detected perpendicular to the illumination axis. Optical clearing of specimens removes water from the sample, replacing it with a liquid that has similar refraction indices like cellular components (e.g. lipids, proteins), which leads to increased specimen transparency. This technique provides high resolution images with almost no autofluorescence,

leading to an extremely well signal-to-noise ratio and enabling imaging of samples up to 5 mm in diameter with spatial resolutions up to 5 μm. To analyse infiltration of Qtracker 525 labelled spheroid polarized MDMs into 3D tumor cell/fibroblast co-culture spheroids, spheroids from one poly-Hema coated 96 well u-bottom plate were collected, washed once with PBS and pelleted at 300xg for 10 min at 4° C. Spheroids were re-suspended in 5 ml 4% Formaldehyde in PBS and fixed for 1 hour at RT. 15 ml PBS was added, cells were centrifuged and transferred into one well of a 96 well flat-bottom plate in as little volume as possible using PBS. Spheroids were then embedded in 1 % Agarose in PBS and placed in a paraffin embedding cassette. A dehydration series (3x 70% ethanol, 2x 95% ethanol, 2x 100% ethanol each for 1:30 hour, 3x xylol for 1 hour, 4x paraffin for 1 hour) was performed followed by optical clearing using a clearing solution mixture of benzyl benzoate and benzyl alcohol (2:1) for 6 hours at RT. In Agarose embedded spheroids are then stored in the clearing solution at 4°C until imaging using

3.7 Immunohistochemistry (IHC) staining

Immunohistochemistry refers to the immunological and biochemical imaging technique to selectively identify antigens in cells of a tissue section by tagging cellular components with antibody conjugated labels. The most commonly used technique called chromogenic detection involves the antibody conjugated enzyme peroxidase, which catalyses a chemical reaction to form coloured insoluble precipitates upon substrate addition. To analyse infiltration and marker expression of spheroid polarized MDMs within 3D tumor cell/fibroblast co-culture spheroids, IHC was performed. Spheroids containing MDMs from one poly-Hema coated 96 well u-bottom plate were collected, washed once with PBS and pelleted at 300xg for 10 min at 4° C. Spheroids were re-suspended in 5 ml 4% Formaldehyde in PBS and fixed for 1 hour at RT. 15 ml PBS was added, cells were centrifuged and transferred into one well of a 96 well flat-bottom plate in as little volume as possible using PBS. Spheroids were then embedded in 1 % Agarose in PBS and placed in a paraffin embedding cassette. A dehydration series (3x 70 % ethanol, 2x 95 % ethanol, 2x 100 % ethanol each for 1:30 hour, 3x xylol for 1 hour, 4x paraffin for 1 hour) was performed, spheroids were then embedded in paraffin and 1.5 μm sections were cut using a microtome. Sections were placed on SuperFrost glass slides (ThermoFischer Scientific) and dried at 37°C overnight. Sections were stained by using an automated staining protocol on a BenchMark XT instrument (Ventana Medical Systems) (Appendix, Figure 34). Single marker staining was performed for CD68 (clone PG-M1, DAKO, #M0876) with chromogenic detection using diaminobenzidine (DAB) to show myeloid cell infiltration into spheroids.

3.8 RNA sequencing

RNA sequencing, also called whole transcriptome shotgun sequencing, is used to quantify and profile RNAs in a biological sample at a given time point and can discriminate different RNA populations such as tRNA, miRNA or small RNA. RNA sequencing is based next-generation sequencing (NGS) and the most commonly used method is known as Illumina (sequencing-by-synthesis technology). Isolated mRNA is converted into a library of cDNA, which is fragmented and ligated with 5` and 3` adaptors for polymerase chain reaction (PCR) amplification. The library is loaded onto a flow cell and fragments are captured by surface-bound oligos complementary to the library adaptors. Each fragment is amplified into specific, clonal clusters through bridge amplification, which are then used as templates for sequencing by Illumina. Reversible terminator-bound deoxyribose nucleoside trisphosphates (dNTPs) are incorporated into DNA template strands. As each fluorescent labelled dNTP is added and cleaved to allow incorporation of the next base, the fluorescent terminator dyes are imaged and signal intensity is measured during each cycle allowing a highly accurate base-by-base sequencing. For RNA extraction of spheroid polarized MDMs, 3D co-culture spheroids were harvested and dissociated with Accutase as previously described. The cell suspension was centrifuged at 300xg for 10 min at 4° C and re-suspended in 80 µl isolation buffer. 20 µl human anti-CD11b micro beads (Miltenyi Biotec) per 10^7 cells were added and incubated for 15 at 4° C. Cells were washed once with isolation buffer and up to 10^8 cells were re-suspended in 500 µl isolation buffer. MACS LS columns were then prepared by rinsing columns once with 3 ml isolation buffer. The cell suspension was applied to the column, allowing unlabelled cells to pass through while keeping CD11b$^+$ cells back in the column. 3 washing steps were performed by adding 3 ml of isolation buffer to the column once it is empty. The column was then removed, 5 ml isolation buffer was added on top to flush out the magnetically labelled CD11b cells with a plunger. Up to 50.000 CD11b$^+$ myeloid cells were pelleted and re-suspended in 200 µl RNA extraction buffer (PicoPure RNA isolation Kit, ThermoFisher) and stored at -80° C. RNA samples were then processed, measured and quantified using the KAPA qPCR library quantification kit (KAPA Biosystems) at F. Hoffmann- La Roche, Basel.
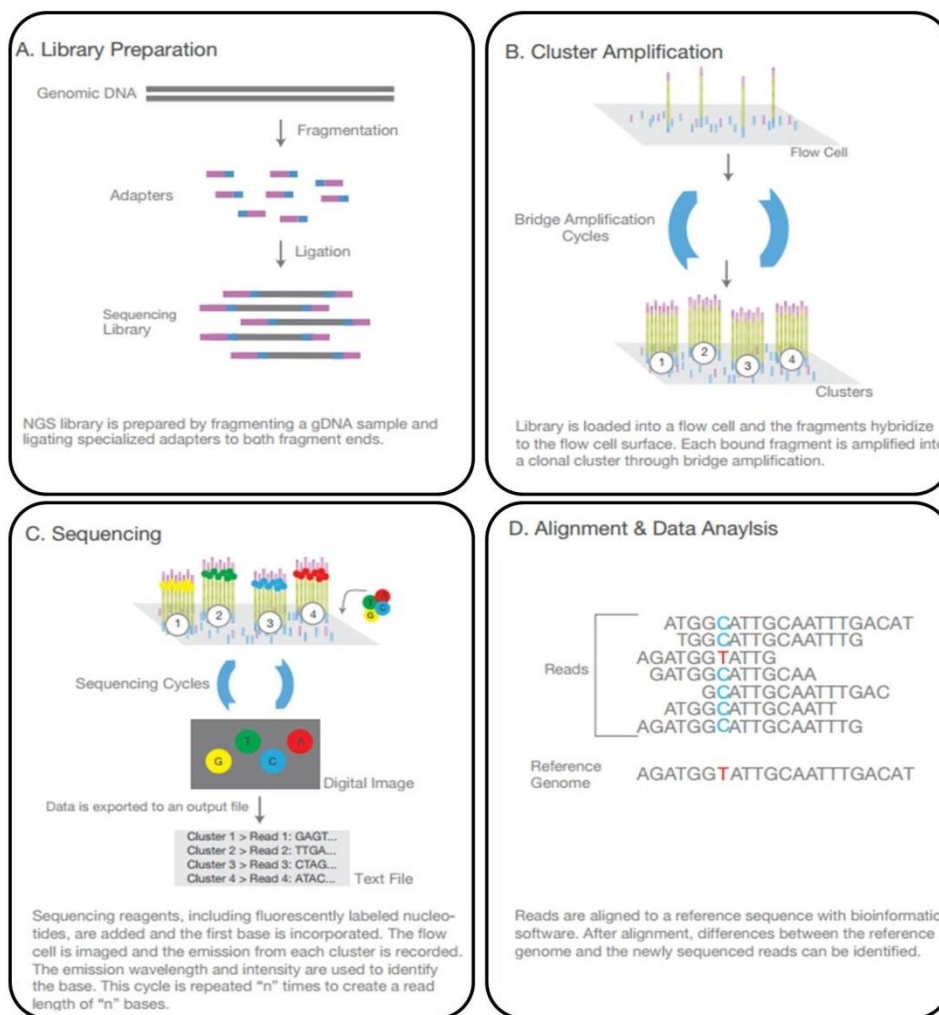
Figure 12: Next-Generation-Sequencing by the Illumina Sequencing-By-Synthesis (SBS) method [61].

3.9 Statistics

All data are presented as mean ± SD from at least 4 independent experiments unless otherwise indicated in the figure legends. Figures were analysed and prepared by using GraphPad Prism V6.04 software, Microsoft Excel 2010 and Microsoft PowerPoint 2010. Statistical significances were calculated by using an unpaired Student´s *t* test with unequal variances; *p < 0.05, **p < 0.01, ***p < 0.001.

4. Results

The following sections describe the establishment of our 3D tumor cell/fibroblast co-culture model, characterizes differentiated MDMs within co-culture spheroids. In several experiments regarding the establishment of a 3D co-culture model with 4 different cell types (tumor cells, fibroblasts, monocytes and T cells), cell numbers, spheroid formation and viability, appropriate concentration and time points of the cells used and the applied activating and inhibitory molecules needed to be optimized in order to obtain a 3D system, which can be used for analysing the functional behaviour of immune cells, which are influenced by soluble factors and cell-cell communication in a 3D co-culture system.

4.1 Establishment of 3D tumor cell/fibroblast co-culture

To develop an *in vitro* 3D co-culture model, we used different pancreatic cancer cell lines and the fetal lung fibroblast cell line MRC5 to create a tumor microenvironment that is able to represent a physiologically relevant system to investigate cell-cell behaviour.

4.1.1 3D co-culture of tumor cells with fibroblasts supports spheroid formation

Tumor cell lines differ in their ability to aggregate or to form spheroids in 3D forced floating systems such as poly-Hema coated plates. In order to determine the ability of 4 different pancreatic cancer cell lines, namely Pa-Tu 8902, BxPC3, HPAC and MiaPaCa-2, to form tight spheroids, cancer cells were cultured alone or in combination with the fibroblast cell line MRC5 for 11 days. Measuring the diameter of the spheroids, we observed that spheroid growth (Fig. 13 A) and spheroid formation (Fig. 13 B) was strongly supported in co-culture with MRC5 in a tumor cell line dependent manner. Spheroid growth of Pa-Tu 8902 and HPAC were strongly dependent on the addition of MRC5 fibroblasts, whereas the spheroid growth of BxPC3/MRC5 and MiaPaCa-2/MRC5 were comparable to tumor cell mono-culture. The spheroid diameter of BxPC3 and MiaPaCa-2 mono-culture decreased within 5 days after seeding as cells slowly start to aggregate. Addition of MRC5 accelerated the process of spheroid formation for BxPC3 and MiaPaCa-2 co-cultures and supported spheroid growth in Pa-Tu 8902 and HPAC co-cultures more than in BxPC3 and MiaPaCa-2 (Fig. 13 A). When looking closely at all co-culture spheroids, we observed a clear and well-differentiated spheroid border for PA-Tu 8902, BxPC3 and HPAC co-culture spheroids, but not for MiaPaCa-2/MRC5 spheroids (Fig 13

B). MRC5 fibroblasts cultured alone in poly-Hema coated plates formed tight spheroids within 5 days in contrast to all tumor cell line mono-cultures, which only formed loose cell aggregations except for HPAC (Fig. 13 B). Furthermore, tumor cell/fibroblast co-culture differed strongly regarding spheroid size. Pa-Tu 8902, HPAC and MiaPaCa-2 co-culture spheroids reached a diameter up to 500 μm, whereas BxPC3/MRC5 spheroids were the smallest with up to 350 μm in diameter. These data indicate that MRC5 fibroblasts are necessary for the chosen pancreatic cancer cell lines for spheroid formation and growth.
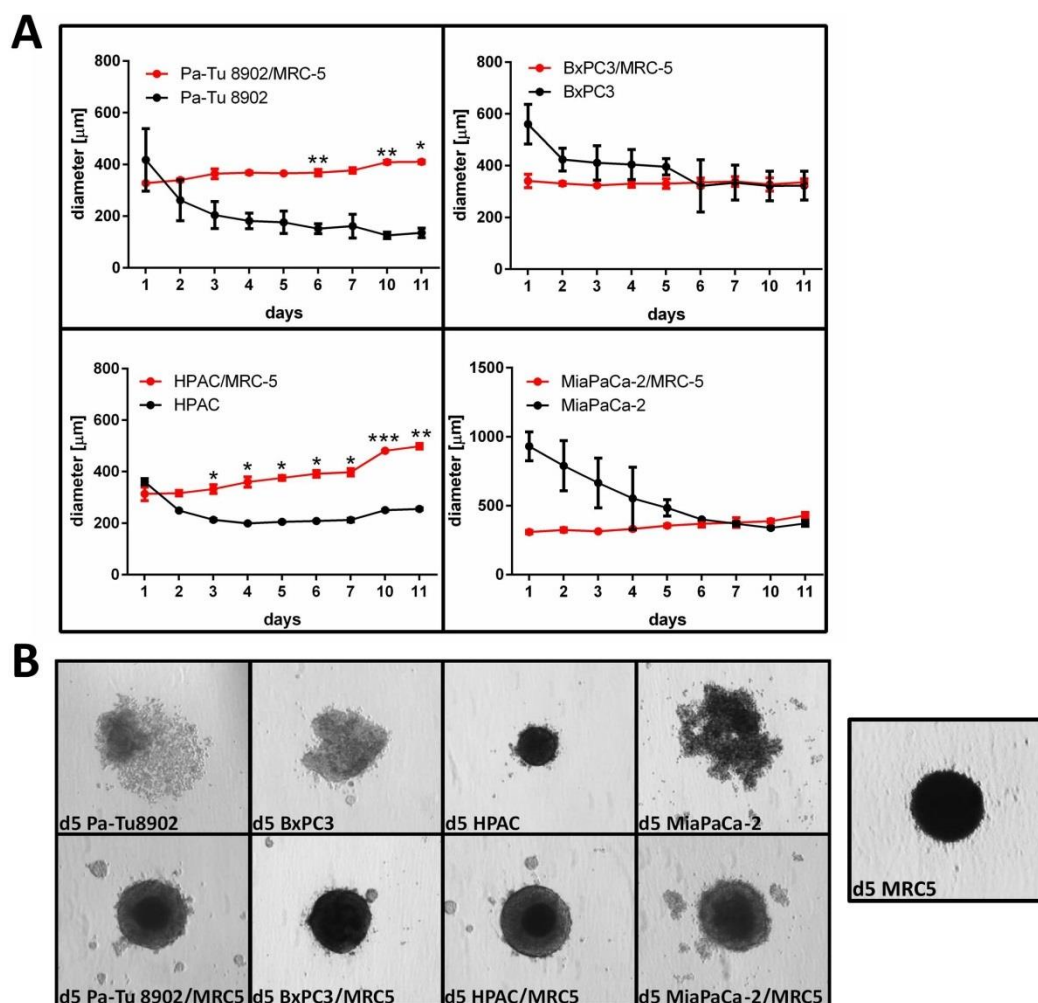

Figure 13: Size and formation of 3D tumor cell/fibroblast spheroids.
Tumor cells were cultured alone or with fibroblasts in a poly-Hema-coated 96 well plate for 5 days as described before. 3D spheroid formation and cell viability was measured by CellTiterGlo assays. A) Co-culturing Pa-Tu 8902 and HPAC tumor cells with MRC5 fibroblasts strongly led to an increase of spheroid size, whereas the size of BxPC3 and MiaPaCa-2 monoculture spheroids resembled the size of co-culture spheroids with MRC5 fibroblasts by day 6. B) All tumor cell lines showed tight spheroid formation in co-culture with fibroblasts (MRC5) compared to tumor cell monoculture. MRC5 cells cultured alone formed a tight spheroid by day 5. Statistical significance was calculated of n= 5 independent experiments by using an unpaired Student´s *t* test with unequal variances; *p < 0.05, **p < 0.01, ***p < 0.001.

To further illustrate the vast phenotypic difference in cell morphology of tumor cells and fibroblasts co-cultured in 2D and 3D, the same numbers of Pa-Tu 8902 and BxPC3 cells were co-cultured with fibroblasts as monolayer and forced-floating spheroids (Fig. 14). Different growth rates of both tumor cell lines were observed for 2D and 3D culturing, with BxPC3 showing a slower tumor cell growth compared to Pa-Tu8902. Thus, the survival of tumor cell/fibroblast spheroids for all 4 pancreatic cancer cell lines was then measured and compared to survival of tumor cells alone.
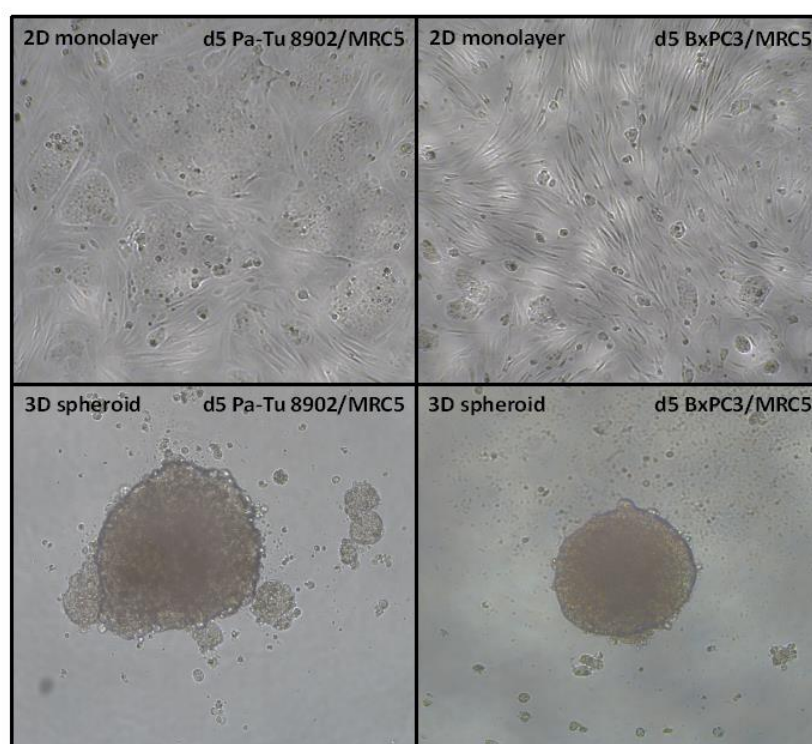

Figure 14: Co-culture of tumor cells with fibroblasts as 2D monolayers and 3D spheroids.
Tumor cells were cultured with fibroblasts either in a poly-Hema-coated 96 well u-bottom plate or in a uncoated 96 well flat-bottom plate or for 5 days as described before. On day 5, images were taken using a light microscope.

4.1.2 MRC5 co-cultured with pancreatic cancer cell lines support viability of 3D co-culture

To further investigate if 3D co-culture of tumor cells with MRC5 fibroblasts affects cell viability, we co-cultured different pancreatic cancer cell lines with fibroblasts for 11 days. Cell viability was measured using a CellTiterGlo assay. All tumor cell lines showed increased survival in co-culture with fibroblasts and 3 out of 4 tumor cell lines reached the highest viability on day 5 (Fig. 15 A) compared to tumor mono-culture. BxPC3 co-cultured with fibroblast exhibited strongly increased cell survival until day 11. For the pancreatic cancer cell lines Pa-Tu 8902, HPAC and MiaPaCa-2, we observed a decrease of co-culture viability from 7 to day 9 or day 11, respectively.
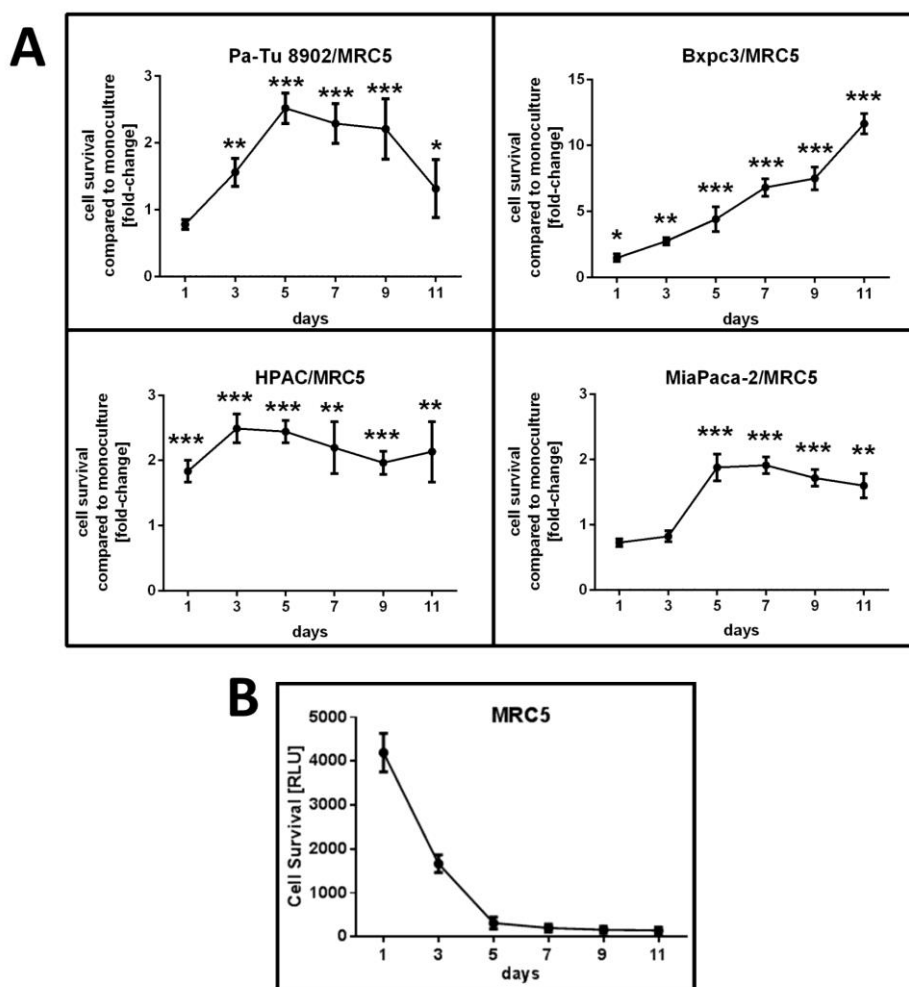
Figure 15: Cell viability and survival of 3D tumor cell/fibroblast co-culture spheroids.
Tumor cells were cultured alone or with fibroblasts in a poly-Hema-coated 96 well plate for 5 days. 3D spheroid viability was measured by CellTiterGlo assays. A) Cell viability of tumor cells was strongly increased in co-culture with MRC5 and reached the maximum on day 5 for most of the cell lines. BxPC3 exhibited the greatest increase of viability upon co-culturing with MRC5, whereas the other cell lines reached a plateau at day 5. B) MRC5 cells cultured without tumor cells in a poly-Hema coated plate died within 5 days. Statistical significance was calculated of n= 5 independent experiments by using an unpaired Student´s t test with unequal variances; *$p < 0.05$, **$p < 0.01$, ***$p < 0.001$.

For MRC5 mono-culture, we observed a continuous cell death within 5 days of culturing in poly-Hema coated plates, indicating that MRC5 fibroblasts support tumor cell survival and showing the dependency of tumor cells on fibroblasts in an *in vitro* 3D system (Fig 15 B).

4.2 Expanding the 3D tumor cell/fibroblast co-culture by addition of monocytes

To study the influence of tumorcell fibroblast co-culture on monocyte differentiation and phenotype, we added freshly isolated monocytes from healthy donors to our 3D tumor cell/fibroblast co-culture.

4.2.1 Monocyte titration for 3D tumor cell/fibroblast co-culture

Since formation of tight spheroids can take up to 5 days depending on the cell lines and differentiation of monocytes to macrophages needs 6 days, the appropriate number of monocytes added to the 3D tumor cell/fibroblast co-culture needs to be determined to obtain a stable and viable 3D co-culture system for up to 11 days of co-culturing. The pancreatic cancer cell lines Pa-Tu 8902 and BxPC3 were co-cultured with MRC5 to evaluate the addition of either 4000, 10.000 or 25.000 monocytes on day 5 of 3D tumor cell/fibroblast co-culture (Fig. 16 A).
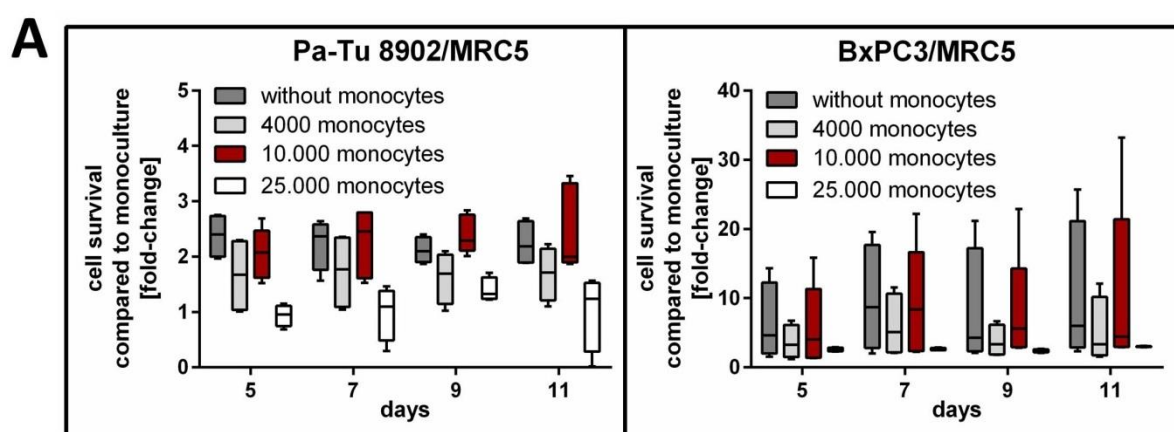

Figure 16: Monocyte titration for 3D tumor cell/fibroblast co-culture.
Tumor cells were co-cultured with fibroblasts for 5 days. Either 4000,10.000 or 25.000 freshly isolated naïve monocytes were added to tumor cell/fibroblast co-culture on day 5 and cell viability was measured every 2 days from day 5 to 11. A) Addition of 4000 and 25.000 monocytes decreased the co-culture viability in a slight, but non-significant way for both tumor cell lines. The addition of 10.000 monocytes did not influence the co-culture´s viability and tumor cell/fibroblast co-cultures with monocytes were as viable as co-cultures without monocytes for each day and tumor cell line, even showing a slight, but non-significant increase of viability for Pa-Tu 8902. Using an unpaired Student´s t test with unequal variances, no significances were observed between tumor cell/fibroblast co-cultures with and without monocytes.

Cell viability was measured every 2 days for 6 days starting from day 5 using CellTiterGlo. A change of co-culture viability depending on the number of monocytes added to the tumor cell/fibroblast co-culture was observed for both Pa-Tu 8902 and BxPC3. Adding either 4000 or 25.000 monocytes to

the 3D tumor cell/fibroblast co-culture led to a decrease of viability compared to the tumor cell/fibroblast co-culture without monocytes. The inclusion of 10.000 monocytes showed comparable survival to tumor cell/fibroblast co-culture without monocytes and did not seem to negatively influence the viability of the 3D tumor cell/fibroblast co-culture. For Pa-Tu 8902 co-cultured with MRC5 and 10.000 monocytes, a slight, but non-significant increase of cell survival could even be observed over the time course of 6 days (Fig. 16 A). 10.000 monocytes were cultured alone in a poly-Hema coated plate for 11 days. The viability of these monocytes decreased rapidly until day 11, showing that monocytes cultured in serum-free medium without tumor cell fibroblast spheroids could not survive (Fig. 16 B). As monocytes were not able to attach to the plate bottom, cells accumulated in the centre of the well of a poly-Hema coated 96 well u-bottom plate and formed loose cell aggregates within 5 days of culturing (Fig. 16 B). Based on these data, 10.000 monocytes were used for further 3D co-culture experiments.

4.2.2 Monocyte addition does not influence the viability of tumor cell/fibroblast co-cultures

Subsequently, 10.000 monocytes were added to all pancreatic cancer cell lines including Pa-Tu 8902, BxPC3, HPAC and MiaPaCa-2 in co-culture with MRC5 fibroblasts to determine the influence of monocyte addition to co-culture viability and proliferation for each tumor cell line (Fig. 17). As previously described, the viability of the co-culture spheroids with monocytes was measured every 2 days starting from day 5 by using CellTiterGlo. As observed for Pa-Tu 8902 and BxPC3 (Fig. 17 A and 17 A and B), the addition of monocytes did also not negatively influence the cell survival of HPAC and MiaPaCa-2 co-cultures and tumor cell/fibroblast co-cultures without monocytes were as viable to co-culture with monocytes (Fig. 17). These data show that the viability of all co-cultures was maintained for 6 days, resulting in a stable 3D co-culture using 3 different cell types.
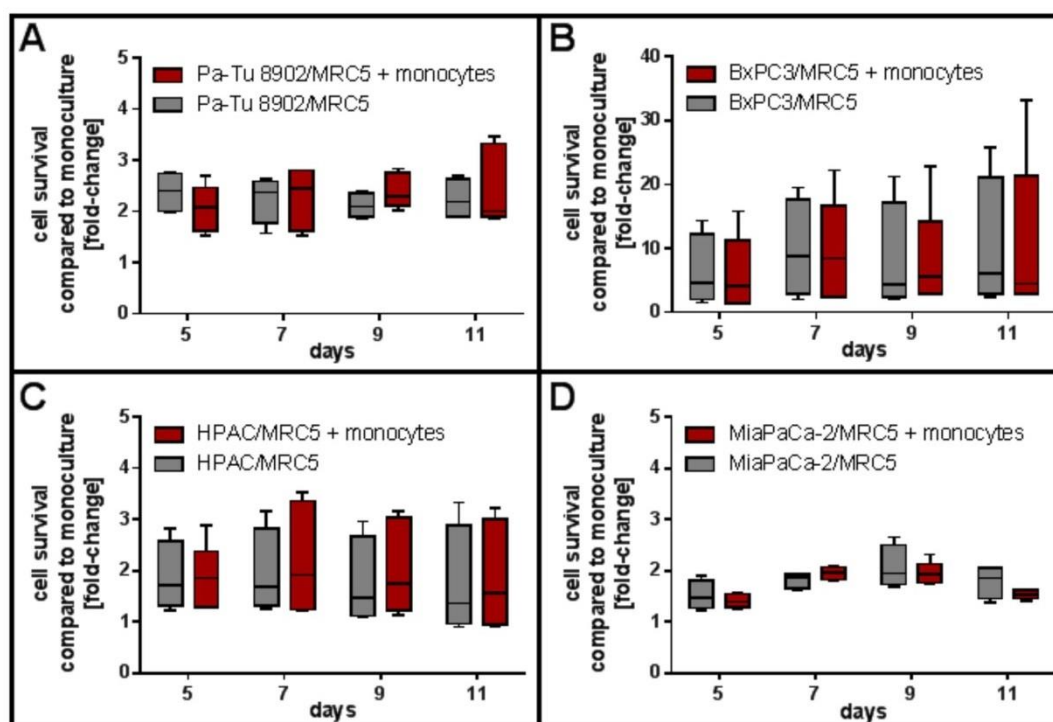
Figure 17: Viability of 3D tumor cell/fibroblast co-culture with monocytes.
Tumor cells were co-cultured with fibroblasts for 5 days. 10.000 freshly isolated naïve monocytes were added to tumor cell/fibroblast co-culture on day 5 and cell viability was measured every 2 days from day 5 to 11. Addition of monocytes did not influence the co-culture´s viability and tumor cell/fibroblast co-cultures with monocytes were as viable as co-cultures without monocytes for each day and tumor cell line. Represented are n=5 independent experiments. Using an unpaired Student´s t test with unequal variances, no significances were observed between tumor cell/fibroblast co-cultures with and without monocytes.

4.2.3 Monocytes do not survive without tumor cell/fibroblast spheroids in a 3D setting

To determine if monocytes are able to survive in serum-free medium without cell contact to tumor cell/fibroblast co-culture spheroids, 10.000 monocytes were cultured alone in a poly-Hema coated 96 well u-bottom plate. As cell attachment was prevented, monocytes accumulated in the centre of the well, forming loose cell aggregates (Fig. 18 A). Within 11 days, a rapid decrease of monocyte viability could be observed (Fig. 18 A). In order to investigate if monocyte survival depends on cell-cell contact to tumor cells or fibroblasts or can be influenced only by soluble molecules produced by tumor cell/fibroblast spheroids, supernatant of all 4 different pancreatic cancer cell lines co-cultured with MRC5 was harvested and used for culturing 10.000 monocytes in a 3D forced-floating setting. By day 6, survival of monocytes was similar or slightly decreased compared to monocytes cultured in serum-free medium for 3 out of 4 pancreatic cancer cell lines (Fig. 18 B). However, monocytes cultured with supernatant obtained from MiaPaCa-2/MRC5 co-culture spheroids showed a

significant increase of cell viability on day 6 in contrast to monocytes in serum-free medium. In summary, monocytes could not survive without attachment to either plate bottom or tumor cell/fibroblast spheroids and viability was not increased upon addition of tumor cell and fibroblast specific soluble molecules.
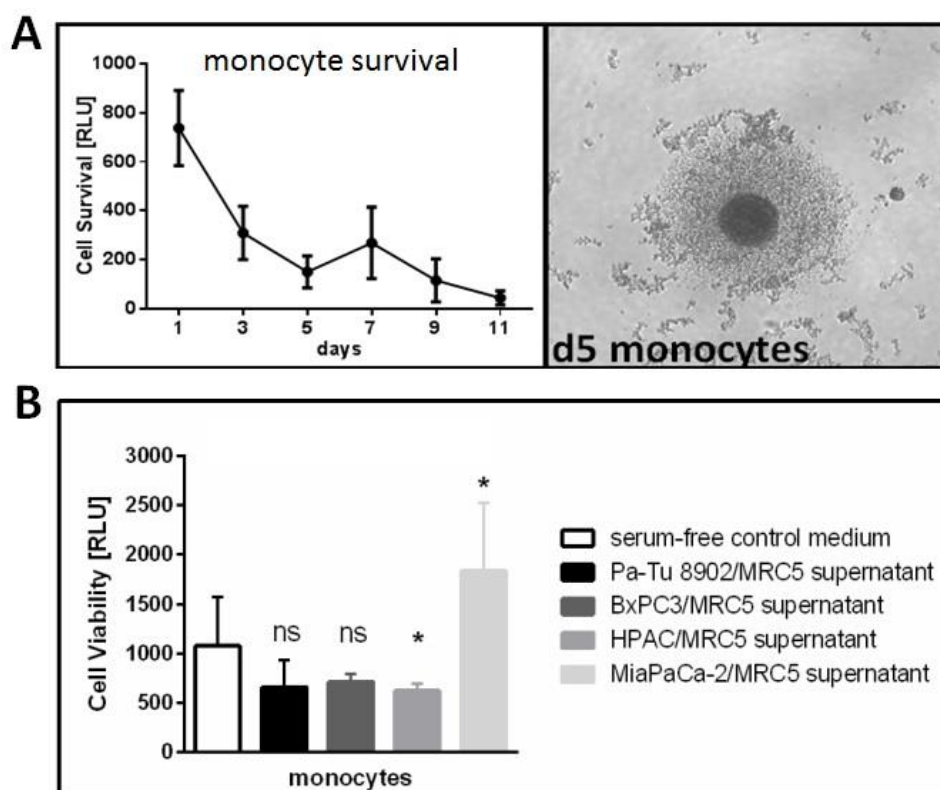

Figure 18: Viability of monocytes cultured in serum-free medium or with 3D tumor cell/fibroblast supernatant.
Tumor cells were co-cultured with fibroblasts for 5 days. Supernatant was collected and 10.000 freshly isolated naïve monocytes were cultured in either serum-free medium or 3D tumor cell/fibroblast supernatant for 6 days. Cell viability was measured at different time points. A) For 10.000 monocytes cultured alone in serum-free medium in poly-Hema coated plates, a strong decrease of cell viability and loose cell aggregations within 5 days was observed. B) On day 6, monocytes showed increased survival when cultured with MiaPaCa-2/MRC5 supernatant, whereas survival of monocytes cultured with supernatant of Pa-Tu 8902, BxPC3 and HPAC co-cultures was comparable to survival of monocytes in serum-free medium. Statistical significance was calculated of n= 4 independent experiments by using an unpaired Student´s t test with unequal variances; *p < 0.05, **p < 0.01, ***p < 0.001.

4.3 Evaluation of MDM infiltration into 3D tumor cell/fibroblast spheroids

To analyse whether monocytes added to the 3D tumor cell/fibroblast co-culture migrate into the spheroids, different imaging techniques were used, starting with Pa-Tu 8902 and BxPC3 tumor cell lines to evaluate the appropriate method.

4.3.1 Analysing MDM infiltration using confocal microscopy

Confocal microscopy was used to track monocytes, which migrated into tumor cell/fibroblast spheroids. Monocytes were labelled with Qtracker 525 nanocrystals before addition to co-culture spheroids and infiltration was analysed on day 6. All cells within the spheroid were counterstained using DAPI shortly before imaging.
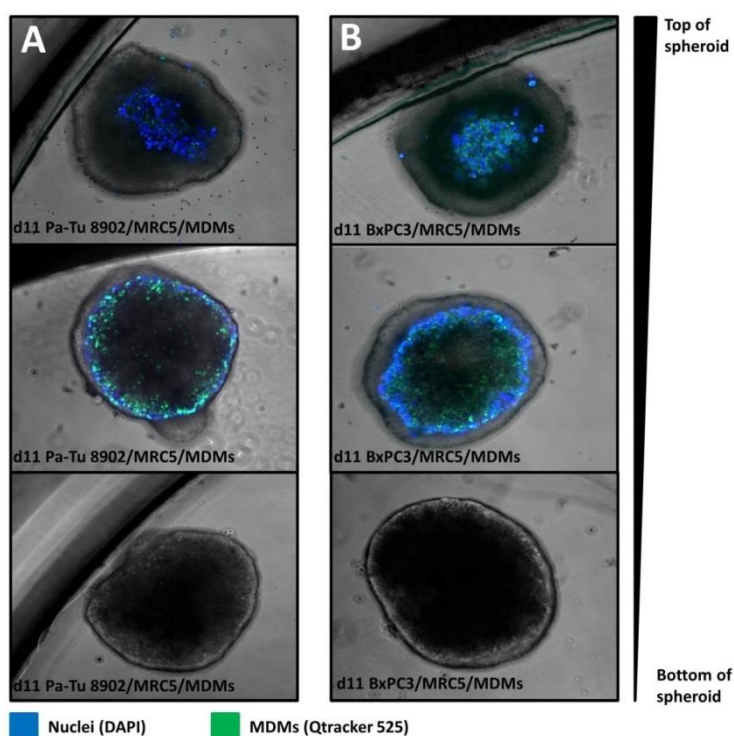

Figure 19: Evaluation of MDM infiltration into tumor cell/fibroblast spheroid by confocal microscopy.
Tumor cells were co-cultured with fibroblasts for 5 days. 10.000 freshly isolated Qtracker 525 labelled monocytes were added to spheroids for 6 days. Cell nuclei were counterstained using DAPI and monocyte infiltration into spheroids was measured by confocal microscopy. A) Images of monocyte infiltration into Pa-Tu 8902/MRC5 spheroids, starting from the top to the bottom of the spheroid B) Images of monocyte infiltration into BxPC3/MRC5 spheroids starting from the top to the bottom of the spheroid. Represented is one of n=3 experiments.

As described before, Pa-Tu 8902 spheroids reached up to 500 µm in diameter, whereas BxPC3 spheroids represented smaller sized spheroids with a diameter up to 350 µm (Fig. 13 A). For both Pa-Tu 8902 and BxPC3 co-culture spheroids, different images of the z-plane of the spheroid, starting from the top of to the bottom, revealed incomplete staining of cells with DAPI (Fig. 19 A and B). DAPI stained cells as well as Qtracker 525 labelled monocytes could only be observed at the outer rim of the spheroid, but not in the spheroid centre or at the spheroid bottom. By making this observation, it is not clear whether monocytes did not migrate into spheroids or if migrated monocytes could not be detected due to limitation of the confocal laser depth, which is around 200 µm. This indicated that this method might not be an appropriate choice to analyse monocyte infiltration into tumor cell/fibroblast spheroids.

4.3.2 Analysing MDM infiltration using light sheet ultramicroscopy

Ultramicroscopes are able to better image 3D structures compared to confocal microscopes by using a set of 6 focused laser lights placed in a specific position to allow high imaging resolution. To evaluate monocyte migration by light sheet ultramicroscopy, monocytes were labelled using Qtracker 585 nanocrystals and added to BxPC3/MRC5 spheroids on day 5. After 6 days, spheroids were harvested, embedded in Agarose and optically cleared to obtain fluorescence images of the whole specimen without high absorption and light scattering. Using focus stacking, also called z-stacking, multiple images at different focus distances were generated by 6 focused light sheets to homogeneously illuminate samples from the side and were then combined to one image in order to produce an image with a greater depth of field. Qtracker 585 labelled monocytes were detectable within BxPC3/MRC5 spheroids throughout the spheroid (Fig. 20). Nevertheless, the number of monocytes that infiltrated the spheroid could not be quantified due to the heterogeneous distribution of Qtracker 585 nanocrystals within the cytoplasm of the monocytes. Counterstains of tumor cells and fibroblasts was not performed due to limited penetration of DAPI into the spheroid, leading to incomplete cell staining as shown before (Fig. 19). As single cell analysis of infiltrated monocytes is restricted, light sheet ultramicroscopy did not appear to be a method of choice for further experimental analysis.
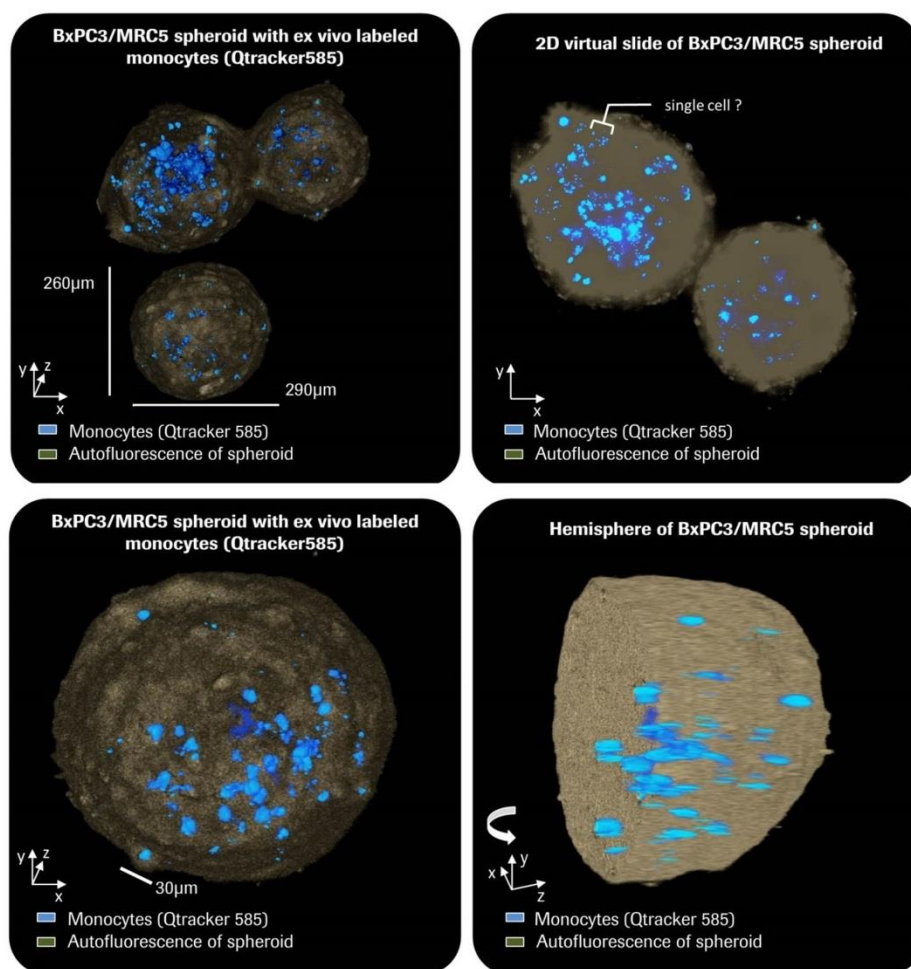
Figure 20: Evaluation of MDM infiltration into BxPC3/MRC5 spheroid by light sheet ultramicroscopy.
Tumor cells were co-cultured with fibroblasts for 5 days. 10.000 freshly isolated Qtracker 525 labelled monocytes were added to spheroids for 6 days. Spheroids were cleared optically and monocyte infiltration into BxPC3/MRC5 spheroids was measured by multispectral fluorescence ultramicroscopy. Limitations of single cell resolution regarding the identification of single spheroid polarized MDMs can be observed. Represented is one of n=3 experiments.

4.3.3 Analysing MDM infiltration using immunohistochemistry

In order to observe monocyte migration into tumor cell/fibroblast spheroids and to be able to determine single cells within a spheroid, monocytes were added to tumor cell/fibroblast co-cultures for 6 days. Harvested spheroids were embedded in paraffin and microtome sections were stained with an automatized staining process using the Ventana Benchmark XT. Myeloid cells infiltrating the spheroids were identified by immunohistochemistry staining with CD68, a pan macrophage marker. CD68^{+} myeloid cell infiltration into spheroids was observed in all co-culture spheroids, although at different rates (Fig. 21 A). MiaPaCa-2/MRC5 spheroids, which did not form tight spheroids with a clear spheroid border, were strongly infiltrated by CD68^{+} myeloid cells compared to other co-culture

spheroids (Fig. 21 B). These data suggested that tumor cell/fibroblast spheroid tightness correlates with the number of monocytes that migrate into spheroids.
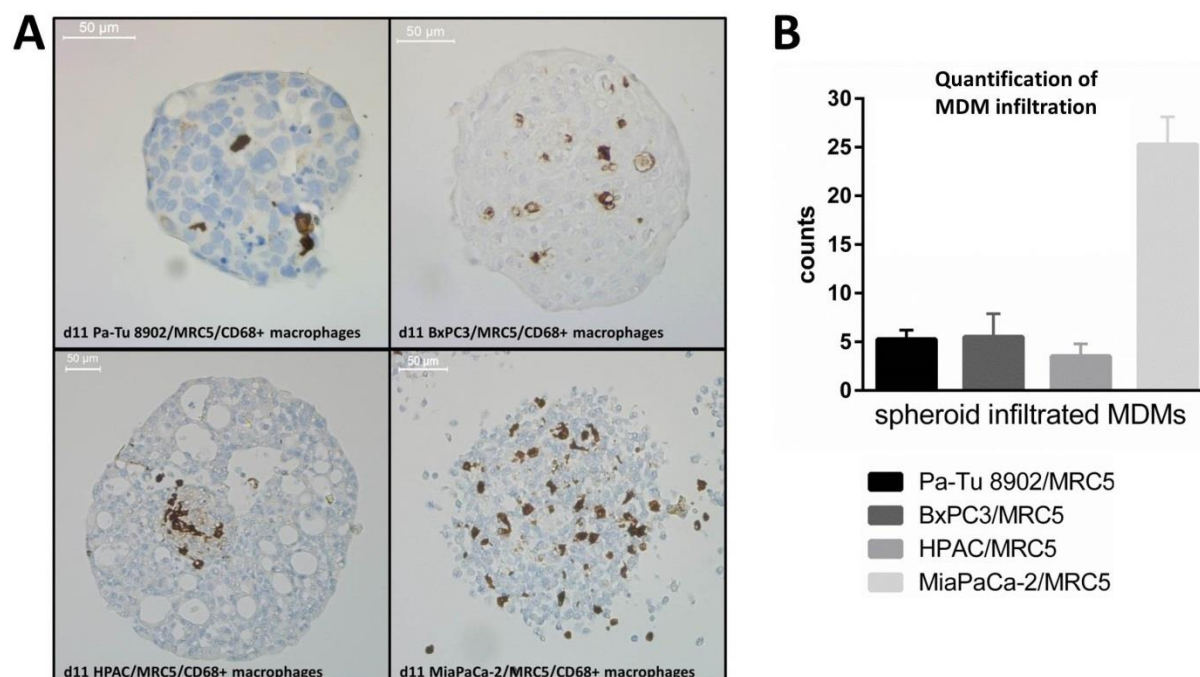

Figure 21: Infiltration of MDMs into 3D tumor cell/fibroblast spheroids.
Tumor cells and fibroblasts were 3D co-cultured for 5 days to form tight spheroids. On day 5 of tumor cell/fibroblast spheroid formation, monocytes were added for 6 days to determine cell migration into spheroids. A) The pan-macrophage marker CD68 on myeloid cells was detected with DAB by performing IHC using a Benchmark XT instrument. Infiltration of spheroid polarized MDMs could be observed for all co-cultures, but was highest in MiaPaCa-2/MRC5 co-culture. One representative picture is shown for each tumor cell line. B) Quantitative analysis of spheroid infiltrated MDMs of n=4 independent experiments.

4.4 Differential cytokine secretion in 3D tumor cell/fibroblast co-cultures

To determine if soluble factors including cytokines, chemokines and growth factors influence monocyte differentiation in the 3D co-culture setting, supernatants from tumor cell/fibroblast co-cultures were measured prior to and 6 days after monocyte addition by using the Luminex multiplex technology. Tumor cell/fibroblast spheroids differed in their cytokine/growth factor profile depending on the tumor cell line. However, all tumor cell lines co-cultured with MRC5 fibroblasts secreted high levels IL-6, CCL-2 and IL-8 and low levels of IL-10 on day 5 after spheroid formation (Table 1). The levels of VEGF, CCL-2 and IL-8 increased significantly in all co-culture supernatants on day 6 after monocyte addition. IL-10 secretion was up-regulated in all tumor cell line co-cultures except for MiaPaCa-2. M-CSF was 2 to 3-fold higher in HPAC/MRC5 co-culture after monocyte

addition. Secretion of IL-6, IL-10 and IP-10 decreased in tumor cell/fibroblast co-cultures from day 5 to day 11, but was strongly elevated once monocytes were added to the co-culture (Table 1 and Fig. 22).

Cytokines/ chemokines	Pa-Tu 8902/MRC5 co-culture day 5	Pa-Tu 8902/MRC5 w/o MDMs co-culture day 11	Pa-Tu 8902/MRC5 + MDMs co-culture day 11	BxPC3/MRC5 co-culture day 5	BxPC3/MRC5 w/o MDMs co-culture day 11	BxPC3/MRC5 + MDMs co-culture day 11	HPAC/MRC5 co-culture day 5	HPAC/MRC5 w/o MDMs co-culture day 11	HPAC/MRC5 + MDMs co-culture day 11	MiaPaCa-2/MRC5 co-culture day 5	MiaPaCa-2/MRC5 w/o MDMs co-culture day 11	MiaPaCa-2/MRC5 + MDMs co-culture day 11
G-CSF	385,45	n.d.	n.d.	62,07	n.d.	n.d.	337,30	n.d.	n.d.	4927,37	n.d.	n.d.
GM-CSF	37,35	23,77	20,03	12,21	21,55	144,40	35,49	19,195	24,52	43,77	23,755	29,61
M-CSF	83,09	76,89	175,55	317,45	407,64	474,09	131,49	115,51	274,54	1171,17	2213,88	1170,09
IL-1ra	n.d.	n.d.	118,36	n.d.	9,12	154,22	n.d.	n.d.	61,18	n.d.	6,31	65,06
IL-6	2277,29	994,53	4099,86	2332,89	764,02	2488,55	651,72	554,11	1469,86	946,49	544,71	1917,26
IL-10	16,37	n.d.	97,65	36,79	n.d.	76,90	14,65	n.d.	124,93	14,72	n.d.	n.d.
TNFalpha	n.d.	n.d.	29,13	n.d.	8,99	85,77	n.d.	n.d.	17,59	n.d.	4,115	9,75
CCL-2	1025,65	1978,50	5817,36	1205,52	166,42	6881,74	701,32	169,765	4211,92	1939,97	1664,3	3692,68
IL-8	5578,71	10034,77	25020,83	2332,48	3035,94	4344,72	1002,85	3103,385	6456,33	3216,73	8870,735	5677,12
IP-10	68,94	35,03	304,02	341,78	31,18	294,29	99,46	19,66	308,63	157,36	41,675	555,04
MIP-1alpha	n.d.	n.d.	114,52	n.d.	7,73	105,90	n.d.	n.d.	26,34	n.d.	5,79	11,91
MIP-1beta	n.d.	10,62	166,90	n.d.	8,00	217,89	n.d.	n.d.	102,24	n.d.	8,11	50,02
VEGF	138,90	696,59	85,85	233,72	187,61	78,11	136,34	108,955	442,64	466,38	546,21	609,93
IFNalpha	n.d.	10,05	n.d.	n.d.	21,66	6,34	n.d.	n.d.	n.d.	n.d.	16,61	n.d.
IFNgamma	n.d.	n.d.	n.d.	n.d.	6,59	n.d.	n.d.	n.d.	n.d.	n.d.	3,57	n.d.
IL-2	n.d.	n.d.	n.d.	n.d.	n.d.	n.d.	n.d.	n.d.	n.d.	n.d.	n.d.	n.d.
IL-4	n.d.	n.d.	n.d.	n.d.	10,42	n.d.	n.d.	n.d.	n.d.	n.d.	8,63	n.d.
sCD40L	n.d.	n.d.	n.d.	n.d.	n.d.	n.d.	n.d.	n.d.	n.d.	n.d.	n.d.	n.d.
TGFalpha	n.d.	n.d.	n.d.	n.d.	n.d.	n.d.	n.d.	n.d.	n.d.	n.d.	n.d.	n.d.

Table 1: Summary of differentially expressed cytokines and chemokines in the supernatant of 3D tumor cell/fibroblast co-cultures with and without spheroid polarized MDMs.
Tumor cells and fibroblasts were co-cultured for 5 days. Monocytes were added to co-culture on day 5 and further cultivated for 6 days. Supernatants were collected on day 5 before monocyte addition and on day 11 from co-cultures without and with monocytes. A panel of 19 soluble factors was measured using Luminex multiplex technology or ELISA. Increased levels of several cytokines and chemokines could be detected on day 11 after addition of monocytes (n.d.= not detectable). Shown is the mean concentration in pg/ml of n=3 independent experiments.

Furthermore, tumor cell/fibroblast spheroids did not secrete pro-inflammatory cytokines and chemokines such as TNF-α, MIP1-α and MIP1-β on day 5 after spheroid formation, however an up-regulation of these molecules could be detected once monocytes were added to co-cultures for 6 days (Table 1). The addition of monocytes to all 3D co-cultures led to a significant increase of GM-CSF and CCL-2 as well as a slight, but non-significant increase of M-CSF, IL-10 and IL-8 compared to 3D co-cultures without monocytes (Fig. 22). These data showed that apart from the tumor cell line used, the addition of monocytes to the co-cultures influenced the cytokine/growth factor profile of the 3D tumor cell/fibroblast co-cultures.
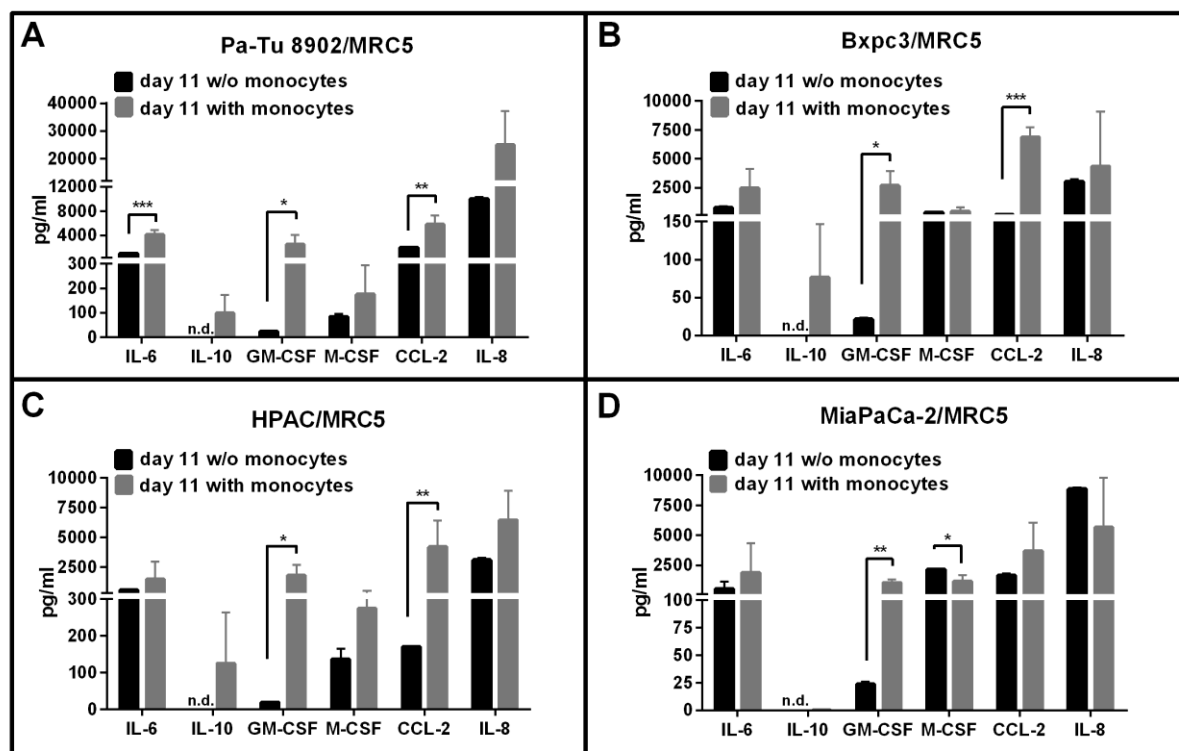
Figure 22: 3D tumor cell/fibroblast co-culture with monocytes induces differential secretion of cytokines, chemokines and growth factors.

Tumor cells and fibroblasts were co-cultured for 5 days. Monocytes were added to co-culture on day 5 and further cultivated for 6 days. Supernatants were collected on day 5 before monocyte addition and on day 11 from co-cultures with monocytes. A panel of 19 soluble factors was measured using Luminex multiplex technology or ELISA. Depicted are the most relevant soluble molecules at detectable levels. Increased levels of several cytokines and chemokines could be detected on day 11 after addition of monocytes. Statistical significance was calculated of n= 3 independent experiments by using an unpaired Student´s t test with unequal variances; *$p < 0.05$, **$p < 0.01$, ***$p < 0.001$.

4.5 M2-like polarization of monocytes in 3D tumor cell/fibroblast co-cultures

Freshly isolated monocytes, which were added to 3D tumor cell/fibroblast spheroids on day 5, were differentiated for 6 days followed by the analysis of cell surface marker expression. To phenotypically analyse spheroid polarized MDMs by flow cytometry, spheroids were dissociated to single cell suspensions (Fig 23). For characterization of spheroid polarized MDMs, single cell suspensions of 3D co-cultures were first gated on morphology (SSC-A vs. FCS-A) followed by gating of single viable cells (DAPI vs. FCS-W). To discriminate different cell types, EpCAM was used as tumor marker, CD11b as myeloid cell marker and cells negative for both EpCAM and CD11b expression were identified as fibroblasts. CD11b^{+} cells were then gated for further analysis (Fig. 23 A). Different methods to obtain

single cell suspensions were evaluated using large Pa-Tu 8902/MRC5 spheroids and small BxPC3/MRC5 spheroids for optimal spheroid digestion (Fig. 23 B and C).
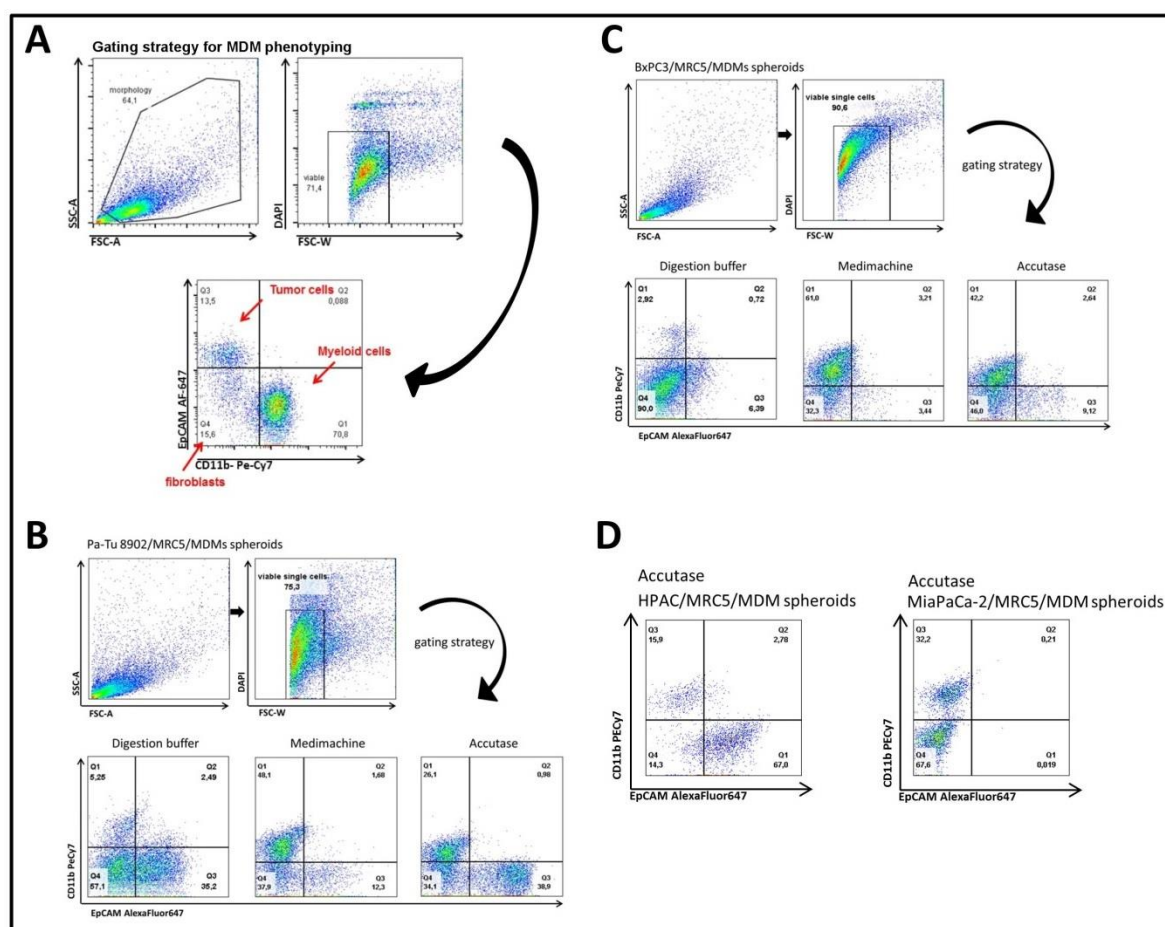

Figure 23: Evaluation of different spheroid digestion methods.
Tumor cells and fibroblasts were co-cultured for 5 days. Monocytes were added to co-culture on day 5 to differentiate for 6 days. Spheroids were harvested to obtain single cell suspensions. A) The gating strategy is shown to discriminate tumor cells, fibroblasts and CD11b^{+} spheroid polarized MDMs for further flow cytometry analysis. B and C) Spheroids were collected and dissociated by either using Accutase, digestion buffer or the MediMachine to obtain a single cell suspension as shown for Pa-Tu 8902 and BxPC3 co-culture spheroids. D) HPAC and MiaPaCa-2 co-cultured were dissociated using Accutase. MiaPaCa-2 tumor cells did not show expression of the tumor marker EpCAM. Shown is one representative out of n=5 experiments.

Using digestion buffer containing the enzymes DNase I, Dispase II, Collagenase D and Hyaluronidase could not sufficiently separate spheroid polarized MDMs from either Pa-Tu 8902 or BxPC3 co-culture spheroids as only a small population of CD11b^{+} cells could be observed. The MediMachine showed better separation of CD11b^{+} cells, however only small EpCAM^{+} tumor cell populations could be detected. Lastly, spheroid digestion using Accutase was analysed and found to be the best option to obtain single cell suspensions. For Pa-Tu 8902/MRC5 and BxPC3 spheroids, a large population of

both CD11b^{+} cells and EpCAM^{+} tumor cells could be detected compared to spheroid digestion with other protocols (Fig. 23 B and C). Based on these data spheroids were dissociated using Accutase for further analyses (Fig. 23 D).

4.4.1 3D tumor cell/fibroblast spheroids promote M2-like polarization of monocytes

To investigate how pancreatic cancer cell/fibroblast co-cultures influence monocyte differentiation, the phenotype of viable spheroid polarized MDMs was characterized by analysing the expression of cell surface markers by flow cytometry. Typical M2 (CD14, CD163, Arginase-1) and M1 (CD86, HLA-DR, CD40) macrophage marker were measured on CD11b^{+} spheroid polarized MDMs and compared to *in vitro* generated M2c macrophages, MDSCs and activated M1 macrophages (Table 2 and Fig. 23).

| marker	monocytes	activated M1 macrophages	M2c macrophages	MDSCs	Pa-Tu 8902/MRC5 spheroid polarized MDMs	BxPC3/MRC5 spheroid polarized MDMs	HPAC/MRC5 spheroid polarized MDMs	MiaPaCa-2/MRC5 spheroid polarized MDMs
CD206	0,71	58,52	28,50	20,33	4,92	8,29	5,73	6,01
CD163	144,84	2,80	33,87	4,70	4,16	4,00	4,45	4,52
CD14	13,35	13,81	46,01	5,73	202,55	55,02	77,83	61,76
CD80	18,29	3,23	1,37	1,98	1,31	1,43	1,34	1,14
CD86	49,45	14,10	6,61	8,85	3,39	3,42	3,48	2,02
HLA-DR	20,48	231,88	37,19	54,64	99,21	154,38	70,75	22,30
CD16	23,06	1,99	56,22	2,41	3,23	1,70	3,04	2,06
CD33	1,93	2,86	2,47	1,24	1,12	0,98	1,02	1,04
PD-L1	-	84,52	4,76	-	7,13	4,20	6,01	4,35
CD40	8,60	54,23	6,04	-	2,19	2,04	2,73	2,33
Arg-1	4,14	1,54	2,84	2,17	1,84	2,12	2,90	2,15
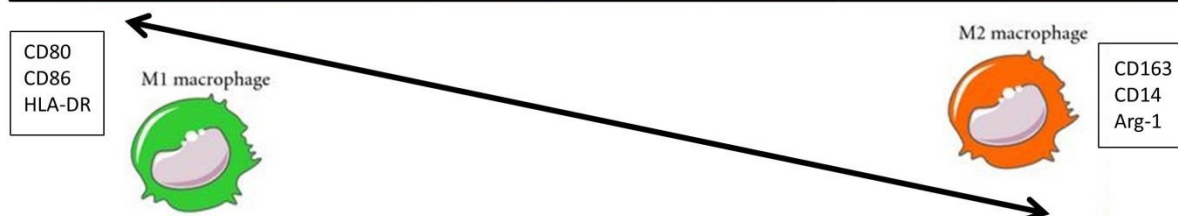
Table 2: Summary of cell surface marker expression on *in vitro* generated macrophages and spheroid polarized MDMs.
Tumor cells and fibroblasts were co-cultured for 5 days. Monocytes were added to co-culture on day 5 to differentiate for 6 days. Spheroids were collected and dissociated by using Accutase to obtain a single cell suspension. Cell surface marker expression of 3D spheroid polarized MDMs was compared to *in vitro* generated MDSCs, M2c, activated M1 macrophages and freshly isolated monocytes. Typical M2 (orange) and M1 macrophage marker (green) were analysed by flow cytometry. Shown is the mean of geometrical mean values of n=6 independent experiments.

As expected, M1 macrophages expressed low levels of CD163 and CD14. In addition, they expressed higher levels of the activation marker CD86, HLA-DR, CD40 and the checkpoint molecule PDL1. M2 macrophages, on the other hand, expressed high levels of CD163 and CD14, lower levels of CD86,

HLA-DR, CD40 and PDL1. Arginase-1, an M2 macrophage marker which is involved in the inhibition of nitric oxide (NO) production, was expressed only by the *in vitro* generated M2 macrophages, MDSCs and freshly isolated monocytes (Table 2). Expression of Arg-1 in spheroid-polarized MDMs was upregulated compared to M1 macrophages and similar to Arg-1 expression found in M2c macrophages.
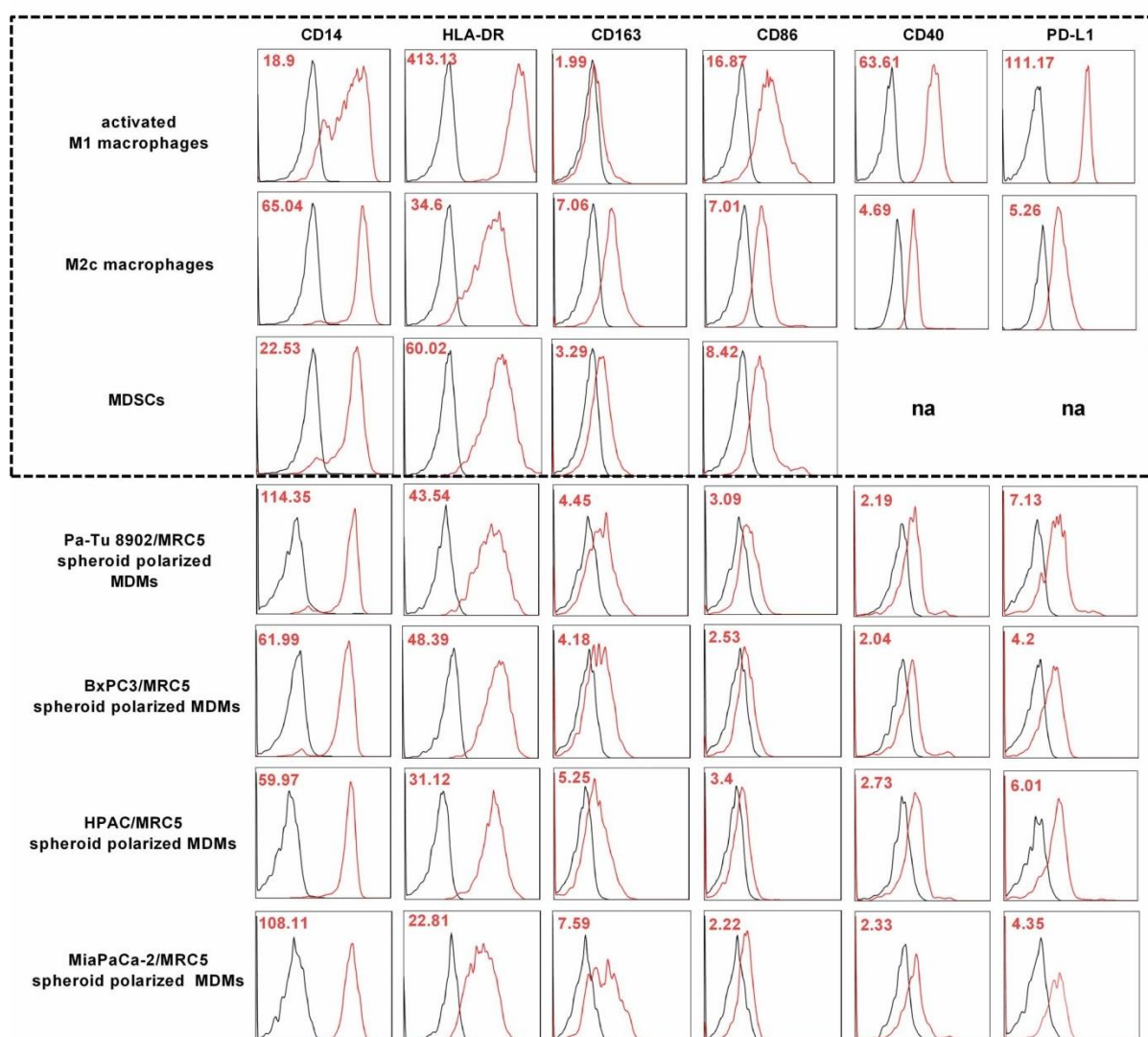

Figure 24: 3D tumor cell/fibroblast co-culture polarized MDMs resemble M2-like macrophages.
Tumor cells and fibroblasts were co-cultured for 5 days. Monocytes were added to co-culture on day 5 to differentiate for 6 days. Spheroids were collected and dissociated by using Accutase to obtain a single cell suspension. Cell surface marker expression of 3D spheroid polarized MDMs was compared to *in vitro* generated MDSCs, M2c and activated M1 macrophages. Typical M2 and M1 macrophage marker were analysed by flow cytometry. 3D co-culture polarized MDMs expressed high levels of CD163 and CD14 and low levels of CD86 and HLA-DR comparable to *in vitro* differentiated M2 macrophages (dotted box). Shown is one representative out of n=5 experiments, red numbers show geometrical mean values for relevant markers.

Cell surface marker expression of CD163 and CD14 on MDSCs was slightly decreased compared to marker expression on M2c macrophages in contrast to the M1 marker HLA-DR and as well as CD86, which were strongly expressed on MDSCs compared to M2c macrophages (Fig. 24). The spheroid polarized MDMs expressed low levels of CD86, HLA-DR and CD40 and high levels of CD14, CD163 and Arginase-1 (Fig. 24 and Table 2). The expression pattern of spheroid polarized MDMs was comparable for each population regardless of the tumor cell line/fibroblast spheroids the myeloid cells were co-cultured with and data showed that spheroid polarized MDMs strongly resembled the *in vitro* generated M2 macrophages.

To show that cell-cell contact of monocytes to tumor cell/fibroblast spheroids is essential for differentiation into M2-like macrophages, freshly isolated monocytes were cultured in supernatant collected from different pancreatic cancer cell lines in co-culture with MRC5. Therefore, the phenotype of monocytes differentiated with 3D tumor cell/fibroblast spheroids was compared to cell surface marker expression of monocytes differentiated only with supernatants of these spheroid co-cultures (Fig. 25). Differential expression of several cell surface markers was observed. The expression of the M2 macrophage marker CD163 was significantly higher in monocytes polarized with tumor cell/fibroblast supernatant, while the expression of Arginase-I in HPAC/MRC5 and MiaPaCa-2/MRC spheroid polarized MDMs significantly exceeded Arginase-I expression in supernatant polarized MDM (Fig. 25 C and D). Along with CD163, the expression of the transmembrane receptor CD33, stated to be an inhibitory molecule, was also strongly up-regulated in MDMs differentiated with only tumor cell/fibroblast supernatant. However, supernatant polarized MDMs also expressed typical M1 macrophage marker such as CD86 and HLA-DR compared to spheroid polarized MDMs, showing that this myeloid cell population combines the expression of both M1 and M2 cell surface marker.
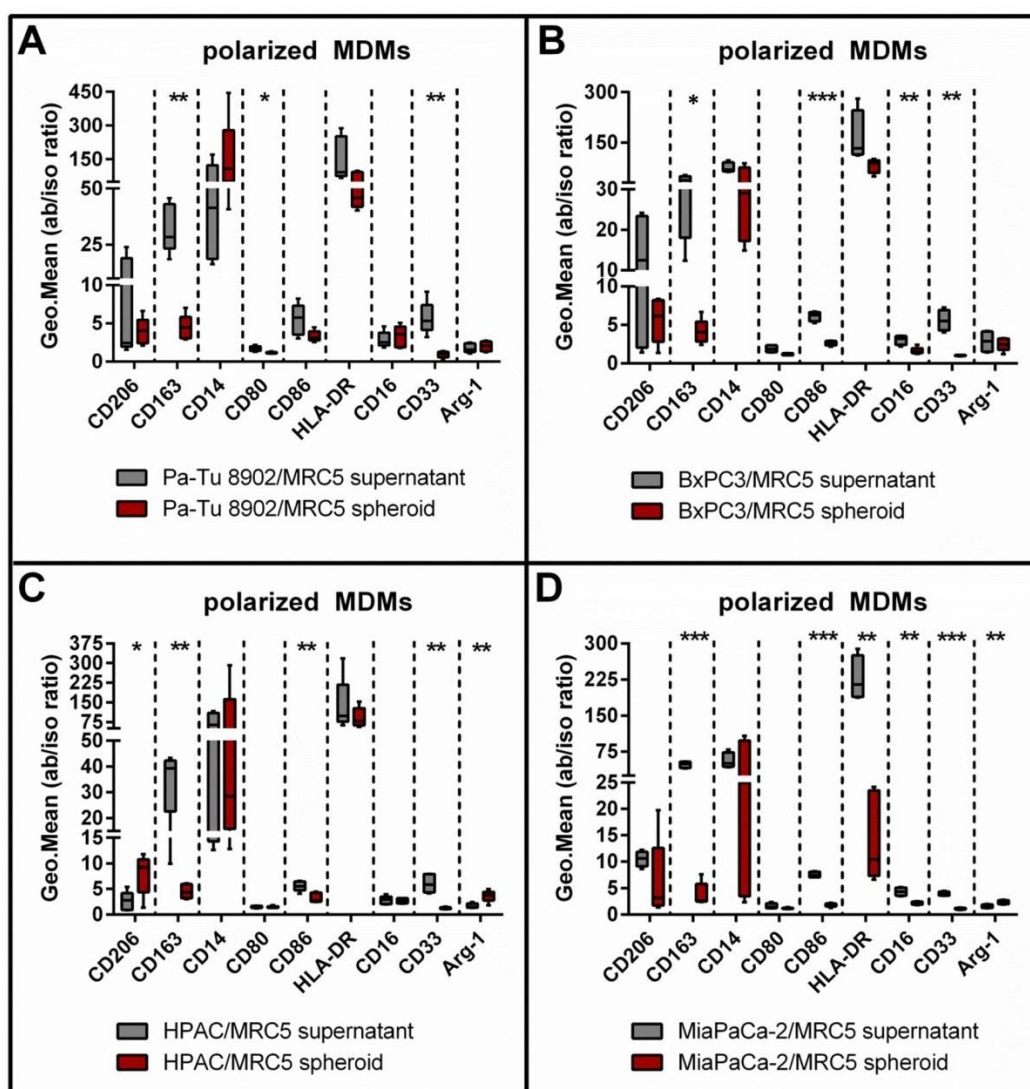
Figure 25: Differential cell surface marker expression of M2 and M1 macrophage marker on MDMs differentiated either with tumor cell/fibroblast spheroids or supernatant.

Tumor cells and fibroblasts were co-cultured for 5 days. Monocytes were either added to co-culture on day 5 to differentiate for 6 days or 3D co-culture supernatant was collected to culture freshly isolated monocytes for 6 days in poly-Hema coated plates without spheroids. Spheroids were collected and dissociated by using Accutase to obtain a single cell suspension. Cell surface marker expression of 3D spheroid polarized MDMs was compared to 3D supernatant differentiated MDMs. Typical M2 and M1 macrophage marker were analysed by flow cytometry. Supernatant differentiated MDMs expressed higher levels of CD163, HLA-DR, CD86 and CD33 compared to spheroid polarized MDMs. Statistical significance was calculated of n= 5 independent experiments by using an unpaired Student´s t test with unequal variances; *$p < 0.05$, **$p < 0.01$, ***$p < 0.001$.

4.4.2 Analysis of RNA transcriptome of tumor cell/fibroblast spheroid polarized MDMs

To determine the differential gene expression of typical M1 and M2 macrophage marker (Fig. 26) as well as from pro- and anti-inflammatory cytokines and chemokines (Fig. 27) on RNA transcriptome level, spheroid polarized MDMs were isolated from tumor cell/fibroblast co-cultures and analysed by RNA sequencing. Interestingly, both M1 and M2 macrophage marker expression could be detected in spheroid polarized MDMs in a tumor cell line dependent manner (Fig. 26). High expression of CD163 and CD14, typical M2 macrophage marker, was observed in MDMs co-cultured with BxPC3, MiaPaCa-2 and Pa-Tu 8902 tumor cells, and was comparable to CD163 expression in *in vitro* generated M2c macrophages. Inhibitory molecules such as Arg-1 and IDO were slightly upregulated in MDMs co-cultured with spheroids compared to M2c macrophages or monocytes. Although increased expression of M1 macrophage marker such as HLA-DR could also be detected here, expression on protein level measured by flow cytometry clearly showed an M2-like phenotype of the mentioned markers.
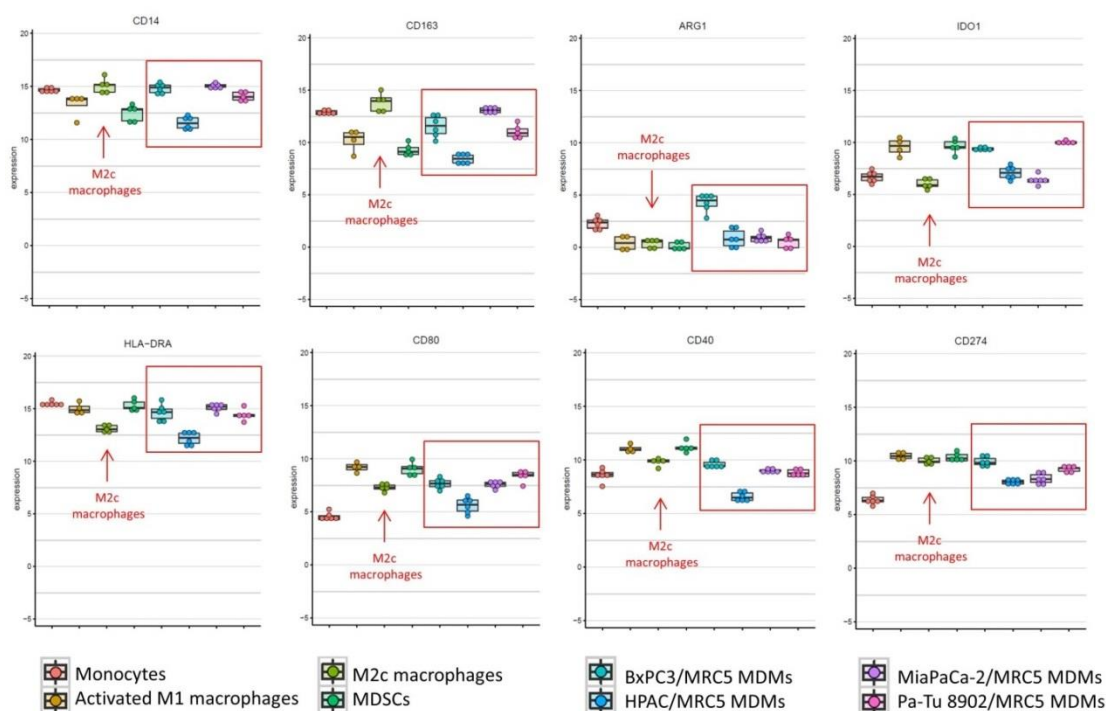

Figure 26: Differential M1/M2 macrophage gene expression profile of spheroid polarized MDMs.
Tumor cells and fibroblasts were co-cultured for 5 days. Monocytes were added to co-culture on day 5. CD11b^{+} myeloid cells were isolated from spheroids after 6 days. Gene expression of 3D myeloid cells was compared to *in vitro* generated MDSCs, M2c and activated M1 macrophages as well as to freshly isolated blood monocytes. Expression of typical M2 and M1 macrophage marker were analyzed by RNA whole transcriptome sequencing. Shown are n= 6 independent experiments.

The up-regulated expression of immunosuppressive cytokines like IL-10 or angiogenic chemokines such as IL-8 and down-regulated inflammatory cytokines including TNF and IL-12β by spheroid polarized MDMs is comparable to the expression profile of M2c macrophages (Fig. 27). Even though, spheroid polarized MDMs showed differential gene expression profiles of both M1 and M2 macrophage marker, the expression of several immunosuppressive and angiogenic cytokines and chemokines led to the conclusion that spheroid polarized more closely resemble *in vitro* generated M2c macrophages than activated M1 macrophages. Cytokines and chemokines secreted in tumor cell/fibroblast supernatants with and without spheroid polarized MDMs were therefore analysed by Luminex technology to characterize the cytokine milieu more closely.
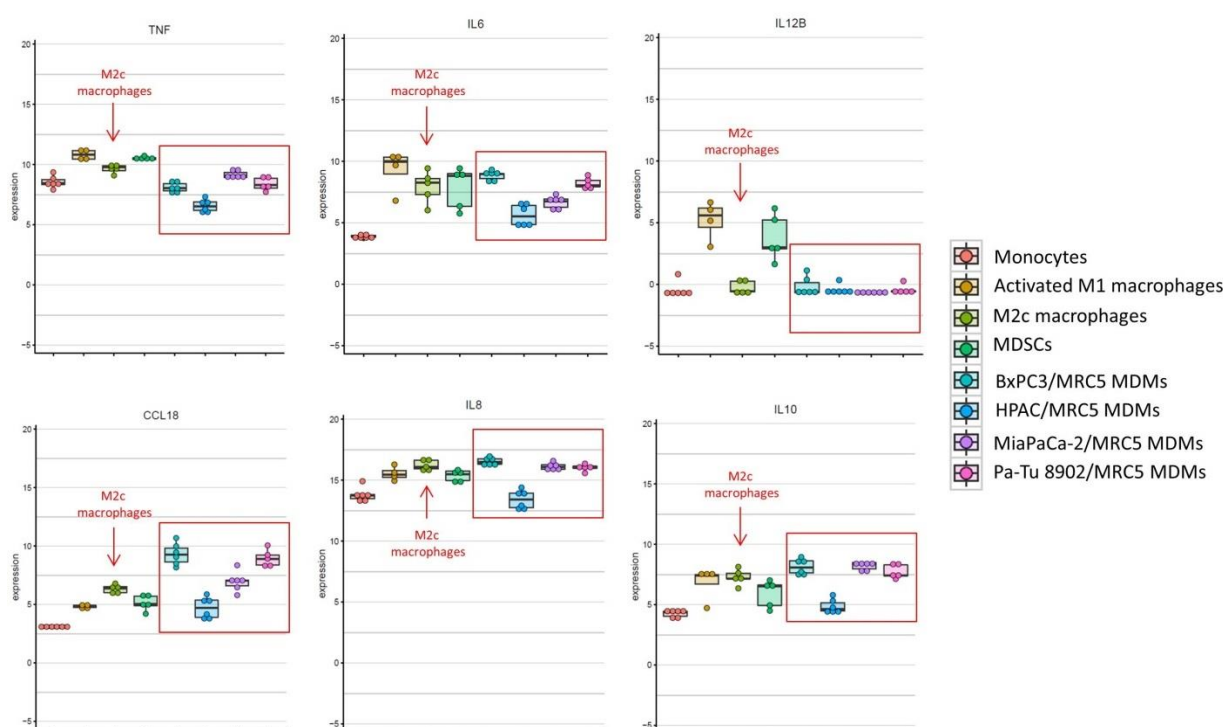

Figure 27: Differential cytokine/chemokine gene expression profile of spheroid polarized MDMs.
Tumor cells and fibroblasts were co-cultured for 5 days. Monocytes were added to co-culture on day 5. CD11b^{+} myeloid cells were isolated from spheroids after 6 days. Gene expression of 3D myeloid cells was compared to *in vitro* generated MDSCs, M2c and activated M1 macrophages as well as to freshly isolated blood monocytes. Expression of pro- and anti-inflammatory cytokines and chemokines were analyzed by RNA whole transcriptome sequencing. Shown are n= 6 independent experiments.

4.6 Expanding the 3D tumor cell/fibroblast/MDM co-culture with CD3⁺ T cells

M2 macrophages are known to induce a suppressive tumor microenvironment by secreting anti-inflammatory cytokines and inhibiting T cell activation and proliferation. To analyse the functional abilities of M2-like spheroid polarized MDMs, autologous CD4⁺ and CD8⁺ T cells were activated with CD3/CD28 activation beads in the presence of 3D tumor cell/fibroblast co-cultures with polarized MDMs on day 11. CD3/CD28 activation beads were titrated in order to determine the optimal degree of T cell activation to be able to see inhibitory effects of spheroid polarized MDMs. According to the applied CD3/CD28 activation bead : T cell ratio, differences in T cell proliferation were detected when comparing T cells in co-culture with tumor cell/fibroblast spheroids with and without polarized MDMs (Fig. 28). For the assay to choose the appropriate bead concentration, the pancreatic cancer cell lines Pa-Tu 8902 and BxPC3 in co-culture with MRC5 fibroblasts were used. As expected, the T cell proliferation for both CD4⁺ and CD8⁺ T cells strongly declined with the reduced concentration of CD3/CD28 activation beads (Fig. 28 A and B). T cells co-cultured with tumor cells, fibroblasts and spheroid polarized MDMs did not proliferate as much as T cells in tumor cell/fibroblast co-culture without spheroid polarized MDMs. Bead: T cell ratios of 1:8 and 1:16 led to significant effects with regard to the inhibition of T cell proliferation by spheroid polarized MDMs, therefore a concentration of 1 bead to 16 T cells was chosen for future experiments.
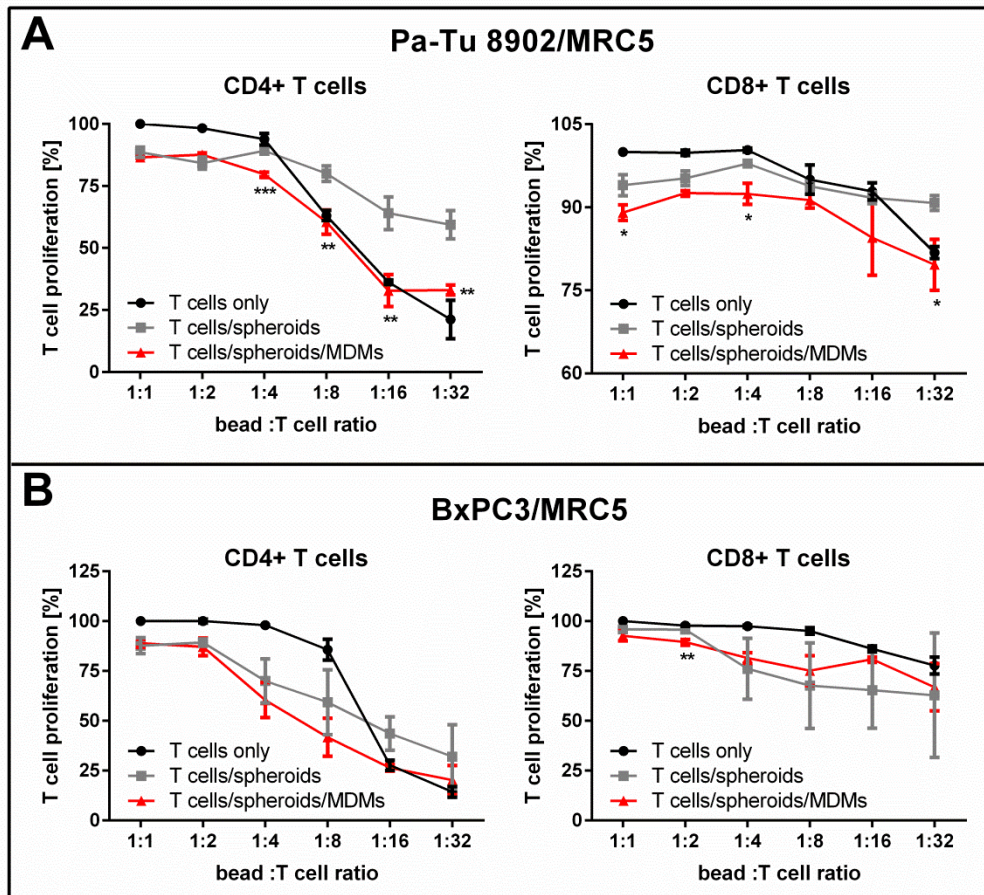
Figure 28: Titration of CD3/CD28 activation beads for optimal CD3^{+} T cell proliferation.
Tumor cells and fibroblasts were co-cultured for 5 days to form tight spheroids. Freshly isolated monocytes were added on day 5 to differentiate for 6 days. Autologous CD3^{+} T cells were labeled with CFSE on day 11, added to co-cultures with and without 10.000 monocytes and stimulated with different concentrations of CD3/CD28 activation beads. Proliferation was measured after 6 days using flow cytometry. T cells alone proliferated strongly for each bead concentration (black) similar to T cells in co-culture with tumor cell and fibroblasts (grey). The strongest suppression of T cell proliferation in tumor cell/fibroblast co-culture with MDMs (red) compared to co-culture without MDMs was observed. Statistical significance (T cells/spheroids vs. T cells/spheroids/MDMs) was calculated of n= 3 independent experiments by using an unpaired Student´s *t* test with unequal variances; *p < 0.05, **p < 0.01, ***p < 0.001.

4.6.1 Spheroid polarized MDMs inhibit T cell proliferation in 3D co-culture

Spheroid polarized MDMs closely resembling *in vitro* generated M2c macrophages, expressing typical M2-like macrophage marker such as CD163 and also secreting molecules that have immunosuppressive functions subsequently led us to investigate if these cells had the functional ability to inhibit T cell activation and proliferation.
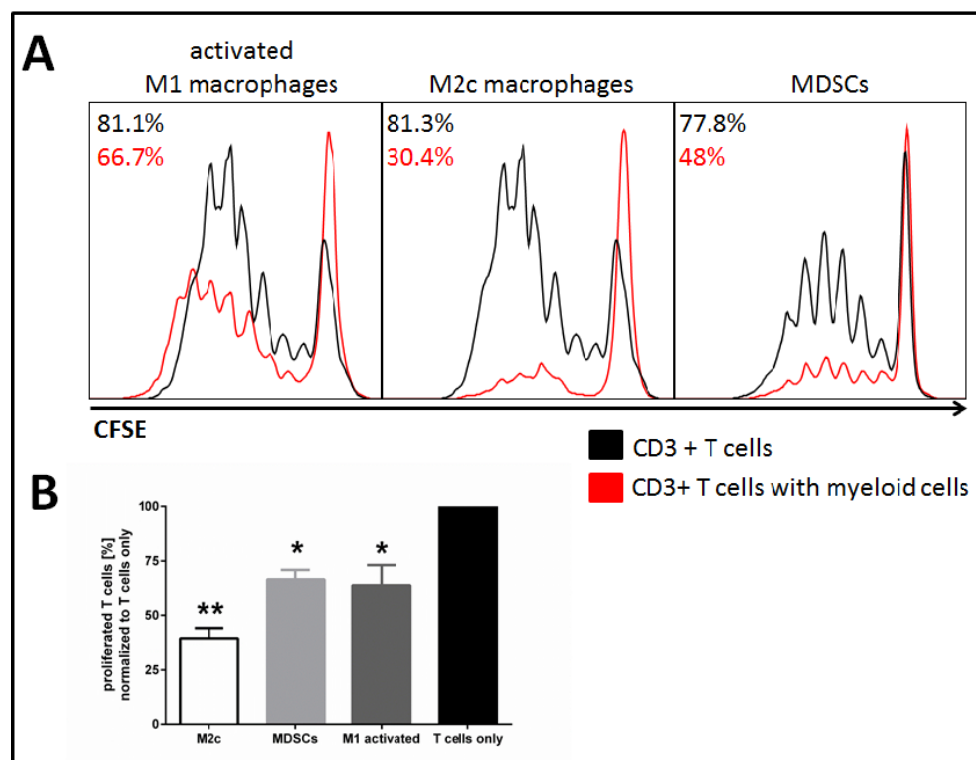

Figure 29: *In vitro* **generated M2c macrophages strongly suppress CD3+ T cell proliferation compared to MDSCs and activated M1 macrophages.**
Freshly isolated monocytes were differentiated into M2c macrophages, activated M1 macrophages and MDSCs within 6 days as described before. On day 6, macrophages were detached using Accutase and seeded into 96 well flat-bottom plates. Autologous CD3+ T cells were labelled with CFSE, added to macrophages in a ratio of 1:5 and stimulated with CD3/CD28 activation beads. Proliferation was measured after 6 days using flow cytometry. A) T cells alone proliferated strongly (black), whereas M2c macrophages strongly suppressed T cell proliferation in contrast to MDSCs and activated M1 macrophages (red) B) CD3+ T cell proliferation was more effectively suppressed in co-culture with *in vitro* generated M2c macrophages compared to co-culture with MDSCs and activated M1 macrophages. Statistical significance was calculated of n= 4 independent experiments by using an unpaired Student´s *t* test with unequal variances; *p < 0.05, **p < 0.01, ***p < 0.001.

First, *in vitro* generated MDSCs, M2c and activated M1 macrophages were co-cultured with autologous CFSE labelled CD3^{+} T cells and proliferation was measured by flow cytometry (Fig 29 A). As expected, immunosuppressive M2c macrophages strongly inhibited T cell proliferation (30 %

proliferating T cells) in contrast to activated M1 macrophages (67 % proliferating T cells). Around 48 % of T cells co-cultured with MDSCs, which express both M2 and M1 cell surface markers, were able to proliferate and therefore showed suppressive capacity comparable to activated M1 macrophages (Fig. 29 A and B).
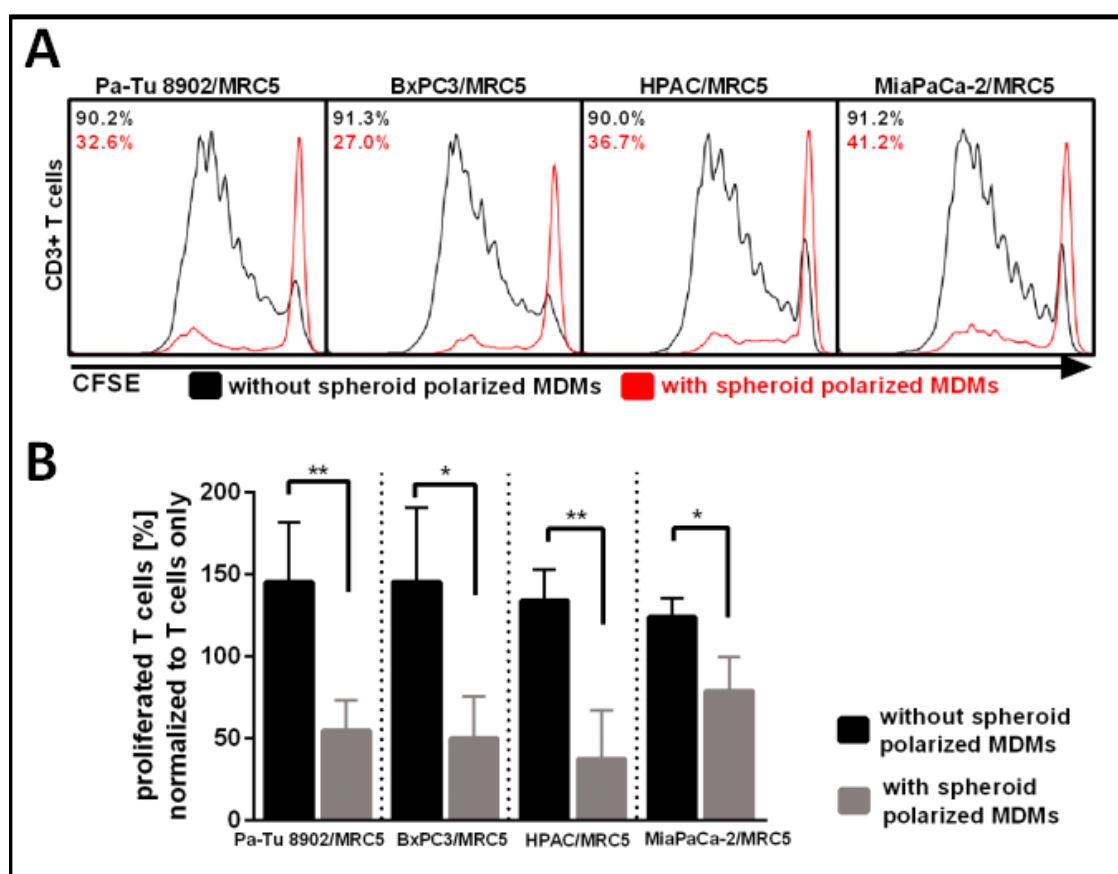

Figure 30: 3D co-culture polarized MDMs suppress CD3+ T cell proliferation.
Tumor cells and fibroblasts were co-cultured for 5 days to form tight spheroids. Freshly isolated monocytes were added on day 5 to differentiate for 6 days. Autologous CD3$^+$ T cells were labelled with CFSE on day 11, added to co-cultures with and without 10.000 monocytes and stimulated with CD3/CD28 activation beads. Proliferation was measured after 6 days using flow cytometry. A) T cells proliferated strongly in co-culture with tumor cell and fibroblasts (black), but were suppressed in co-culture with 10.000 spheroid polarized MDMs (red). B) Strongest suppression of T cell proliferation was observed in Pa-Tu 8902/MRC5 and HPAC/MRC5 co-cultures with spheroid polarized MDMs. Statistical significance was calculated of n= 4 independent experiments by using an unpaired Student´s t test with unequal variances; *p < 0.05, **p < 0.01, ***p < 0.001.

The immunosuppressive function of spheroid polarized MDMs was compared to *in vitro* generated macrophages and MDSCs. Data obtained from the T cell proliferation assays showed that proliferation was indeed significantly inhibited (27% - 41% of proliferating T cells) in co-cultures containing spheroid polarized MDMs (Fig. 30). T cell suppression of MDMs was tumor cell line independent, however, MDMs co-cultured with Pa-Tu 8902/MRC5 and HPAC/MRC5 spheroids most

effectively inhibited T cell proliferation. T cell suppression induced by the spheroid polarized MDMs was comparable to the *in vitro* generated M2c macrophages (30% proliferating T cells) in contrast to activated M1 macrophages (67% proliferating T cells) or MDCs (48% proliferating T cells) (Fig. 29 A and 30). These findings indicated that spheroid polarized MDMs co-cultured with pancreatic tumor cell lines and MRC5 fibroblasts not only showed an M2-like macrophage phenotype in terms of cell surface marker expression and cytokine profile, but could also functionally suppress T cell proliferation.

4.6.2 Impaired activation of CD4$^+$ and CD8$^+$ T cells in the presence of spheroid polarized MDMs in 3D co-culture

After observing a strong inhibition of proliferation of T cells by spheroid polarized MDMs, we investigated the phenotypic changes that occurred in the T cells co-cultured with tumor cell/fibroblast spheroids with or without MDMs. 6 days after CD3/CD28 mediated T cell activation, the expression of several cell surface markers was measured by flow cytometry. We evaluated the expression of the early activation markers CD25 and CD69, immune-modulatory molecules like 4-1BB and the cell surface checkpoint molecules PD1 and CTLA4 (Fig. 31). Early activation markers CD69 and CD25 were both up-regulated upon T cell stimulation in co-culture with pancreatic cancer cells and fibroblasts. However, in the presence of spheroid polarized MDMs independent of the tumor cell line MDMs and T cells have been co-cultured with, the expression for CD25 was significantly lower on both CD4$^+$ and CD8$^+$ T cell sub-populations. A clear but non-significant decrease regarding the expression of CD69 was also observed in both CD4$^+$ and CD8$^+$ T cells. Furthermore, we observed a decrease in the expression of the activating co-stimulatory molecule 4-1BB up to 5-fold on CD4$^+$ T cells and 2-fold on CD8$^+$ T cells in the presence of spheroid polarized MDMs in comparison to activated T cells in co-culture with tumor cells and fibroblasts alone (Fig. 31). Surface expression of the immune check point molecules PD-1 and CLTA-4 was significantly down-regulated in the presence of spheroid polarized MDMs. Taken together, we observed that the functional inhibition of T cell proliferation by spheroid polarized MDMs was also reflected by a significant reduction of cell surface activation markers on both CD4$^+$ and CD8$^+$ T cells.
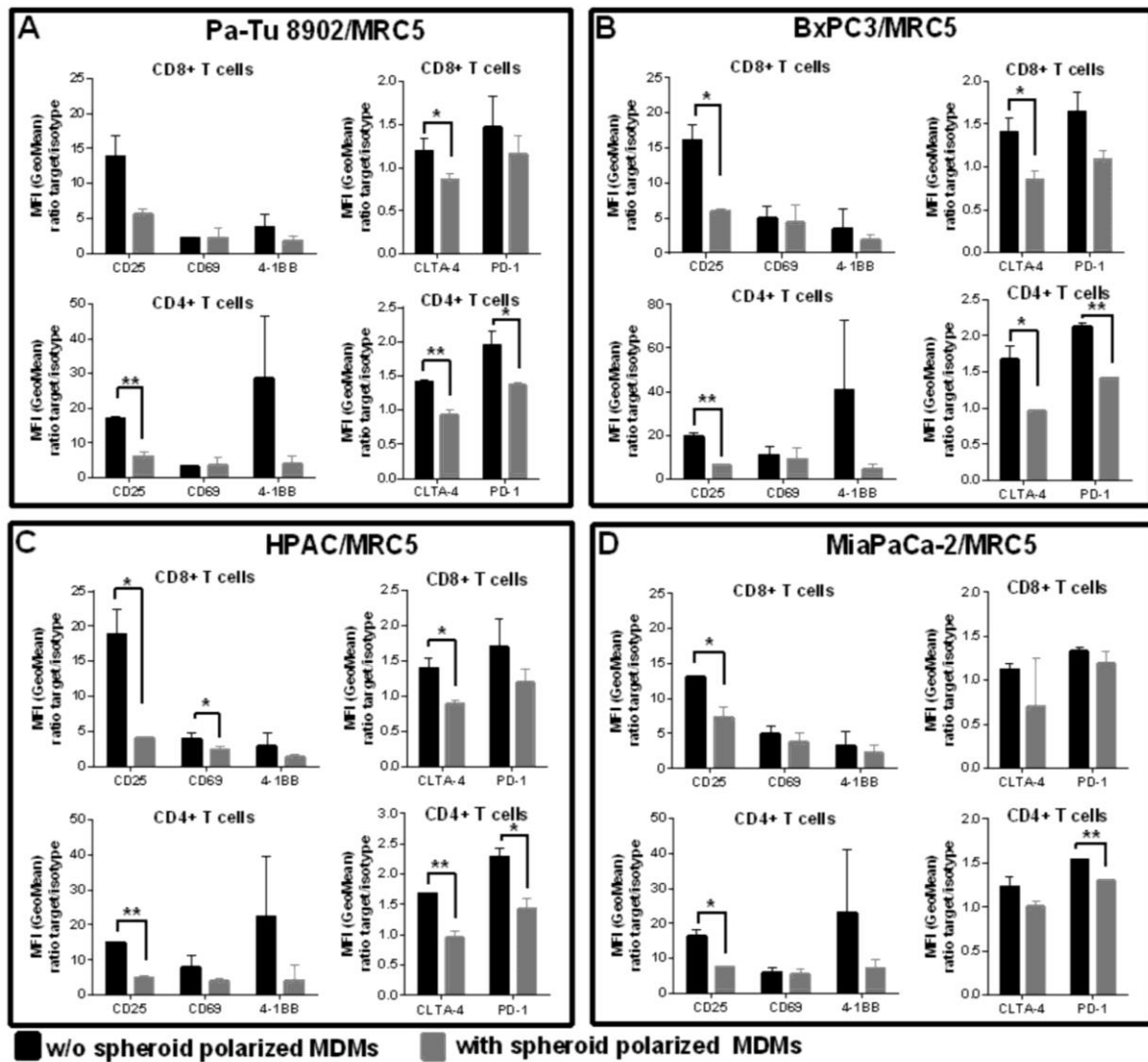
Figure 31: Expression of cell surface activation and checkpoint marker on CD4^{+} and CD8^{+} decreases in 3D tumor cell/fibroblast co-culture with spheroid polarized MDMs.

Tumor cells and fibroblasts were co-cultured for 5 days to form tight spheroids. Freshly isolated monocytes were added on day 5 to differentiate for 6 days. Autologous CD8^{+} and CD4^{+} T cells were added to co-cultures with and without spheroid polarized MDMs on day 11 and stimulated with CD3/CD28 activation beads. The expression of all markers were measured on the cell surface of CD8^{+} and CD4^{+} T cells 6 days after T cell activation by flow cytometry. Statistical significance was calculated of n= 3 independent experiments by using an unpaired Student´s t test with unequal variances; *p < 0.05, **p < 0.01, ***p < 0.001.

4.6.3 Treatment of spheroid polarized MDMs with immune modulating agents partially restores T cell proliferation in 3D co-cultures

Suppression of T cell proliferation and the reduction of cell surface activation markers on both CD4^{+} and CD8^{+} T cells induced by spheroid polarized MDMs raised the question whether we would be able to influence immune cell behaviour by applying either activating or inhibitory immune modulating agents to the 3D co-culture (Fig 32). We therefore evaluated if we could revert T cell suppression by using CD40 and TLR8 ligands to re-activate spheroid polarized immunosuppressive MDMs as well as by using Arginase-I and iNOS inhibitors to block T cell suppressing enzymes. For all of these compounds used, a clear, but non-significant cell line dependent tendency of increased CD4^{+} and CD8^{+} T cell proliferation compared to T cell proliferation in untreated 3D co-culture could be observed (Fig. 32 A and B). The inhibiting molecules Arginase-I and iNOS only showed a slight, but non-significant cell-line dependent reversion of T cell proliferation for both CD8^{+} and CD4^{+} T cells (Fig. 32 A). The combination of Arginase-I and iNOS inhibitors did not lead to improved T cell proliferation in comparison to single compound treatment. Furthermore, CD4^{+} and CD8^{+} T cells cultured with BxPC3/MRC5/MDMs spheroids did not respond to Arginase-I and iNOS treatment, whereas the proliferation of 10% - 20% of the T cells co-cultured with MiaPaCa-2 tumor cells could be restored again. The activating molecules CD40 and TLR8 ligands reverted T cell proliferation for both CD8^{+} and CD4^{+} T cells co-cultured with tumor cells, fibroblasts and spheroid polarized MDMs stronger than the inhibiting molecules (Fig. 32 B). The combination of CD40/TLR8 ligands did seem to be slightly more effective in a cell line dependent way than the single agent treatment, showing the increased T cell proliferation especially in HPAC/MRC5/MDM co-culture. We observed that combined treatment of CD40 and TLR8 ligands seemed to affect CD4^{+} and CD8^{+} T cells differently, with 40% proliferating CD8^{+}, but only 20% proliferating CD4^{+} T cells. Although no statistically significant differences could be detected for most of the treatments, we observed a strong donor variation in response to the compounds regarding the reversal of T cell proliferation. These data indicated that the treatment of spheroid polarized MDMs with molecules that block immune suppressive factors such as Arginase-I and iNOS as well as with molecules that re-activate MDMs has the potential to influence and restore T cell proliferation in our 3D co-culture model.
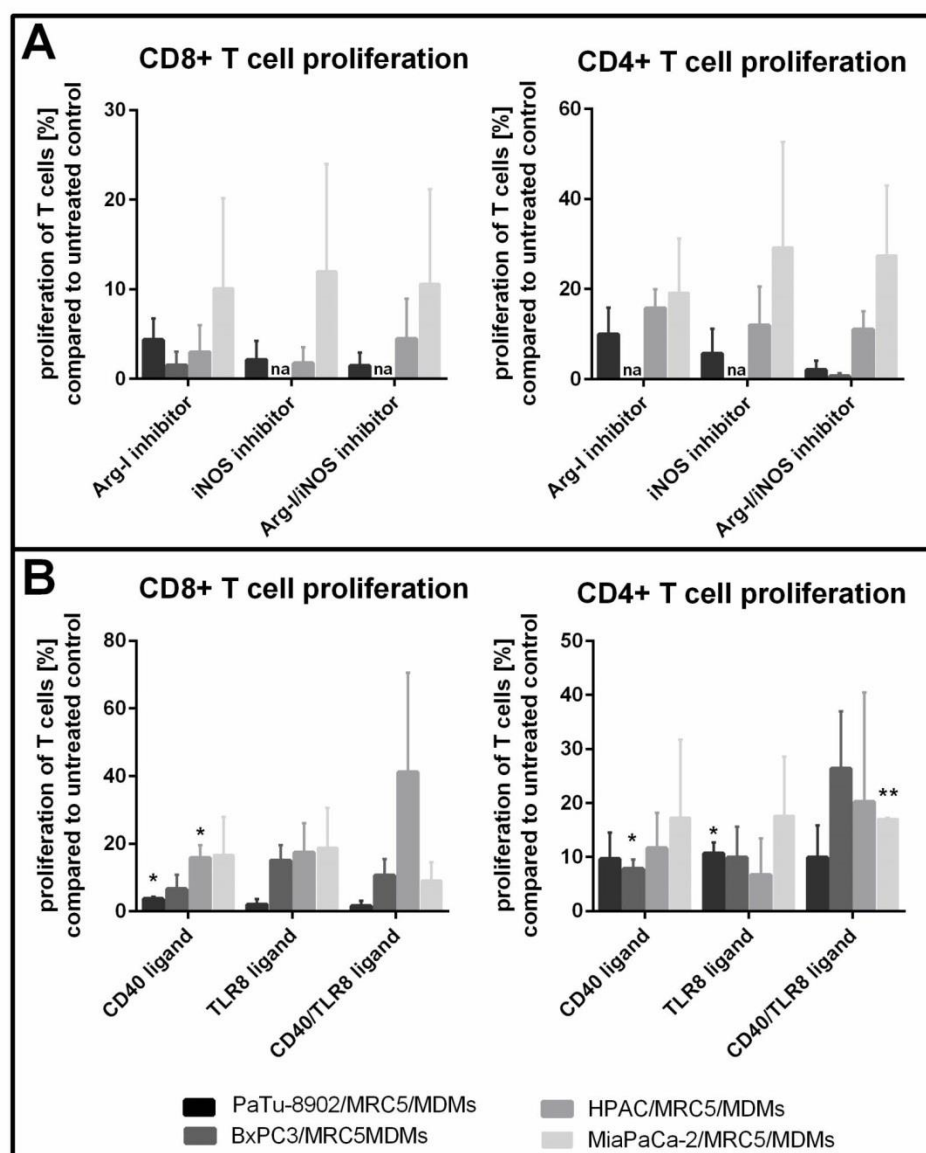
Figure: 32: Compound treatment of 3D co-culture spheroids, MDMs and T cells to restore T cell proliferation. Tumor cells and fibroblasts were co-cultured for 5 days to form tight spheroids. 10.000 freshly isolated monocytes were added on day 5 to differentiate for 6 days. One day prior T cell addition, co-cultures were treated with A) inhibiting or B) activating compounds either alone or in combination. Autologous CD3^{+} T cells were labelled with CFSE on day 11, added to co-cultures with and without spheroid polarized MDMs and stimulated with CD3/CD28 activation beads. Proliferation was measured after 6 days using flow cytometry. Statistical significance was calculated of n= 3 independent experiments by using an unpaired Student´s *t* test with unequal variances; *p < 0.05, **p < 0.01, ***p < 0.001.

5. Discussion

The development of cell cultures has marked a breakthrough regarding the versatility of research studies and advancement of scientific field trials. The development of synthetic growth media and the establishment of cell lines such as hybrid mammalian cells revolutionized the implementation and study of cell culture methods. Fundamental knowledge about cell culture technology was gained throughout the last decades, highlighting the importance of the cell microenvironment and leading to investigations about composition and physiochemical properties of the cell microenvironment to support the emulation of cell lines to their physiological origins [62].

Since the establishment of these *in vitro* 2D cell monolayers, cell culture models have become increasingly important not only to obtain basic knowledge about cell morphology, signalling and behaviour, but also to study cell-cell interactions, to produce antibodies and vaccines as well as to support drug discovery and screening. The increasing challenges and requirements, which *in vitro* methods need to fulfil, has led to the development of more complicated *in vitro* systems such as 3D cell culture or bioreactors mimicking a more physiologically relevant cell microenvironments. In cancer research, the importance of investigating the tumor cell microenvironment and the interaction between tumor cells and immune cells as well as assessing therapeutic drug efficacy requires the establishment of such 3D co-culture models involving more than two or even three cell types [63].

To address this issue, we designed a 3D co-culture model involving tumor cells, fibroblasts, monocytes and T cells. We focused on pancreatic cancer cell lines, since hallmarks of pancreatic cancer are strong desmoplastic reactions depending on fibroblasts, high infiltration of immune cells interacting with tumor cells and fibroblasts and leading to chemotherapeutic resistance of the tumor. The established 3D co-culture model may lead to better understanding of cellular mechanism between different cell types within the tumor microenvironment and can provide solutions to help overcome tumor resistance.

5.1 *In vitro* 3D model of tumor cell - fibroblast - immune system interactions

Although it is clear that crosstalk between tumor cells und tumor stroma plays an important role in tumor growth, tumor-mediated immune suppression and drug resistance, most of the data has been gained by investigating co-cultures with traditional 2D monolayers. Findings and observations made by using 2D cell culture methods are most often not reproducible in *in vivo* situations and can hardly predict outcomes of clinical trials given the unique characteristics of the tumor and its immune composition [64]. Pre-clinical studies to test different therapeutic strategies include both *in vivo* mouse models and *in vitro* studies. Both methods have their own advantages and drawbacks. Although mouse models are closer to patient tumors, differences between mouse and human immune mechanisms and lack of cross reactivity limit the relevance of these experiments. Reflecting the *in vivo* situation in a superior way compared to 2D monolayers, 3D co-culture systems are able to provide critical insight into the role of the inflammatory tumor microenvironment and its interaction between desmoplastic fibroblasts as well as with immune cells in cancer progression and therapy resistance. Studies have already reported that drug responsiveness is limited in 3D systems compared to 2D monolayers [65, 66]. To establish 3D models, most studies focus on one or two cell lines to observe cell-cell interaction, but to achieve a more realistic *in vivo* situation, not only tumor cells and fibroblasts, but also immune cells have to be kept into account [67]. Fibroblasts and immune cells have been reported to play a key role in tumor initiation, progression and metastasis of PDAC and various strategies including immunotherapies are currently being tested [68-70]. Tumor-associated macrophages, in particular, have been linked to poor prognosis in more than 80% of analysed cancer types [15, 71].

We previously established a 3D co-culture model to investigate crosstalk between pancreatic, breast as well as lung cancer cells and fibroblasts and showed that the model reflected the clinical situation and influenced therapeutic response *in vitro* [56]. In this previous study, different cell number ratios of tumor cells and fibroblasts were analysed to optimize the cell viability and survival of the co-culture [56]. Based on these data, a ratio of 1 tumor cell to 1.5 fibroblasts was chosen for the establishment of 3D co-cultures in this research project. As described for lung and breast cancer cells co-cultured with fibroblasts, we also observed differences in morphology when cells were either co-cultured in a 2D monolayer setting or in 3D spheroids [72]. Tumor cells and especially fibroblasts were found to be flattened on the bottom of the cell culture plate with each cell type forming islands around the other. The 3D co-culture spheroid however, provides an architectural scaffold for pancreatic cancer cells, which is critical for their form and function and better supports cellular

interactions that also occur *in vivo*. The 4 different pancreatic cancer cell lines we co-cultured with MRC5 fibroblasts and showed increased survival and the ability of all tumor cell lines to form similar sized dense spheroids indicated that interactions between tumor cells and fibroblasts strongly support tumor growth in a cell line dependent manner. Nevertheless, studies to show the promotional effect of fibroblasts on tumor growth of various cancer cell lines provide conflicting data depending on the fibroblast cell line and the 3D method used, again displaying the complexity of tumor microenvironments and pointing out challenges, which *in vitro* 3D models still need to overcome [73, 74].

To better reflect tumor-mediated immune suppression *in vitro*, we extended our 3D tumor cell/fibroblast model with freshly isolated monocytes. We systematically analysed the viability and the cytokine profile of the co-cultures, phenotype of the spheroid polarized MDMs and their functional behaviour and influence on T cells. So far, there are only limited 3D studies with 3 or more different cell types. In a human breast cancer model, the survival and progression of breast cancer cells in the presence of fibroblasts and either M1 or M2 differentiated macrophages has shown a reduction of tumor cell growth if co-cultured with M1 differentiated macrophages, whereas the presence of M2 differentiated macrophages seemed to promote tumor cell growth [75]. High infiltration of TAMs into different types of tumor tissue correlate with unfavourable clinical outcomes and promote tumor growth, which points out the importance of determining the appropriate number of monocytes included to our 3D co-culture model [32, 76]. The viability of our 3D tumor cell/fibroblast co-culture differed in regard to the number of monocytes added to the co-cultures. Too few monocytes did not influence the tumor cell/fibroblast survival in contrast to high numbers of monocytes, which led to a strong decrease of the co-culture viability most likely due to excessive nutrient uptake and increased production of cellular waste. As further experiments aimed to analyse the phenotype and function of spheroid polarized MDMs, we proved the necessity of cell-cell contact between tumor cells, fibroblasts and monocytes to keep monocytes alive in a 3D culture setting by culturing monocytes alone with co-culture supernatants. Even though soluble molecules including growth factors were present, the moncytes were not able to survive without cell-cell interactions and spheroid contact.

5.2 Infiltration of M2-like MDMs into 3D spheroids and the role of soluble molecules within tumor microenvironments

The most common leukocyte cell population accounting for 30 % to 50 % of the total inflammatory cells found within the tumor microenvironment are TAMs. Depending on the tumor stage and microenvironment, they are able to cause contrasting effects on tumor progression [77]. The correlation between the presence of TAMs in tumors and tumor growth has been shown widely for a variety of tumor malignancies including laryngeal carcinoma, breast cancer, gastric cancer as well as pancreatic cancer [76-78]. Infiltration of immune cells into tumor tissue alters the response and sensitivity of tumors towards chemotherapeutic compounds, often leading to drug resistant tumours. Hence, establishing a model to assess infiltration of immune cells into 3D spheroids in high-throughput screenings is important [79]. In this study, we evaluated 3 methods to optically detect spheroid polarized MDMs that infiltrated the 3D tumor cell/fibroblast spheroids. As previously pointed out, the analysis of 3D spheroids is often limited by their size and other morphological parameters, making it difficult to obtain images of the whole specimen and to quantify single cells within such a 3D spheroid [58]. So far, the need to generate a, for example, stable green fluorescent protein (GFP) reporter gene cell line provides the best possibility to trail immune cells, which migrate into tumor spheroids *in vitro*. Furthermore, cell lines which only form loose cell aggregations instead of tight spheroids and have small spheroid diameters of up to 250 μm facilitate the penetration of cell dyes as well as the migration of immune cells into the whole spheroid [80]. To be able to optically examine 3D spheroids, the choice of the appropriate 3D culturing method and imaging technology may also be essential for further analysis [81]. In our study, we evaluated confocal microscopy, light sheet ultra-microscopy and immunohistochemistry to detect myeloid cell migration into tumor spheroids. 3 of 4 tumor cell lines used in co-culture with fibroblasts turned out to form tight spheroids with diameter up to 500 μm. Penetration of dyes such as DAPI or Hoechst into the centre of the spheroid could not be achieved, although spheroids were fixed and permeabilized prior to the staining process, making it difficult to analyse spheroids using confocal or light sheet ultra-microscopy. Using immunohistochemistry, we were able to detect spheroid infiltrated myeloid cells within spheroids in a cell line dependent manner in the best possible way. Recruitment of myeloid cells into tumor tissue is regulated by cytokines, chemokines and growth factors, which are derived from cancer cells and stroma tissue in the microenvironment [27]. High numbers of infiltrated TAMs have been shown to correlate with poor prognosis [82, 83]. High density of TAMs within tumor tissue are associated with angiogenesis, differentiation of cancer cells and the expression of tumor-promoting cytokines [84]. In our model, we could reproduce infiltration of myeloid cells into tumor

tissue and thus provide a realistic model to investigate tumor cell – immune cell interactions and immune cell – mediated resistance of tumors against chemotherapeutic compounds.

Not only has immune cell infiltration been associated with secretion of various soluble molecules such as cytokines and chemokines but also worse clinical outcomes the. Cytokines regulate biological processes including cell differentiation, cell migration, metabolism, immunity and inflammation. In pancreatic cancer, many pro- and anti-inflammatory cytokines and chemokines have been found to be overexpressed, modulating the tumor microenvironment and directly influencing cancer cells and immune cells in a paracrine manner [85]. Since cytokine profiles differ dramatically from tissue to tissue, act redundantly and almost always work in concert, reliable predictions based on *in vitro* experiments regarding outcomes of clinical trials need to be handled with care [86]. In our 3D co-culture model, we systematically analysed the cytokine profile of the tumor cell/fibroblast co-cultures with and without spheroid polarized MDMs. CCL2 is a potent chemoattractant for monocyte recruitment into tumor tissue and promotes a shift of monocytes towards M2 macrophages and polarization of T helper cells towards T_H2 cells. High levels of the chemokine CCL-2 in pancreatic cancer, has been shown to be closely related to macrophage infiltration into tumors and could be detected in high levels in our 3D co-culture [27]. GM-CSF and M-CSF along with other cytokines like IL-6 and IL-8 have been shown to be involved in recruitment and differentiation of myeloid cells into M2 macrophages and myeloid derived suppressor cells (MDSCs) in the tumor apart from promoting tumor angiogenesis. So far, increased levels of IL-6 could be used as predictor of patient performance, as studies have shown a prognostic link between the elevated levels of inflammatory cytokines such as IL-6, IL-8 and TNF-α and tumor severity [87]. Increased levels of IL-6 and IL-8 often correlate with levels of IL-10, which has also been shown to impact patient survival in pancreatic cancer as well as in other malignancies like lung and colorectal cancer [86]. IL-10 is well known for its role in M2 macrophage differentiation and suppression of various myeloid cells and T cells. These cytokines were detected in the supernatants of our 3D co-culture and have also been shown to be present in PDAC patients [88, 89]. The presence of these cytokines has been linked to advanced tumor stages, angiogenesis and reduced effector cell functions, leading to a poor performance status and worse prognosis [90, 91].

A comprehensive analysis of the crosstalk between tumor cells, immune cells and the surrounding tissue microenvironment can provide better insights into the development and progression of cancer malignancies. Although the composition of immune cells found within tumor microenvironment varies from tumor to tumor, they can all be found in higher densities in tumor tissue than in non-

cancerous tissue. Immune cell infiltration and varying immune cell components depend on a complex cytokine and chemokine milieu within the tumor microenvironment, which allows and regulates activation and suppression of the immune system [92].

5.3 Macrophage polarization in pancreatic cancer

In the recent years, myeloid cell populations have been found to play a major role in the inflammatory tumor microenvironment of different tumor types. Myeloid cells like macrophages regulate and stimulate immune responses by antigen presentation to lymphocytes or suppress immune responses by releasing immune-suppressive molecules or expression of inhibitory receptors. In tumors of both mouse and humans, myeloid cells are able to promote tumor growth, neo-vascularization, metastasis and immune-suppression [93]. Monocytes recruited to the site of the tumor differentiate depending on the composition of the tumor milieu, which involves cytokines, chemokines and growth factors.

Tumor-associated macrophages represent a key factor, which contributes to the pathogenesis of PDAC. Several regulators have been reported to mediate M2 macrophage polarization in pancreatic cancer, including soluble molecules such as cytokines and chemokines, enzymes like the heparanase and various proteins as well as transcription factors [27]. Previous studies reported that the phenotypes of TAMs often differ based on the location and the stage of the tumor [94]. Evidence shows that cancer cells are able to modify phenotype and activity of TAMs and shift polarization towards a pro-tumorigenic phenotype, which then support tumor growth, survival and angiogenesis. TAMs in PDAC are defined as CD68$^+$ CD163$^+$ and CD204$^+$ positive and are associated with lymphatic metastasis [82]. It has also been shown that TAMs show high expression of CD14 and to some extent expression of the typical M1 macrophage marker HLA-DR and CD86 in breast cancer [95]. Expression of type-I Arginase, which is known to promote tumor growth by suppression of effector T cells, has been described as a marker of M2-like macrophages [96, 97]. Nevertheless, a number of studies reveal conflicting data concerning the plastic phenotype of macrophages within the tumor tissue of patients and the vast heterogeneity has yet not been intensively described. Clinical data shows that around 70 % of TAMs were M2 polarized macrophages, whereas the remaining 30 % present an M1 macrophage phenotype. Phenotype shifting from M1 into M2 then occurs during progression of cancer [98, 99]. In our 3D co-culture model, we observed that tumor/fibroblast spheroids induced an

M2 polarization of co-cultured monocytes with a CD14$^+$ CD163$^+$ HLA-DR^{low} CD86^{low} ARG-1$^+$ phenotype that strongly resembles the phenotype of TAMs reported in PDAC.

Studies using only tumor cell culture supernatant to differentiate the myeloid cell line THP-1 induced a mixed M1/M2 macrophage polarization, highlighting the importance of cell-cell interactions within the tumor microenvironment [100]. We also found that cell-cell contact between tumor cell/fibroblast spheroids and monocytes was essential to polarize monocytes towards an M2-like phenotype, whereas tumor cell/fibroblast supernatant led to a mixed phenotype of MDMs expressing high levels of typical M1 marker such as HLA-DR and CD86.

Although we identified the spheroid polarized MDM population as M2-like macrophages, this only seemed to apply on protein/receptor level. Transcriptome analysis revealed a mixed M1/M2 genotype and to some extend high similarities to the genotype of naïve monocytes and MDSCs. Along TAMs, MDSCs have also been described as immune cell subset with profound immune-suppressive abilities within the tumor microenvironment. They typically represent a mixture of immature myeloid cells at different differentiation stages and can be grouped into monocytic and polymorphonuclear granulocytic MDSCs [101]. In our study, we exclusively focused on monocytic MDSCs characterized by CD14$^+$, HLA-DR$^{low/neg}$ and CD33$^+$ marker expression, since we established a 3D co-culture model with freshly isolated CD14$^+$ monocytes [102]. Looking at the gene expression levels of several macrophage markers such as CD14, CD163 and IL-10, HPAC/MRC5 spheroid polarized MDMs resembled *in vitro* differentiated MDSCs more closely than *in vitro* generated M2c macrophages, although the boundaries between MDSCs and TAMs are not fully defined and monocytic MDSCs may be able to rapidly differentiate into TAMs [103, 104].

Using our 3D co-culture model, we were able to generate immune-suppressive myeloid cell subsets, which strongly resemble TAMs and MDSCs found in *in vivo* tumor tissues. It stands to reason that spheroid polarized MDMs behave in a more realistic and physiological way compared to 2D *in vitro* differentiated macrophages, which led us to investigate the immune-suppressive abilities and functions of our spheroid polarized MDMs. Understanding immune-suppression within the tumor microenvironment and targeting TAMs and MDSCs can open new therapeutic possibilities to control tumor growth and prevent metastasis.

5.4 TAM – mediated immunosuppression of T cells in the tumor microenvironment

Along immunosuppressive myeloid cells, tumor infiltrating lymphocytes (TILs) make up a large majority of hematopoietic cells and are typically localized in peritumoral fibrotic interstitial tissue. Few studies investigated the correlation between TIL infiltrates and patient survival and depending on the type of the tumor, the density and the distribution of TILs at different areas within the tumor tissue and stroma, TILs may either have an anti- or a pro-tumoral functions [105]. To escape T cells, tumors exploit a mechanism called T cell exhaustion, which is characterized by T cell effector dysfunction, up-regulation of inhibitory molecules and defective proliferative capacities. During the progression of the tumor, T cells step-wise lose these functional and phenotypic characteristics, facilitating the escape of tumor cells from the immune system [106]. Recruitment of TAMs to the site of the tumor leads to the generation of an immunosuppressive milieu and supports tumor immune evasion. The secretion of suppressive cytokines such as TGF-β and IL-10 by TAMs and expression of inhibitory molecules such as the enzyme Arginase-I, which metabolizes L-arginine to L-ornithine and urea thus depleting T cells of vital L-arginine, negatively affect TILs in the tumor microenvironment [107]. We observed some of these immune-suppressive mechanisms in our 3D co-culture system. Addition of monocytes to tumor cell/fibroblast co-cultures, which then differentiated into M2-like macrophages, led to the upregulation of immune-suppressive cytokines such as IL-10 and inhibitory molecules like Arginase-I.

So far, it has been reported that TILs in solid tumors may be functionally defective or incompletely activated, since often the presence of TILs, mostly CD3$^+$ T cells, does not prevent tumor growth and progression [108]. The presence of additional markers such as CD45RO indicate that most of the CD3$^+$ T cells found in tumors are memory T cells [105]. Infiltration of CD8$^+$ and CD4$^+$ T cells were shown to be a potential marker to better predict patient survival and high densities of T cells have been associated with good clinical outcomes for PDAC [105]. However, studies have revealed that cytotoxic CD45RO$^+$ CD8$^+$ memory T cells represent the major anti-tumor effector cells while the complex role of CD4$^+$ T cells more strongly depends on interactions with antigen-presenting cells (APCs) and the cytokine milieu [109, 110]. In our study, we observed that CD4$^+$ and CD8$^+$ T cells highly expressed CD45RO in co-culture with 3D tumor cell/fibroblast spheroids. Expression of CD45RO on T cells only was slightly reduced in co-culture with tumor cell/fibroblast spheroids and spheroid polarized MDMs. For ovarian cancer, it has been shown that TAMs could modulate the phenotype of memory T cells depending on secreted cytokines, allowing TAMs to maintain local

inflammation required for angiogenesis and metastasis [111]. However, the expression of CD45 isoforms does not give details about the activation status of these T cells.

The analysis of the activation status of T cells has shown that high expression of the T cell activation marker CD25 (Interleukin 2 receptor α) on T cells in cutaneous malignant melanoma correlates with longer survival. Low expression of CD25, however, indicated functional impairment of T cells, whereas the early T cell activation marker, CD69, could not be used to successfully predict the T cell activation status [112, 113]. These data are in line with our findings that the activation of T cells in co-culture with the spheroid polarized MDMs in our model down-regulate CD25 and CD69, indicating impaired activation of these cells. Other immune check point/modulatory markers like 4-1BB; PD1 and CTLA4 are known to be up-regulated upon T cell activation. 4-1BB is reported to be a biomarker for tumor-reactive T cells which are able to inhibit tumor growth *in vivo* [114]. T cell expression of PD-1 and CTLA-4 showed impaired T cell function during the effector phase when engaged with their ligands and restrain anti-tumor immunity [115]. These markers were down-regulated in our co-culture model when T cells were co-cultured with spheroid polarized MDMs but not when co-cultured with 3D tumor cell/fibroblast spheroids only. TAMs have also been reported to not only suppress T cell activation but also inhibit proliferation of T cells in the tumor microenvironment *in vivo* [116, 117]. Presence of spheroid polarized MDMs in our co-culture model not only suppressed T cell activation as reflected by low expression of T cell activation markers, but also inhibited T cell proliferation in our *in vitro* system. In breast cancer, it has been shown that up-regulation of PD-L1 on TAMs and receptor engagement with PD-1 on T cells results in T cell exhaustion and apoptosis. In addition, TAMs can indirectly inhibit T cell proliferation by the production anti-inflammatory cytokines such as IL-10, PGE_2 and prostanoids [117].

To better understand the complex crosstalk between immune cells within the tumor microenvironment, a physiologically relevant model for further *in vitro* studies is essential. So far, our findings show that our 3D co-culture model created such a suitable niche to mimic *in vivo* conditions and induced *in vivo* like phenotype in the immune cell types involved. The characterization of the distribution of immune cells within the tumor as well as their highly heterogeneous phenotype and function can help to find new potential biomarkers and to develop new treatment strategies in order to improve the clinical outcome for patients.

5.5 Cancer immunotherapy in pancreatic cancer

The role of the immune system in the development of tumor malignancies has now been discussed and investigated intensively for decades. Tumor cells, which are recognized and eliminated by immune cells, develop several mechanism to evade immune controls, including the production of immunosuppressive molecules and the up-regulation of inhibitory receptors [118]. Despite all the efforts to continuously gain better understanding of deregulated pathways in PDAC, immune evasion strategies and resistance mechanisms, therapeutic advances and the development of better treatment options has remained static [119]. In the recent past, developing new cancer immunotherapies has been the focus of research due to the limited success in treating PDAC patients with standard of care therapies like chemo- , radiation therapy as well as surgery. Characterizing immune suppression and escape mechanisms and finding suitable targets for immune-based therapies will be the challenge in developing new treatment strategies such as peptide and DNA vaccines against tumor-associated antigens (TAAs), adoptive T cell transfers, usage of checkpoint inhibitors or the modulation of APCs [120].

To overcome immune suppression, studies have focused on targeting checkpoint marker such as PD-1 and CTLA-4, but also on pro-inflammatory receptors such as CD40 to reverse the immunosuppressive phenotype of M2-like macrophages into pro-tumoral M1 macrophages or on immune cell depletion from the tumor [38]. Since high densities of immunosuppressive TAMs are symptomatic for pancreatic cancer and correlate with negative clinical outcomes, aiming at the depleting TAMs from the tumor microenvironment also holds promising treatment potential as shown by Ries and colleagues [89, 94]. Preventing TAMs to infiltrate tumors by blocking the signalling of chemotactic molecules such as CSF-1, they were able to strongly reduce the number of TAMs within several solid tumors using anti-CSF-1R antibodies [89]. Efforts have also been made to target TAMs in order to re-program their immunosuppressive phenotype or to induce activation of APCs to mediate anti-tumor T cell responses. CD40, the member of the tumor necrosis factor receptor superfamily, which is widely expressed on APCs such as dendritic cells and monocytes, has been intensively studies as potential target in cancer immunotherapy [121]. Anti-CD40 antibodies have been found to mimic the CD40 ligand, thus triggering to the activation of APCs and leading to stimulation and activation of T cells [122]. In several studies, anti-CD40 antibody has been shown to re-activate macrophages in pancreatic cancer mouse models, which led to the recruitment of anti-tumor M1 macrophages to the tumor site, the depletion of tumor stroma and subsequently to increased efficacy of chemotherapeutical agents such as gemcitabine [122, 123]. Since several years,

the potential of TLR agonists to promote activation of monocytes or dendritic cells is also being investigated. But so far, TLR agonists have to be chosen used with caution as they can promote either anti-tumor and pro-tumor effects depending on costimulatory molecules expressed on APCs and tumor cells. Treatment of single TLR agonist also show limited efficacy, which highlights the need of combination therapies using different TLR agonists or chemotherapeutical compounds [124]. Combination studies of TLR8 agonist and chemotherapeutic agents such as doxorubicin in ovarian cancer already demonstrated positive effects on inhibiting tumor progression [125]. In our study, we investigated the immune modulation of M2-like polarized MDMs and T cells in tumor cell/fibroblast co-cultures using a CD40 ligand and TLR8 agonist. The natural TLR8 ligand is foreign single-stranded RNA and upon ligand engagement, the activation of APCs and secretion of T_H1-polarizing cytokines is induced [125]. Using these immune-stimulatory compounds, we could already observe increased, but non-significant T cell proliferation due to re-activation of spheroid polarized MDMs by CD40 ligand treatment, also in combination with TLR8 in our 3D co-culture model. These effects were cell line dependent and though non-significant due to high donor variations, showed that certain treatments cannot be applied to all patients, hence highlighting the importance of personalized medicine and healthcare. Nevertheless, this could further be improved by different combinations of various activating molecules such as different TLR ligands. Among different therapies such as aiming to reduce the recruitment and survival of macrophages, switching the pro-tumoral phenotype of immunosuppressive M2-like macrophages to immune-activating anti-tumoral M1 macrophages holds the most promising potential, since macrophages react highly sensitive to stimuli within the PDAC microenvironment [126].

Therapeutic strategies modulating tumor-infiltrated leukocytes such as CD4$^+$ and CD8$^+$ T cells targeting immunosuppressive enzymes produced by macrophages such as Arginase-I or iNOS, have been investigated intensively [127]. Furthermore, checkpoint molecules such as CTLA-1 or PD-1, which both belong to the CD28 receptor family, represent promising targets and are expressed on activated T cells, essentially regulating immune cell responses. Engagement of these receptors leads to the inhibition of T cell activation and hence the down-regulation of immune cell responses [128]. In clinical studies, patients with tumors and TAMs highly expressing PD-L1 or CTLA-4 were shown to have a worse clinical prognosis [38]. But to date, clinical trials regarding pancreatic cancer with molecules such as anti-PD-1 and anti-CTLA-4 ended with disappointing outcomes, emphasizing the need for combination therapies that focus on multiple immune cells and checkpoint markers to treat tumors of patients who do not respond to single agent therapies [37, 38]. In our co-culture model however, the expression level of these molecules is rather low on T cells (PD-L1 and CTLA-4). In line

with the outcomes of clinical studies and based on our data, one could speculate that targeting PD1/PDL1 or CTLA4 would not be a successful approach in the long-run. Instead, a combination therapies need to be investigated more closely, starting with molecules that increase the expression of the above mentioned molecules (for e.g. CD40 activation) or remove the suppressive factors/cells (IL-10/Arginase-I inhibition or depletion of M2 macrophages by targeted therapy like CSF1R) would be more effective. Focusing on cancer immunotherapy as potential treatment for pancreatic cancer has been a challenge so far. In future, a profound understanding of the tumor microenvironment as well as of tumor resistance mechanisms may help to develop new therapeutic treatment strategies.

6. Conclusion and perspective

Pancreatic cancer is still one of the most complex and lethal tumor malignancies world-wide, despite intensive research investigations over the last decades [129]. There is an urgent need to develop physiologically relevant tumor models in order to gain better knowledge and understanding regarding tumor progression and immune system evasion. Since novel immunotherapy strategies hold the most promising potential in combating PDAC, the establishment of *in vitro* 3D tumor models has become a major focus of cell culture research [130].

We established a 3D co-culture tumor model and have extended tumor cells and fibroblasts co-culture by the inclusion of immune cell components. TAMs and T cells have been major targets of cancer immunotherapies, so investigating the complex interplay between these cell types and how they contribute to drug resistance needs to be fully addressed in future [119]. Our 3D co-culture model represents a potential tool to study cell-cell interactions and to better predict drug efficacy, nevertheless, based on the complexity of the *in vivo* tumor microenvironment, it comes along with potential limitations. In the context of PDAC, many cell types other than TAMs and T cells as well as soluble factors are involved in the process leading to tumor immune escape. Granulocytes, granulocytic MDSCs or NK cells have also been reported to be present in the PDAC microenvironment and are absent in our 3D co-culture model [26]. *In vitro* cell culture models are still simplistic compared to *in vivo* models and even though 3D cell cultures can combine specific tumor attributes such as providing a 3D architecture as well as different immune cell types, they are not able to represent all ECM components as well as angiogenic factors [131]. Research is now focused on developing bio-engineered multi-organ tissues that provide a more realistic and predictive approach to assess drug toxicity and investigate cell-cell interactions more closely [132]. These systems are very close to the patient situation and offer flexibility in analysing various cell types within a tumor microenvironment.

In conclusion, 3D co-culture models are a reliable and suitable tool to study the complex crosstalk between the different cell types in the tumor to further advance the development of novel therapeutic therapies. However, limitations that come along with these systems need to be carefully evaluated and new methods must be critically assessed. In future, 3D cell culture models may be able to effectively close the gap between traditional *in vitro* 2D monolayers and *in vivo* animal models by focusing on understanding resistance mechanisms to existing immunotherapies and identification of alternative mechanisms for therapeutic targeting, subsequently clearing the way for improving personalized medical health care.

7. References

1.   Society, A.C. *Cancer Facts and Figures*. Atlanta, GA: Am. Cancer Soc. 2017; Available from: https://cancerstatisticscenter.cancer.org/#/.

2.   Lowenfels, A.B. and P. Maisonneuve, *Epidemiology and risk factors for pancreatic cancer.* Best practice & research. Clinical gastroenterology, 2006. **20**(2): p. 197-209.

3.   Gandini, S., et al., *Tobacco smoking and cancer: a meta-analysis.* International journal of cancer, 2008. **122**(1): p. 155-64.

4.   Pandol, S., et al., *Epidemiology, risk factors, and the promotion of pancreatic cancer: role of the stellate cell.* Journal of gastroenterology and hepatology, 2012. **27 Suppl 2**: p. 127-34.

5.   Li, D., et al., *Body mass index and risk, age of onset, and survival in patients with pancreatic cancer.* JAMA, 2009. **301**(24): p. 2553-62.

6.   Hidalgo, M., *Pancreatic cancer.* The New England journal of medicine, 2010. **362**(17): p. 1605-17.

7.   Hruban, R.H. and N. Fukushima, *Pancreatic adenocarcinoma: update on the surgical pathology of carcinomas of ductal origin and PanINs.* Modern Pathology, 2007. **20**: p. S61-S70.

8.   Maitra, A. and R.H. Hruban, *Pancreatic cancer.* Annual review of pathology, 2008. **3**: p. 157-88.

9.   Lavina Malhotra, D.A., Mark Bloomston, *The Pathogenesis, Diagnosis, and Management of Pancreatic Cancer.* Journal of Gastrointestinal & Digestive System 2015. **5**: p. 278.

10.   Mazur, P.K. and J.T. Siveke, *Genetically engineered mouse models of pancreatic cancer: unravelling tumour biology and progressing translational oncology.* Gut, 2012. **61**(10): p. 1488-500.

11.   Michl, P., S. Pauls, and T.M. Gress, *Evidence-based diagnosis and staging of pancreatic cancer.* Best practice & research. Clinical gastroenterology, 2006. **20**(2): p. 227-51.

12.   Klauss, M., et al., *Value of three-dimensional reconstructions in pancreatic carcinoma using multidetector CT: Initial results.* World Journal of Gastroenterology, 2009. **15**(46): p. 5827-5832.

13.   Rasheed, Z.A., W. Matsui, and A. Maitra, *Pathology of pancreatic stroma in PDAC*, in *Pancreatic Cancer and Tumor Microenvironment*, P.J. Grippo and H.G. Munshi, Editors. 2012: Trivandrum (India).

14.   Erkan, M., et al., *The Activated Stroma Index Is a Novel and Independent Prognostic Marker in Pancreatic Ductal Adenocarcinoma.* Clinical Gastroenterology and Hepatology, 2008. **6**(10): p. 1155-1161.

15.   Joyce, J.A. and J.W. Pollard, *Microenvironmental regulation of metastasis.* Nature reviews. Cancer, 2009. **9**(4): p. 239-52.

16.   Carr, R.M. and M.E. Fernandez-Zapico, *Pancreatic cancer microenvironment, to target or not to target?* EMBO molecular medicine, 2016. **8**(2): p. 80-2.

17.   Erkan, M., et al., *Tumor microenvironment and progression of pancreatic cancer.* Experimental oncology, 2010. **32**(3): p. 128-31.

18.   Feig, C., et al., *The pancreas cancer microenvironment.* Clinical cancer research : an official journal of the American Association for Cancer Research, 2012. **18**(16): p. 4266-76.

19.   Lohr, M., et al., *Transforming growth factor-beta1 induces desmoplasia in an experimental model of human pancreatic carcinoma.* Cancer research, 2001. **61**(2): p. 550-5.

20. Frantz, C., K.M. Stewart, and V.M. Weaver, *The extracellular matrix at a glance.* Journal of Cell Science, 2010. **123**(24): p. 4195-4200.

21. Rozario, T. and D.W. DeSimone, *The extracellular matrix in development and morphogenesis: a dynamic view.* Developmental biology, 2010. **341**(1): p. 126-40.

22. Schaefer, L. and R.M. Schaefer, *Proteoglycans: from structural compounds to signaling molecules.* Cell and tissue research, 2010. **339**(1): p. 237-46.

23. Grivennikov, S.I., F.R. Greten, and M. Karin, *Immunity, inflammation, and cancer.* Cell, 2010. **140**(6): p. 883-99.

24. DeNardo, D., P. Andreu, and L.M. Coussens, *Interactions between lymphocytes and myeloid cells regulate pro- versus anti-tumor immunity.* Cancer and Metastasis Reviews, 2010. **29**(2): p. 309-316.

25. Shiao, S.L., et al., *Immune microenvironments in solid tumors: new targets for therapy.* Genes & Development, 2011. **25**(24): p. 2559-2572.

26. Chang, J.H., Y. Jiang, and V.G. Pillarisetty, *Role of immune cells in pancreatic cancer from bench to clinical application: An updated review.* Medicine, 2016. **95**(49): p. e5541.

27. Cui, R., et al., *Targeting tumor-associated macrophages to combat pancreatic cancer.* Oncotarget, 2016. **7**(31): p. 50735-50754.

28. Quatromoni, J.G. and E. Eruslanov, *Tumor-associated macrophages: function, phenotype, and link to prognosis in human lung cancer.* American journal of translational research, 2012. **4**(4): p. 376-89.

29. Lin, W.W. and M. Karin, *A cytokine-mediated link between innate immunity, inflammation, and cancer.* Journal of Clinical Investigation, 2007. **117**(5): p. 1175-1183.

30. Karnevi, E., R. Andersson, and A.H. Rosendahl, *Tumour-educated macrophages display a mixed polarisation and enhance pancreatic cancer cell invasion.* Immunology and cell biology, 2014. **92**(6): p. 543-52.

31. De Palma, M. and C.E. Lewis, *Macrophage regulation of tumor responses to anticancer therapies.* Cancer cell, 2013. **23**(3): p. 277-86.

32. Hao, N.B., et al., *Macrophages in tumor microenvironments and the progression of tumors.* Clinical & developmental immunology, 2012. **2012**: p. 948098.

33. Ghaneh, P., E. Costello, and J.P. Neoptolemos, *Biology and management of pancreatic cancer.* Gut, 2007. **56**(8): p. 1134-1152.

34. Kanji, Z.S. and S. Gallinger, *Diagnosis and management of pancreatic cancer.* CMAJ : Canadian Medical Association journal = journal de l'Association medicale canadienne, 2013. **185**(14): p. 1219-26.

35. Herreros-Villanueva, M., et al., *Adjuvant and neoadjuvant treatment in pancreatic cancer.* World Journal of Gastroenterology, 2012. **18**(14): p. 1565-72.

36. Vincent, A., et al., *Pancreatic cancer.* Lancet, 2011. **378**(9791): p. 607-20.

37. Foley, K., et al., *Current progress in immunotherapy for pancreatic cancer.* Cancer letters, 2016. **381**(1): p. 244-51.

38. Kunk, P.R., et al., *From bench to bedside a comprehensive review of pancreatic cancer immunotherapy.* Journal for immunotherapy of cancer, 2016. **4**: p. 14.

39. Long, J., et al., *Overcoming drug resistance in pancreatic cancer.* Expert opinion on therapeutic targets, 2011. **15**(7): p. 817-28.

40. Chand, S., et al., *The Landscape of Pancreatic Cancer Therapeutic Resistance Mechanisms.* International journal of biological sciences, 2016. **12**(3): p. 273-82.

41.   Ireland, L., et al., *Chemoresistance in Pancreatic Cancer Is Driven by Stroma-Derived Insulin-Like Growth Factors.* Cancer research, 2016. **76**(23): p. 6851-6863.

42.   Hwang, C.I., et al., *Preclinical models of pancreatic ductal adenocarcinoma.* The Journal of pathology, 2016. **238**(2): p. 197-204.

43.   Behrens, D., W. Walther, and I. Fichtner, *Pancreatic cancer models for translational research.* Pharmacology & therapeutics, 2017.

44.   Edmondson, R., et al., *Three-Dimensional Cell Culture Systems and Their Applications in Drug Discovery and Cell-Based Biosensors.* Assay and Drug Development Technologies, 2014. **12**(4): p. 207-218.

45.   Pampaloni, F., E.G. Reynaud, and E.H.K. Stelzer, *The third dimension bridges the gap between cell culture and live tissue.* Nature Reviews Molecular Cell Biology, 2007. **8**(10): p. 839-845.

46.   Lee, J.M., et al., *A three-dimensional microenvironment alters protein expression and chemosensitivity of epithelial ovarian cancer cells in vitro.* Laboratory investigation; a journal of technical methods and pathology, 2013. **93**(5): p. 528-42.

47.   Ravi, M., et al., *3D Cell Culture Systems: Advantages and Applications.* Journal of Cellular Physiology, 2015. **230**(1): p. 16-26.

48.   King, S.C.a.M., *Gather Round: In Vitro tumor spheroids as improved models of in vivo tumors.* Bioengineering & Biomedical Science, 2012. **2**(4).

49.   Kim, J.B., *Three-dimensional tissue culture models in cancer biology.* Seminars in Cancer Biology, 2005. **15**(5): p. 365-77.

50.   Hongisto, V., et al., *High-Throughput 3D Screening Reveals Differences in Drug Sensitivities between Culture Models of JIMT1 Breast Cancer Cells.* PloS one, 2013. **8**(10).

51.   Birgersdotter, A., R. Sandberg, and I. Ernberg, *Gene expression perturbation in vitro--a growing case for three-dimensional (3D) culture systems.* Seminars in Cancer Biology, 2005. **15**(5): p. 405-12.

52.   Loessner, D., et al., *Bioengineered 3D platform to explore cell-ECM interactions and drug resistance of epithelial ovarian cancer cells.* Biomaterials, 2010. **31**(32): p. 8494-506.

53.   Breslin, S. and L. O'Driscoll, *Three-dimensional cell culture: the missing link in drug discovery.* Drug Discovery Today, 2013. **18**(5-6): p. 240-249.

54.   Ivascu, A. and M. Kubbies, *Rapid generation of single-tumor spheroids for high-throughput cell function and toxicity analysis.* Journal of biomolecular screening, 2006. **11**(8): p. 922-32.

55.   Kelm, J.M., et al., *Method for generation of homogeneous multicellular tumor spheroids applicable to a wide variety of cell types.* Biotechnology and Bioengineering, 2003. **83**(2): p. 173-180.

56.   Majety, M., et al., *Fibroblasts Influence Survival and Therapeutic Response in a 3D Co-Culture Model.* PloS one, 2015. **10**(6): p. e0127948.

57.   Chambers, K.F., et al., *3D Cultures of prostate cancer cells cultured in a novel high-throughput culture platform are more resistant to chemotherapeutics compared to cells cultured in monolayer.* PloS one, 2014. **9**(11): p. e111029.

58.   Antoni, D., et al., *Three-dimensional cell culture: a breakthrough in vivo.* International journal of molecular sciences, 2015. **16**(3): p. 5517-27.

59.   Yamada, K.M. and E. Cukierman, *Modeling tissue morphogenesis and cancer in 3D.* Cell, 2007. **130**(4): p. 601-10.

60.   Cunningham, B., *[Illinois] ECE 416 Fluorescent Beads*, M.b. assay, Editor. 2013.

61. Illumina, I. *An introduction to next-generation sequencing technology*. 2016; Available from: https://www.illumina.com/content/dam/illumina-marketing/documents/products/illumina_sequencing_introduction.pdf.

62. Carlos Omar Rodríguez-Hernandez, S.E.T.-G., Carlos Olvera-Sandoval, Flor Yazmín Ramírez-Castillo, Abraham Loera Muro, Francisco Javier Avelar-Gonzalez, Alma Lilián Guerrero-Barrera, *Cell Culture: History, Development and Prospects.* International Journal of Current Research and Academic Review 2014. **2**(12): p. 188-200.

63. Shin, C.S., et al., *Development of an in vitro 3D tumor model to study therapeutic efficiency of an anticancer drug.* Molecular pharmaceutics, 2013. **10**(6): p. 2167-75.

64. Levinger, I., Y. Ventura, and R. Vago, *Life is Three Dimensional-As In Vitro Cancer Cultures Should Be.* Advances in Cancer Research, Vol 121, 2014. **121**: p. 383-414.

65. Imamura, Y., et al., *Comparison of 2D-and 3D-culture models as drug-testing platforms in breast cancer.* Cancer research, 2015. **75**.

66. Lee, J.M., et al., *A three-dimensional microenvironment alters protein expression and chemosensitivity of epithelial ovarian cancer cells in vitro.* Laboratory Investigation, 2013. **93**(5): p. 528-542.

67. Koeck, S., et al., *Infiltration of lymphocyte subpopulations into cancer microtissues as a tool for the exploration of immunomodulatory agents and biomarkers.* Immunobiology, 2016. **221**(5): p. 604-617.

68. Inman, K.S., A.A. Francis, and N.R. Murray, *Complex role for the immune system in initiation and progression of pancreatic cancer.* World Journal of Gastroenterology, 2014. **20**(32): p. 11160-11181.

69. Evans, A. and E. Costello, *The role of inflammatory cells in fostering pancreatic cancer cell growth and invasion.* Frontiers in Physiology, 2012. **3**.

70. Paniccia, A., et al., *Immunotherapy for pancreatic ductal adenocarcinoma: an overview of clinical trials.* Chinese Journal of Cancer Research, 2015. **27**(4): p. 376-391.

71. Weizman, N., et al., *Macrophages mediate gemcitabine resistance of pancreatic adenocarcinoma by upregulating cytidine deaminase.* Oncogene, 2014. **33**(29): p. 3812-9.

72. Liu, X.Q., et al., *Interactions among Lung Cancer Cells, Fibroblasts, and Macrophages in 3D Co-Cultures and the Impact on MMP-1 and VEGF Expression.* PloS one, 2016. **11**(5).

73. Morales, J. and M.L. Alpaugh, *Gain in cellular organization of inflammatory breast cancer: A 3D in vitro model that mimics the in vivo metastasis.* BMC cancer, 2009. **9**: p. 462.

74. Jaganathan, H., et al., *Three-Dimensional In Vitro Co-Culture Model of Breast Tumor using Magnetic Levitation.* Scientific Reports, 2014. **4**.

75. Teresa DesRochers, L.H., Lauren O´Donnell, Christina Mattingly, Stephen Shuford, Mark O´Rourke, Mary Rippon, William Edenfield, Matthew Gevaert, David Orr, Howland Crosswell *Macrophage incorporation into a 3D perfusion tri-culture model of human breast cancer.* Journal for Immunotherapy of cancer, 2015. **3(Suppl 2)**: p. P401.

76. Zhang, Y., et al., *High-infiltration of tumor-associated macrophages predicts unfavorable clinical outcome for node-negative breast cancer.* PloS one, 2013. **8**(9): p. e76147.

77. Lin, J.Y., et al., *Clinical significance of tumor-associated macrophage infiltration in supraglottic laryngeal carcinoma.* Chinese journal of cancer, 2011. **30**(4): p. 280-6.

78. Ishigami, S., et al., *Tumor-associated macrophage (TAM) infiltration in gastric cancer.* Anticancer research, 2003. **23**(5A): p. 4079-83.

79.   Giannattasio, A., et al., *Cytotoxicity and infiltration of human NK cells in in vivo-like tumor spheroids.* BMC cancer, 2015. **15**: p. 351.

80.   Robertson, F.M., et al., *Imaging and analysis of 3D tumor spheroids enriched for a cancer stem cell phenotype.* Journal of biomolecular screening, 2010. **15**(7): p. 820-9.

81.   Zanoni, M., et al., *3D tumor spheroid models for in vitro therapeutic screening: a systematic approach to enhance the biological relevance of data obtained.* Scientific Reports, 2016. **6**: p. 19103.

82.   Kurahara, H., et al., *Significance of M2-polarized tumor-associated macrophage in pancreatic cancer.* The Journal of surgical research, 2011. **167**(2): p. e211-9.

83.   Heusinkveld, M. and S.H. van der Burg, *Identification and manipulation of tumor associated macrophages in human cancers.* Journal of translational medicine, 2011. **9**: p. 216.

84.   Yuan, A., J.J.W. Chen, and P.C. Yang, *Pathophysiology of tumor-associated macrophages.* Advances in Clinical Chemistry, Vol 45, 2008. **45**: p. 199-223.

85.   Roshani, R., F. McCarthy, and T. Hagemann, *Inflammatory cytokines in human pancreatic cancer.* Cancer letters, 2014. **345**(2): p. 157-63.

86.   Feurino, L.W., et al., *Current update of cytokines in pancreatic cancer: pathogenic mechanisms, clinical indication, and therapeutic values.* Cancer investigation, 2006. **24**(7): p. 696-703.

87.   Wei Li, A.A., Min Li, *Inflammation and Pancreatic Cancer: A Tale of Two Cytokines.* Cell Biology: Research & Therapy, 2012. **1:1**.

88.   Bayne, L.J., et al., *Tumor-derived granulocyte-macrophage colony-stimulating factor regulates myeloid inflammation and T cell immunity in pancreatic cancer.* Cancer cell, 2012. **21**(6): p. 822-35.

89.   Ries, C.H., et al., *Targeting tumor-associated macrophages with anti-CSF-1R antibody reveals a strategy for cancer therapy.* Cancer cell, 2014. **25**(6): p. 846-59.

90.   Ebrahimi, B., et al., *Cytokines in pancreatic carcinoma: correlation with phenotypic characteristics and prognosis.* Cancer, 2004. **101**(12): p. 2727-36.

91.   Delitto, D., et al., *The inflammatory milieu within the pancreatic cancer microenvironment correlates with clinicopathologic parameters, chemoresistance and survival.* BMC cancer, 2015. **15**.

92.   Fridman, W.H., et al., *The immune contexture in human tumours: impact on clinical outcome.* Nature reviews. Cancer, 2012. **12**(4): p. 298-306.

93.   Murdoch, C., et al., *The role of myeloid cells in the promotion of tumour angiogenesis.* Nature reviews. Cancer, 2008. **8**(8): p. 618-31.

94.   Mielgo, A. and M.C. Schmid, *Impact of tumour associated macrophages in pancreatic cancer.* BMB reports, 2013. **46**(3): p. 131-8.

95.   Grugan, K.D., et al., *Tumor-Associated Macrophages Promote Invasion while Retaining Fc-Dependent Anti-Tumor Function.* Journal of Immunology, 2012. **189**(11): p. 5457-5466.

96.   Sharda, D.R., et al., *Regulation of Macrophage Arginase Expression and Tumor Growth by the Ron Receptor Tyrosine Kinase.* Journal of Immunology, 2011. **187**(5): p. 2181-2192.

97.   Schmieder, A., et al., *Differentiation and gene expression profile of tumor-associated macrophages.* Seminars in Cancer Biology, 2012. **22**(4): p. 289-297.

98.   Mantovani, A. and A. Sica, *Macrophages, innate immunity and cancer: balance, tolerance, and diversity.* Current opinion in immunology, 2010. **22**(2): p. 231-7.

99.   Ma, J.L., et al., *The M1 form of tumor-associated macrophages in non-small cell lung cancer is positively associated with survival time.* BMC cancer, 2010. **10**.

100.   Caras, I., et al., *Influence of tumor cell culture supernatants on macrophage functional polarization: in vitro models of macrophage-tumor environment interaction.* Tumori, 2011. **97**(5): p. 647-54.

101.   Greten, T.F., *Myeloid-derived suppressor cells in pancreatic cancer: more than a hidden barrier for antitumour immunity?* British Medical Journal - Gut, 2014. **63**: p. 1690-1691.

102.   Umansky, V., et al., *The Role of Myeloid-Derived Suppressor Cells (MDSC) in Cancer Progression.* Vaccines, 2016. **4**(4).

103.   Kumar, V., et al., *The Nature of Myeloid-Derived Suppressor Cells in the Tumor Microenvironment.* Trends in immunology, 2016. **37**(3): p. 208-20.

104.   Ugel, S., et al., *Tumor-induced myeloid deviation: when myeloid-derived suppressor cells meet tumor-associated macrophages.* Journal of Clinical Investigation, 2015. **125**(9): p. 3365-3376.

105.   Protti, M.P. and L. De Monte, *Immune infiltrates as predictive markers of survival in pancreatic cancer patients.* Frontiers in Physiology, 2013. **4**.

106.   Patil, S., R.S. Rao, and B. Majumdar, *T-cell Exhaustion and Cancer Immunotherapy.* Journal of international oral health : JIOH, 2015. **7**(8): p. i-ii.

107.   Rodriguez, P.C., et al., *Arginase I production in the tumor microenvironment by mature myeloid cells inhibits T-cell receptor expression and antigen-specific T-cell responses.* Cancer research, 2004. **64**(16): p. 5839-49.

108.   Miescher, S., et al., *Functional properties of tumor-infiltrating and blood lymphocytes in patients with solid tumors: effects of tumor cells and their supernatants on proliferative responses of lymphocytes.* Journal of Immunology, 1986. **136**(5): p. 1899-907.

109.   Ruffell, B., et al., *Lymphocytes in cancer development: polarization towards pro-tumor immunity.* Cytokine & growth factor reviews, 2010. **21**(1): p. 3-10.

110.   Zhu, J., H. Yamane, and W.E. Paul, *Differentiation of effector CD4 T cell populations (*).* Annual review of immunology, 2010. **28**: p. 445-89.

111.   Foucher, E.D., et al., *IL-34-and M-CSF-induced macrophages switch memory T cells into Th17 cells via membrane IL-1 alpha.* European Journal of Immunology, 2015. **45**(4): p. 1092-1102.

112.   Ladanyi, A., et al., *T-cell activation marker expression on tumor-infiltrating lymphocytes as prognostic factor in cutaneous malignant melanoma.* Clinical cancer research : an official journal of the American Association for Cancer Research, 2004. **10**(2): p. 521-30.

113.   Berd, D., et al., *Activation markers on T cells infiltrating melanoma metastases after therapy with dinitrophenyl-conjugated vaccine.* Cancer immunology, immunotherapy : CII, 1994. **39**(3): p. 141-7.

114.   Zhu, Y.W. and L.P. Chen, *CD137 as a Biomarker for Tumor-Reactive T Cells: Finding Gold in the Desert.* Clinical Cancer Research, 2014. **20**(1): p. 3-5.

115.   Winograd, R., et al., *Induction of T-cell Immunity Overcomes Complete Resistance to PD-1 and CTLA-4 Blockade and Improves Survival in Pancreatic Carcinoma.* Cancer Immunology Research, 2015. **3**(4): p. 399-411.

116.   Movahedi, K., et al., *Different tumor microenvironments contain functionally distinct subsets of macrophages derived from Ly6C(high) monocytes.* Cancer research, 2010. **70**(14): p. 5728-39.

117. Williams, C.B., E.S. Yeh, and A.C. Soloff, *Tumor-associated macrophages: unwitting accomplices in breast cancer malignancy.* NPJ breast cancer, 2016. **2**.

118. Paniccia, A., et al., *Immunotherapy for pancreatic ductal adenocarcinoma: an overview of clinical trials.* Chinese journal of cancer research = Chung-kuo yen cheng yen chiu, 2015. **27**(4): p. 376-91.

119. Schnurr, M., et al., *Strategies to relieve immunosuppression in pancreatic cancer.* Immunotherapy, 2015. **7**(4): p. 363-76.

120. Krishna Soujanya Gunturu, G.R., Muhammad Wasif Saif, *Immunotherapy updates in pancreatic cancer: are we there yet?* Therapeutic Advances in Medical Oncology, 2013. **5**(1): p. 81-89.

121. Vonderheide, R.H. and M.J. Glennie, *Agonistic CD40 antibodies and cancer therapy.* Clinical cancer research : an official journal of the American Association for Cancer Research, 2013. **19**(5): p. 1035-43.

122. Vonderheide, R.H., et al., *CD40 immunotherapy for pancreatic cancer.* Cancer immunology, immunotherapy : CII, 2013. **62**(5): p. 949-54.

123. Beatty, G.L., et al., *CD40 agonists alter tumor stroma and show efficacy against pancreatic carcinoma in mice and humans.* Science, 2011. **331**(6024): p. 1612-6.

124. Kaczanowska, S., A.M. Joseph, and E. Davila, *TLR agonists: our best frenemy in cancer immunotherapy.* Journal of Leukocyte Biology, 2013. **93**(6): p. 847-863.

125. Monk, B.J., et al., *Integrative Development of a TLR8 Agonist for Ovarian Cancer Chemoimmunotherapy.* Clinical Cancer Research, 2017. **23**(8): p. 1955-1966.

126. Zheng, X., et al., *Redirecting tumor-associated macrophages to become tumoricidal effectors as a novel strategy for cancer therapy.* Oncotarget, 2017.

127. Zarour, H.M., *Reversing T-cell Dysfunction and Exhaustion in Cancer.* Clinical cancer research : an official journal of the American Association for Cancer Research, 2016. **22**(8): p. 1856-64.

128. Johansson, H., et al., *Immune checkpoint therapy for pancreatic cancer.* World Journal of Gastroenterology, 2016. **22**(43): p. 9457-9476.

129. Wolfgang, C.L., et al., *Recent progress in pancreatic cancer.* CA: a cancer journal for clinicians, 2013. **63**(5): p. 318-48.

130. Hirt, C., et al., *"In vitro" 3D models of tumor-immune system interaction.* Advanced Drug Delivery Reviews, 2014. **79-80**: p. 145-154.

131. Nyga, A., U. Cheema, and M. Loizidou, *3D tumour models: novel in vitro approaches to cancer studies.* Journal of cell communication and signaling, 2011. **5**(3): p. 239-48.

132. Nam, K.H., et al., *Biomimetic 3D Tissue Models for Advanced High-Throughput Drug Screening.* Journal of laboratory automation, 2015. **20**(3): p. 201-15.

8. Abbreviations

5-FU	5-fluorouracil
AJCC	American Joint Committee on Cancer
Arg-1	Arginase-1
APC	Antigen-presenting cell
ATCC	American Type Culture Collection
Bcl-xL	B cell lymphoma-extra large
CEA	Carcinoembryonic antigen
CFSE	Carboxyfluorescein succinimidyl ester
c-IAP	C-inhibitor of apoptosis protein
CSF-1	Colony-stimulating factor-1
CT	Computed tomography
CTL	Cytotoxic T lymphocytes
DMEM	Dulbecco´s modified eagle medium
DMSO	Dimethy sulfoxide
dNTPs	Deoxyribose nucleoside trisphosphates
DR	Desmoplastic reaction
ECM	Extracellular matrix
EDTA	Ethylenediaminetetraacetic acid
EGF	Epidermal growth factor
EMEM	Eagle´s minimum essential medium
EMT	Epithelial-mesenchymal transition
EpCAM	Epithelial cell adhesion molecule
FACS	Fluorescence activated cell sorting
FCS	Fetal calf serum
FGF	Fibroblast growth factor
Fig.	Figure
GFP	Green fluorescent protein
GM-CSF	Granulocyte-macrophage colony-stimulating factor
HLA-DR	Human leukocyte antigen-DR
IDO	Indoleamine-2,3-dioxygenase
IFN-γ	Interferon-γ

IGF	Insulin-like growth factor
IL	Interleukin
IPMN	Intraductal papillary mucinous neoplasm
LPS	Lipopolysaccharide
MCN	Mucinous cystic neoplasm
MDMs	Monocyte-derived macrophages
MDSCs	Myeloid-derived suppressor cells
MHC	Major histocompatibility complex
MMPs	Matrix metalloproteinases
NEAA	Non-essential amino acid
NF-κB	Nuclear factor κB
NK cells	Natural killer cells
NOS	Nitrogen oxide synthases
PanIN	Pancreatic intraepithelial neoplasia
PBMCs	Peripheral blood mononuclear cells
PBS	Phosphate buffered saline
PCR	Polymerase chain reaction
PD1	Programmed cell death protein 1
PDAC	Pancreatic Ductal Adenocarcinoma
PDL1	Programmed cell death ligand 1
Pen/Strep	Penicillin/Streptomycin
poly-Hema	Poly-2-hydroxyethylmethacrylate
PSCs	Pancreatic stellate cells
RLU	Relative luminescence units
RNAi	RNA interference
ROS	Reactive oxygen species
RT	Room temperature
SLRPs	Small leucine-rich proteoglycans
TAA	Tumor-associated antigens
TAMs	Tumor-associated macrophages
TCR	T cell receptor
TGF	Transforming growth factor
Th cells	T helper cells

TIMPs	Tissue inhibitors of metalloproteinases
TNF	Tumor necrosis factor
Treg cells	T regulatory cells
α-SMA	α-smooth muscle actin

9. List of figures

10. List of tables

11. Appendix

11.1 Additional data

11.1.1 Benchmark XT automated immunohistochemistry staining

Procedure: XT OptiView DAB IHC v4 (Protocol Summary)
BenchMark XT IHC/ISH Staining Module
Roche PZ G.241/R.182 GCP BM, TR-G 1 Nonnenwald 2 / 82377 Penzberg

Protocol No   Protocol Name
        472   E_FFPET_CC1_OV_XT

    1 IHC Synchronization Option [Selected]
    2 Paraffin [Selected]
    3 Deparaffinization [Selected]
    4 Cell Conditioning [Selected]
    5 CC1 [Selected]
    6 CC1 8 Min [Selected]
    7 CC1 16 Min [Selected]
    8 CC1 24 Min [Selected]
    9 CC1 32 Min [Selected]
   10 Pre Primary Peroxidase Inhibit. [Selected]
   11 Primary Antibody [Selected]
   12 Primary Antibody Temperature [Selected]
   13 Warmup Slide to Ab Incubation Temperatures [Primary Antibody]
   14 Antibody Titration [Selected]
   15 ***** Hand Apply (Primary Antibody), and Incubate for [1 Hour] *****
   16 Counterstain [Selected]
   17 Apply One Drop of [HEMATOXYLIN II] (Counterstain), Apply Coverslip, and Incubate for [8 Minutes]
   18 Post Counterstain [Selected]
   19 Apply One Drop of [BLUING REAGENT] (Post Counterstain), Apply Coverslip, and Incubate for [8 Minutes]

* one drop is one reagent dispense
Roche PZ G.241/R.182 GCP BM, TR-G 1 Nonnenwald 2 / 82377 Penzberg
NexES v10.6

Figure 33: Immunohistochemistry staining protocol for Benchmark XT.
Automated staining system protocol to detect CD68 on macrophages that have infiltrated tumor cell/fibroblast spheroids.

11.1.2 Expression of cell surface marker on supernatant polarized MDMs

marker	Pa-Tu 8902/MRC5 supernatant polarized MDMs	BxPC3/MRC5 supernatant polarized MDMs	HPAC/MRC5 supernatant polarized MDMs	MiaPaCa-2/MRC5 supernatant polarized MDMs
CD206	8,83	9,83	2,58	10,54
CD163	32,26	34,09	33,79	48,13
CD14	64,95	76,63	62,06	55,79
CD80	1,70	1,75	1,51	1,58
CD86	5,47	6,07	5,59	7,54
HLA-DR	149,80	171,73	136,80	226,24
CD16	2,86	2,92	2,81	4,33
CD33	5,68	5,51	6,07	3,92
CD40	9,43	6,90	6,44	5,50
Arg-1	1,78	2,49	1,70	1,54

Table 3: Summary of cell surface marker expression on MDMs differentiated with tumor cell/fibroblast supernatant.
Tumor cells and fibroblasts were co-cultured for 5 days. Supernatant was collected and 10.000 freshly isolated naïve monocytes were cultured in 3D tumor cell/fibroblast supernatant for 6 days. Typical M2 and M1 macrophage marker were analysed by flow cytometry. Shown is the mean of geometrical mean values of n=5 independent experiments.

11.1.3 Expression of cell surface marker on activated CD4⁺ and CD8⁺ T cells in 3D co-culture

A

marker CD4+ T cells	Pa-Tu 8902/MRC5		BxPC3/MRC5		HPAC/MRC5		MiaPaCa-2/MRC5	
	w/o MDMs	with spheroid polarized MDMs	w/o MDMs	with spheroid polarized MDMs	w/o MDMs	with spheroid polarized MDMs	w/o MDMs	with spheroid polarized MDMs
CLTA-4	1,42	0,93	1,68	0,96	1,68	0,95	1,24	1,01
PD-1	1,95	1,37	2,13	1,41	2,29	1,43	1,54	1,30
CD45RO	103,73	110,64	182,81	122,35	224,84	157,89	114,53	87,13
CD25	17,04	6,14	19,76	6,44	15,05	4,80	16,37	7,50
CD122	2,17	1,51	2,28	1,45	1,79	1,01	2,09	1,33
CD69	3,17	3,70	11,20	9,30	7,94	4,05	6,02	5,62
4-1BB	28,66	3,89	40,84	4,73	22,44	4,23	23,01	7,17
Ox40	1,67	2,37	2,28	2,42	3,66	3,01	4,37	4,28

B

marker CD8+ T cells	Pa-Tu 8902/MRC5		BxPC3/MRC5		HPAC/MRC5		MiaPaCa-2/MRC5	
	w/o MDMs	with spheroid polarized MDMs	w/o MDMs	with spheroid polarized MDMs	w/o MDMs	with spheroid polarized MDMs	w/o MDMs	with spheroid polarized MDMs
CLTA-4	1,19	0,87	1,40	0,86	1,40	0,90	1,12	0,71
PD-1	1,47	1,16	1,64	1,09	1,71	1,20	1,33	1,19
CD45RO	83,44	85,34	31,16	26,42	74,89	58,11	38,13	26,15
CD25	13,82	5,64	16,07	6,06	18,78	4,05	13,08	7,39
CD122	2,46	1,94	2,56	2,02	2,31	1,75	2,20	1,77
CD69	2,22	2,24	4,97	4,35	3,98	2,37	4,94	3,83
4-1BB	3,70	1,79	3,48	1,84	2,90	1,31	3,27	2,21
Ox40	1,32	1,25	1,46	1,82	1,57	1,40	1,84	1,78

Table 4: Summary of cell surface marker expression on CD4⁺ and CD8⁺ T cells co-cultured with 3D tumor cell/fibroblast spheroids with and without MDMs.

Tumor cells and fibroblasts were co-cultured for 5 days. Freshly isolated monocytes were added on day 5 to differentiate for 6 days. Autologous CD8⁺ and CD4⁺ T cells were added to co-cultures with and without spheroid polarized MDMs on day 11 and stimulated with CD3/CD28 activation beads. Cell surface marker expression of CD8⁺ and CD4⁺ T cells was measured 6 days after T cell activation by flow cytometry. A decrease of activation and checkpoint marker was observed for A) CD4⁺ and B) CD8⁺ T cells co-cultured with tumor cell/fibroblast spheroids containing spheroid polarized MDMs. Shown is the mean of geometrical mean values of n=4 independent experiments.